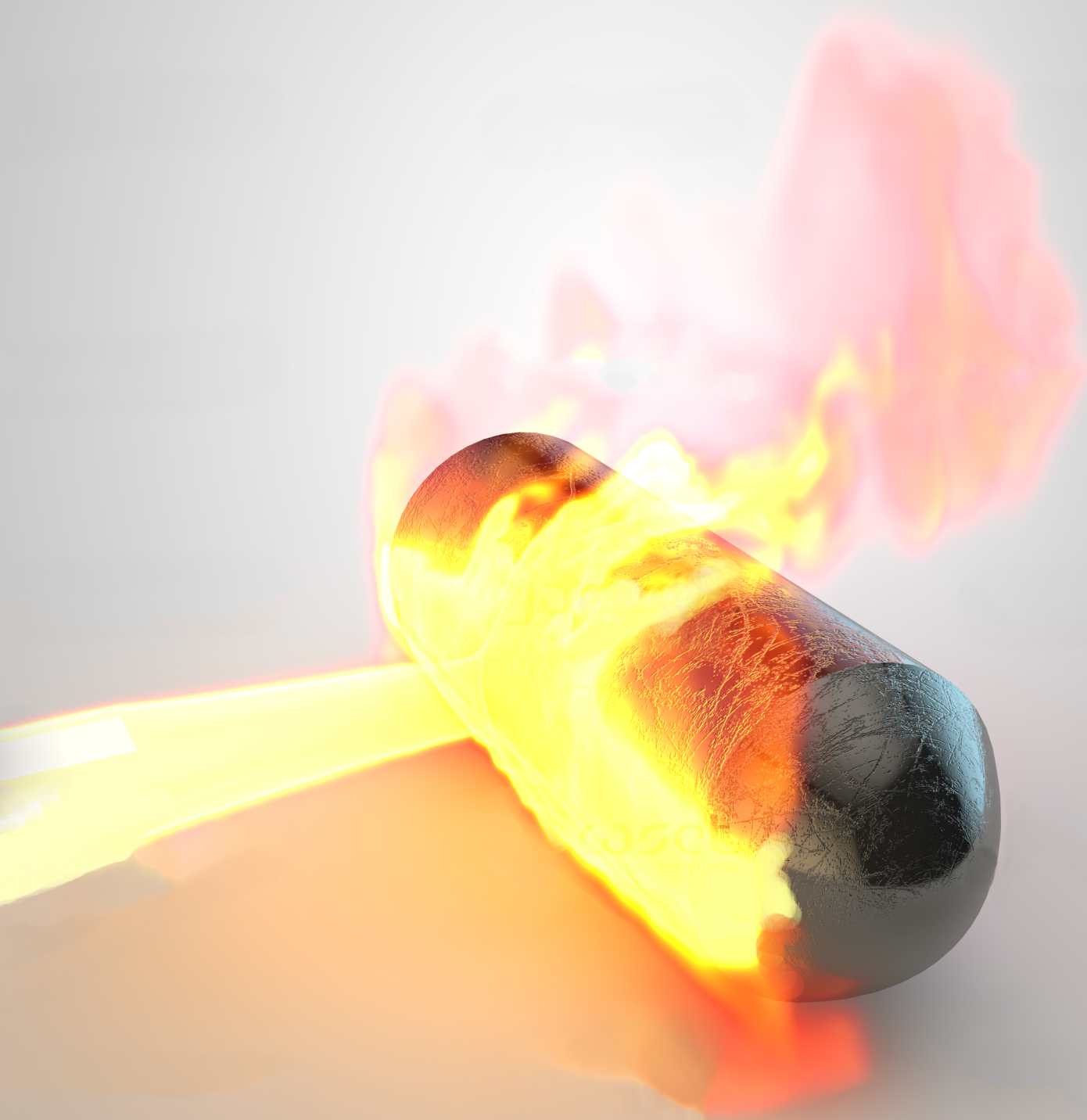


Analysis of the application and sizing of pressure safety valves for fire protection on offshore oil and gas installations

Master thesis
Michael S. Bjerre
Jacob G.I. Eriksen



Master Thesis

Analysis of the application and sizing of pressure safety valves for fire protection on offshore oil and gas installations

By PECT10-1-F15

Abstract

In this master thesis, the effectiveness of a fire PSV has been investigated, when offshore oil and gas process equipment is exposed to a small jet fire, large jet fire, or a pool fire. According to API 521, care should be taken when a fire scenario is affecting the unwetted part of a pressure vessel. Case studies are carried out, by simulating fire scenarios, using a state-of-the-art simulation tool, VessFire, in order to determine the effectiveness of a fire PSV. The case studies showed that a fire PSV does not offer adequate protection, in fire scenarios where the unwetted part of a pressure vessel is subjected to a fire. Alternatives to the use of a fire PSV, such as blowdown and passive fire protection, are discussed. The applicability of the stationary sizing method suggested by API 521, in fire case scenarios, are investigated. API 521 suggests a dynamic model in order to better predict the size of a fire PSV. A model is developed and compared with the stationary sizing equations. Results show that the stationary sizing method, in general, oversizes the fire PSV, and in cases with light hydrocarbons tends to undersize the fire PSV. It is found that a dynamic sizing method is advantageous when sizing a fire PSV.

Jacob G.I. Eriksen

Michael S. Bjerre

Project period for P10: February 2nd 2015 - June 9th 2015

Supervisor: Matthias Mandø

Rambøll supervisors: Anders Andreasen & Carsten Stegelmann

MSc in Process Engineering and Combustion Technology

Aalborg Universitet Esbjerg

Niels Bohrs Vej 8

6700 Esbjerg

Preface

This is a master thesis written by a project group consisting of two students at Aalborg University Esbjerg. The master thesis concludes the education of Process Engineering and Combustion Technology and was written during the 10th semester, spring of 2015. The project is done in collaboration with Rambøll Oil & Gas Esbjerg.

We would like to thank our supervisor Matthias Mandø for guidance throughout the project period, and our counselors at Rambøll Oil & Gas, Anders Andreasen and Carsten Stegelmann, for their help and guidance with the project.

A case study of the effectiveness of a fire PSV is conducted in the project. The results of the case study have resulted in an article draft concerning the subject. The draft article can be seen in annex I.

A model capable of dynamic simulations of a pressure vessel exposed to a fire, is developed in the project. The model is programmed in Excel VBA, and the code is shown in annex II.

Contents

1	Introduction	5
2	Problem analysis	8
2.1	Fire hazards offshore	8
2.1.1	Fire scenario and intensities	8
2.1.2	Fire impact on pressure vessels	11
2.1.3	Mechanics of vessel rupture	12
2.2	Design of offshore oil and gas installations	14
2.2.1	Production process unit	14
2.2.2	Flare system	15
2.3	Safety design of offshore oil and gas installations	17
2.4	Fire PSV	20
2.4.1	Fire PSV sizing	22
2.4.2	Problems with the use of fire PSVs offshore	25
3	Problem statement	28
4	Case study on the effectiveness of a pressure safety valve	29
4.1	Example of VessFire output	31
4.2	Influence of a PSV on the rupture time for various pressure vessels .	34
4.2.1	Peak heat load and wall thickness	42
4.2.2	Effect of insulation on rupture time	43
4.2.3	Rupture time for blowdown cases	44
4.3	Comparison of case study results	45
4.4	Variables influence on rupture time	46
4.4.1	Rupture times with and without a fire PSV	48
5	Dynamic sizing of fire pressure safety valves	50
5.1	Design of dynamic model for fire pressure safety valves	50

5.1.1	Flame heat flux model	54
5.1.2	Transient 1-D conductive heat transfer model for shell wall	55
5.1.3	Peak temperature of shell wall using 3-D heat transfer	61
5.1.4	Thermodynamic properties for the wall	63
5.1.5	Convective heat transfer coupling of fluid and wall	66
5.1.6	Pressure vessel inventory conditions	75
5.1.7	PSV and mass flow calculations	77
5.1.8	Calculation of exerted stress and prediction of rupture	78
5.2	Model validation	81
5.3	Comparison of stationary and dynamic sizing for pressure safety valves	91
6	Conclusion	94
6.1	Case study	94
6.2	Sizing of pressure safety valves	97
	Bibliography	100
A	Appendix: Steam and liquid sizing equations	102
B	Appendix: Vessel inventory	103
C	Appendix: Equivalent PSV size	104
D	Appendix: CasePlanner and Grapher	105
E	Appendix: Thickness of shells under internal pressure	106
F	Appendix: CCD simulation plan	107
G	Derivation of stability criteria	110
H	Appendix: Fluid conductivity	116

Nomenclature

Abbreviations

AFP	Active fire protection
API	American Petroleum Institute
BDV	Blowdown valve
BLEVE	Boiling liquid expanding vapor explosion
CCD	Central composite design
CFD	Computational fluid dynamics
EES	Engineering equation solver
EOS	Equation of state
ESDV	Emergency shutdown valve
FL	Fill level
GUI	Graphical user interface
H	Horizontal
HP	High pressure
IP	Intermediate pressure
KO	Knock out
LAH	Level alarm high
LAHH	Level alarm high high
LAL	Level alarm low
LALL	Level alarm low low
LP	Low pressure
LPG	Liquefied petroleum gas
NGL	Natural gas liquids
PAH	Pressure alarm high
PAHH	Pressure alarm high high
PAL	Pressure alarm low
PALL	Pressure alarm low low
PFP	Passive fire protection
PR EOS	Peng-Robinson equation of state
PRV	Pressure relief valve
PSV	Pressure safety valve
PV	Pressure-volume
SRK EOS	Soave-Redlich-Kwong equation of state
TAH	Temperature alarm high
TAHH	Temperature alarm high high
TAL	Temperature alarm low
TALL	Temperature alarm low low
TEG	Triethylene glycol
TH	Temperature-enthalpy
UTS	Ultimate tensile strength
V	Vertical
VBA	Visual Basic for Applications

1 Introduction

The oil and gas production in Denmark, and generally northern Europe, is centered around offshore platforms in the North Sea. The platforms are subject to various safety and environmental regulations, from clients as well as governments. The safety devices and requirements are mainly in place, in order to protect the personnel on board, by reducing the general risk level and prolonging available evacuation time as stated in API 14C [1].

One such safety device is the Pressure Safety Valve (PSV), which can stabilize the pressure in a vessel during an emergency, by relieving overpressure. A PSV is used to protect against pressure increases, e.g. which happens when an emergency shutdown process closes the outlet of a vessel, while the inlet has not yet been closed. A subcategory of the use of a PSV, is the case of a fire scenario. In this case, it is referred to as a fire PSV, which is intended to specifically protect against emergencies and pressure increases caused by fires near, impinging on, or engulfing the vessel.

The fire PSV sizing methods has been developed for onshore refineries and petrochemical industry, but is also applied for offshore oil and gas installations. However, hazards present on offshore installations differs significantly from those typically seen onshore, so the adoption of the onshore sizing methodology may not be appropriate for offshore applications.

The offshore platforms often contains gas inventories at higher pressures than the onshore facilities, which increases the risk of forming a jet fire. Jet fires are much more violent (heat fluxes of 300-400 kW/m²) and high momentum released compared to pool fires typically seen on refineries onshore (heat fluxes of 100-200 kW/m²).

The standard for the installation and use of pressure relieving equipment, API Standard 521 [2], also presents scenarios in which the PSV will be of little or no use. One scenario mentioned in the standard, is the case of a fire impinging on a gas volume, or gas part of a multiphase vessel. In this scenario, the fire can heat up the vessel wall, which causes a rupture, without increasing the pressure. This means that the fire PSV is not activated before rupture, even though the pressure vessel is subject to a fire.

The problem of using fire PSVs offshore that does not protect effectively against vessel rupture during an offshore fire is twofold:

- 1) The installed PSV may provide a false sense of security, when in fact appropriate fire protection is not in place and other safety barriers should have been installed.
- 2) All systems installed including safety systems has an inherent risk associated

to them, as they need to be maintained. Such maintenance put personnel at risk as they have to work in hazardous process areas.

It is therefore not only costly but also a personnel risk to install fire PSVs offshore if they do not provide any real protection in a fire.

A good example of the risk associated with PSVs comes from the Piper Alpha disaster, where a condensate pump and PSV was taken out of service for maintenance. The PSV was temporarily replaced by a loosely fitted blind flange and on another work shift, the condensate pump was brought online as the operator was unaware that the PSV was out for maintenance, resulting in condensate release exploding and escalating into a riser fire. This was the onset of one of the worst offshore catastrophes, killing 167 men and leading to total loss of the installation. No one was made personally responsible for the disaster, and the responsible insurance company paid out more than 1 billion GBP. More than 100 recommendations were made to improve the safety in the North Sea as a result of the accident [3]. A picture from the accident can be seen in figure 1.1.



Figure 1.1: Piper Alpha on fire caused by the accident in 1988 [4].

In this master thesis, the application of fire PSVs offshore will be investigated by a case study of typical offshore process equipment exposed to fire. This is done using a state of the art vessel fire simulation software, VessFire [5]. The case study should provide guidance and trend indication for the usefulness of fire PSVs offshore.

It is important that a PSV is properly sized when installed on a pressure vessel. Conventional sizing methods are expected to under estimate the heat of vaporisation, which leads to over sized fire PSVs. Over sized PVSs leads to chatter and additional cost.

An investigation of fire PSV sizing methods will be performed by developing a dynamic model for PSV sizing and compare it to the steady-state sizing methods

normally used. The dynamic model will be developed by modelling fire heat input to a vessel, heat conduction through vessel wall and heat transfer into vessel contents and between different fluid phases in the vessel.

The model will be developed in Excel VBA to provide a simple alternative to the use of expensive software for dynamic PSV sizing.

2 Problem analysis

2.1 Fire hazards offshore

In case of an emergency the pressure vessels, on an oil platform, can become subject to a fire exposure. This can be caused by a leakage from a vessel containing flammable hydrocarbons or a defective piping connection, e.g. a flange connection. When the pressure vessel is heated by a fire, the pressure increases (if it is not relieved) and the vessel wall temperature increases, and eventually, the vessel would rupture, releasing its content causing a major escalation of the initial fire. In the worst case, the vessel will rupture in a Boiling Liquid Expanding Vapor Explosion (BLEVE) that could have catastrophic consequences to personnel and assets on an offshore installation. Much of the safety design of an offshore installation is devoted to the prevention of a small and controllable fire escalating into an uncontrolled fire or explosion.

2.1.1 Fire scenario and intensities

The fire that a vessel can be subjected to is generally categorized as either a pool fire or a jet fire. A jet fire is a pressurized release of flammable gas and/or liquid with a high momentum, forming a cone shaped flame envelope in the direction of the release. On an offshore production platform, the flammable material is pressurized hydrocarbons.

Jet fires radiate high heat fluxes of 300-400 kW/m² [2][6] and the momentum can push firewall protection away and burn through steel like a blow torch.

A pool fire is an ignited flammable liquid on a surface, and on an offshore platform, it will typically be fueled by oil. Heat fluxes of hydrocarbon pool fires are significantly lower than for jet fire, and are in the range of 100-200 kW/m² [2][6].

A pool fire can occur if hydrocarbons have leaked onto a surface on which it will remain for a period of time. This containment of the spilled hydrocarbons could be due to intentionally man made bunding to prevent any further spread, or unintentionally placed obstacles. Areas where a grate floor or similar constructions are present, the pool fire is not assumed to be a relevant fire case scenario. Pool fires are assumed to be consisting of liquid hydrocarbons, as any similar amount of gas leaking will be dispersed in the atmosphere or most likely ignite before gathering in any available confinements.

Examples of a jet fire and a pool fire are illustrated in figure 2.1.



Figure 2.1: Example of jet fire (left) [7] and pool fire (right) [8].

The fire from a pool fire will be limited by the extent of the liquid spill, but the flames can rise quite high. As the fire develops, evaporation of the liquid spill increases, bringing more flammable material to the fire. The intensity of the fire can either be limited by fuel supply (evaporation of flammable liquid) or by air supply (enclosed or partially enclosed areas). Figure 2.2 illustrates the heat load from a jet fire and a pool fire as a function of the stoichiometric ratio within the flame volume.

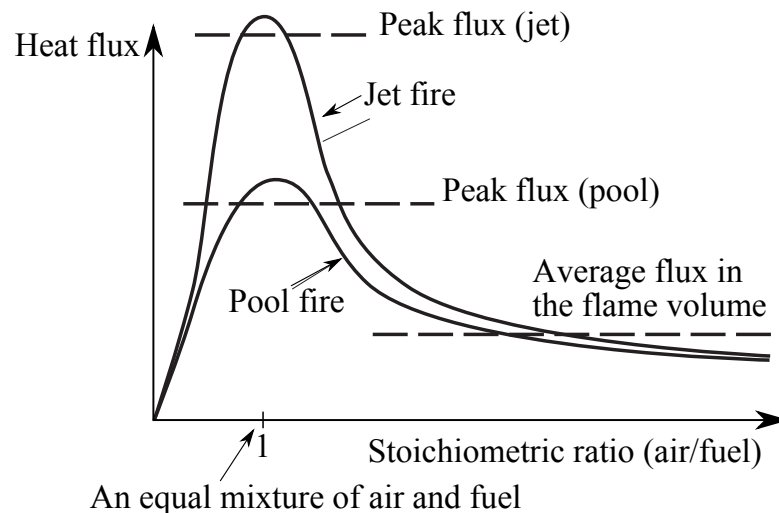


Figure 2.2: Heat flux in a flame volume as a function of the stoichiometric ratio. Modified from API 521 [2].

The stoichiometric ratio will change along the flame direction. Close to the fuel source, the stoichiometric ratio is below unity. Here the heat load will be ventilation controlled and the lack of air to the flame will limit the heat load. There will be a stoichiometric ratio of unity at some points in the flame and this will correspond to the peak heat load. Towards the outer borders of the flame, the stoichiometric ratio will be above unity, and there will be excess air, which will limit the heat load.

The intensity of the fire is categorized into a peak and a background heat load. The heat flux from a flame will change rapidly with time as a consequence of the turbulence in the flame. API 521 [2] describes that for engineering purposes, it is adequate to use average values for the heat flux. The dashed lines in figure 2.2 illustrates the average peak heat load and the average background heat load.

If it is assumed that the vessel is engulfed by the flame, then the peak heat load will affect a local area of the vessel, while the background heat load affects the entire area of the vessel. A pool fire has a low peak heat load and a relatively large background heat load. Jet fire is often divided into a small jet fire with a mass flow of more than 0.1 kg/s, and a large jet fire with a mass flow more than 2 kg/s for design purposes of offshore oil and gas installations. The small jet fire has a peak heat load, but no background heat load, since the flame is not large enough to affect the entire vessel. This is evident when considering the flame volume, i.e. the spatial extent of the flame, which is negligible in relation to a large vessel, and thus it can be assumed that the small jet fire does not provide any significant global (background) heat load. For any given fire scenario the appropriate heat flux will have to be estimated. This can be done by following the Scandpower standard [6], using table 2.1.

	Peak heat load kW/m ²	Background heat load kW/m ²
Small jet fire	250	0
Large jet fire	350	100
Pool fire	150	100

Table 2.1: Fire intensity for a fire case of a small jet fire, large jet fire, and a pool fire [6].

The heat fluxes described in table 2.1, is when no firefighting is included, and is as such, a conservative estimate. Generally the jet fires act like a blowtorch, affecting a small area with high intensity heat and momentum, while the pool fire is affecting a larger area at lower intensity heat and practically no momentum. The heat loads will in any natural case vary both in time and location along the vessel, and thus the heat loads described are average estimates for a flame located relatively close to the vessel. The net heat load from the flame to the vessel will under normal circumstances decrease with time as the vessel temperature increases, thus increasing the reradiation heat from the vessel to its surroundings.

The peak heat load referenced is assumed to only be available at the directly fire affected area, while the background heat load is assumed to be present throughout the entire vessel surface area.

2.1.2 Fire impact on pressure vessels

When a pressure vessel is exposed to a fire, the flames can heat up the inventory and cause a pressure build-up in the vessel, or the flames can cause a high local temperature increase in the vessel wall, which will reduce the strength of the vessel. These factors can cause the pressure vessel to rupture and a subsequent escalation of the situation can be critical.

Several physical phenomena are important to take into account, when predicting the behavior of a vessel subjected to a fire. Important variables and phenomena concerning the vessel, in a heat scenario, are illustrated in figure 2.3.

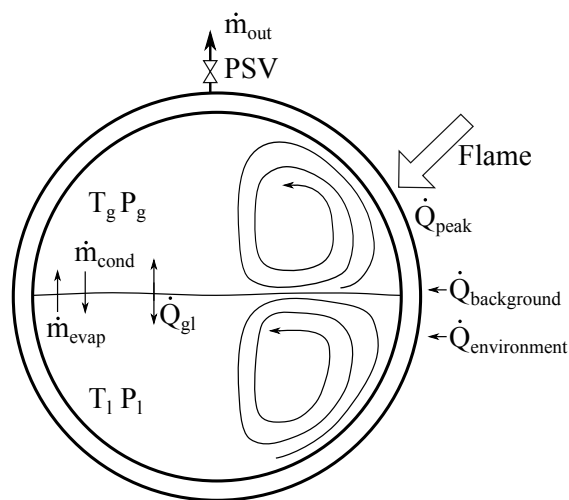


Figure 2.3: Illustration of physical heat transfer phenomena in a vessel affected by a flame.

- \dot{m}_{out} is the mass flow through the PSV orifice.
- \dot{Q} indicates heat flow.
- Subscripts refer to gas (g), liquid (l), and gas-liquid interface (gl).
- \dot{m}_{cond} is the mass flow of condensing gas.
- \dot{m}_{evap} is the mass flow of evaporating liquid.
- T is the temperature.
- P is the pressure.
- $\dot{Q}_{environment}$ refers to the heat loss to the surroundings.
- Indices *background* and *peak* refers to the flame type.

The heat is transported from a flame source through the outer side of the vessel, either as a background heat load or as a peak heat load. The heat is transferred from the flame to the outer vessel wall by means of convection and radiation.

Conduction takes place through the wall, and subsequently the heat is transferred to the liquid and gas by means of convection. The radiation from the exposed

inner wall of the gas volume to the liquid should be taken into account, if the gas is assumed to be transparent.

As the liquid and gas are regarded as being two separate continuous phases, but at different temperatures, a heat transfer process will exist in the phase interface. The convection inside the vessel can be divided into natural convection and forced convection. Forced convection would become evident in the case of opening a valve and producing a velocity field in the gas phase. As illustrated in figure 2.3 natural convection will be present in the liquid and gas phases, which will aid in the transfer of thermal energy through the system.

Due to evaporation and condensation, mass and heat transfer will take place between the two phases. This will change the liquid level, and thus affect the inner area of the vessel exposed to the gas phase and liquid phase, which in turn will affect the heat transfer from the vessel wall to the liquid and gas phases.

When calculating the system response due to the fire, the peak heat input is used to determine the thermal behavior of the wall material, and the background heat input is used to calculate the pressure profile of the system content. By using time and area average values, the heat flux can in some cases be simplified. Several parameters can influence an accurate prediction of the heat flux, including fire duration, fire size, obstacles nearby, further escalation of fire, changes in air-fuel ratio, exposed vessel area, conduction and convection heat transfer coefficients, ambient conditions, vessel heat capacity, and drainage and fire fighting, including active and passive. The best possibility of calculating an accurate solution for a given case, will be to employ Computational Fluid Dynamics (CFD) simulations, but as most problems are widely individual in its conditions, simulating each case with CFD is not a practical solution.

2.1.3 Mechanics of vessel rupture

Each vessel is designed to an optimal range of pressure and temperature, for which the vessel can contain the hydrocarbon content. If the conditions vary beyond the design criteria, the vessel becomes at risk of rupture. To gauge the strength of a material, the concept Ultimate Tensile Strength (UTS) is used, which is the maximum stress that the vessel can sustain before it ruptures. The UTS is a function of temperature and is unique to each individual material. The material strength will decrease either as a consequence of the material becoming brittle at low temperatures, or by the UTS decreasing with increasing temperature.

Figure 2.4 illustrates the effect of material temperature on the UTS of the material. The material UTS is seemingly kept relative constant even when the temperature is increased considerably in the initial period. When the temperature then reaches a critical value the material stress is drastically decreased, through a narrow change in temperature.

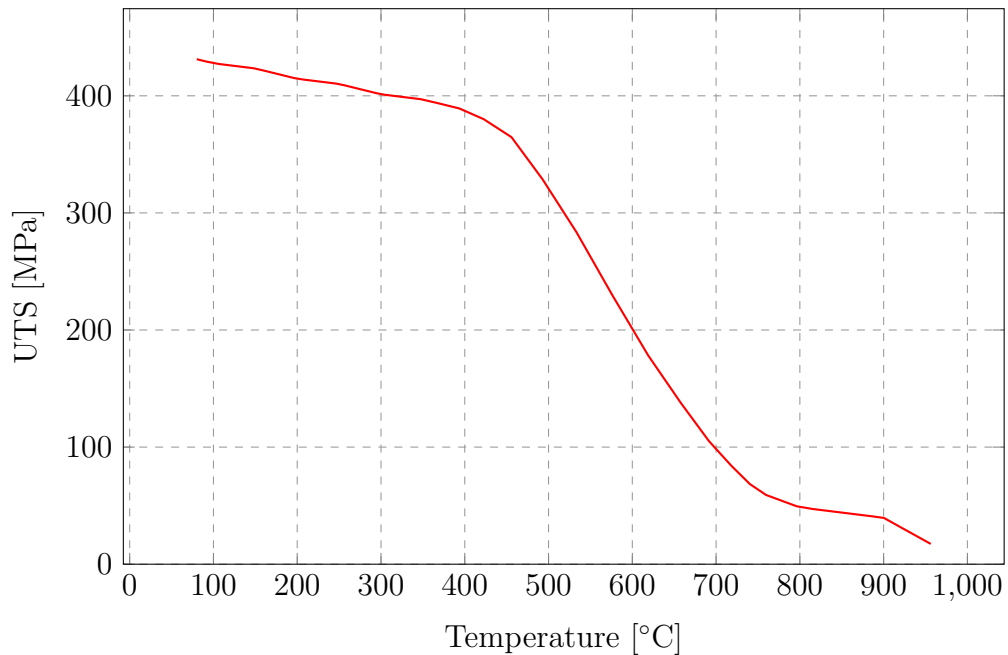


Figure 2.4: The UTS as a function of vessel material temperature. The material illustrated is carbon steel, CS360LT.

When a material is subjected to relative high stress for an extended period of time, or high temperatures, the material will have a tendency to creep, which is a slow permanent deformation process. The creep can still occur even if the stress is below its yield point, i.e. it is still in the region of elastic deformation. The creep tendency is highly affected by temperatures, and thus when a torch flame is applied locally to the vessel material, it may form the beginning of a fissure.

The fissure will weaken the vessel and if the vessel wall thickness is thin enough the fissure will spread, and can only be stopped when it enters an area with an increase in material strength. If the vessel is subjected to a fire engulfing a larger part of the vessel, such as a pool fire or a large jet fire, the fissure could spread across a large part of the vessel, and weaken it severely, causing a BLEVE. A BLEVE occurs when there is a sudden depressurization of the vessel, due to a rupture. When a fissure occurs, it effectively functions as an outlet for the hydrocarbon inventory, and the vessel pressure decreases. If the conditions are near the saturation point of the liquid content, the reduction in pressure may cause a sudden flash evaporation. The depressurization causes the liquid to rapidly boil, and the produced expanding vapors will behave as an explosion. The added amount of gas in the vessel will then cause pressure recovery and if this effect is strong enough to create a large fissure, the BLEVE scenario could arise as a secondary consequence. If the inventory of the vessel is flammable, an ignition can occur, resulting in a widespread fireball or an explosion [9]. An example of a BLEVE can be seen in figure 2.5.



Figure 2.5: Example of a Boiling Liquid Expanding Vapor Explosion [10].

A fissure could still be large, as in the order of the vessel diameter, without causing the BLEVE scenario, but as a significant amount of material is released, and possibly ignited, the ensuing fire or explosion might be just as damaging as a BLEVE.

2.2 Design of offshore oil and gas installations

The purpose of the process equipment on an offshore oil platform is to separate the oil well fluid into its constituent components. When the initial oil well product is extracted from the source it is usually a mixture of oil, gas, and water. This is often referred to as being a three phase mixture. For easier and more cost effective transportation to onshore refinery facilities the three phases will have to be separated. This can be done by a gravity separator, exploiting the fact that the three phases have adequate differences in densities. The lowest density being that of gas, and the heaviest that of water, the gas will flow to the top of the vessel, and the water to the bottom, while the oil will flow as a top-layer on the water.

2.2.1 Production process unit

The purpose of the production process design is to separate the well-fluid, which is extracted from the wells drilled to the reservoirs in its main phases: gas, oil, water and solids (e.g. sand). In the following section, a typical example of an offshore process will be discussed.

A practical way of performing the process is using a three stage separation process.

Each stage of the separation process has a different pressure. By dividing the process into three pressure stages, it is possible to obtain a better separation. A process diagram of the separation process is shown in figure 2.6. The process diagram is an example of the separation train used on an oil and gas production platform in the North Sea.

The multiphase well product enters the first stage separator and the gas, oil, and water is typically separated at a relatively high pressure, typically in the range of 30-35 barg. The oil is sent to the second stage separator where the pressure is reduced to e.g. 10 barg. The separated water from the first and second stage separators are sent to a water treatment facility. The oil is sent to the third stage separator operating at low pressure e.g. 2-3 barg. The oil and water mixture from the third stage separator is sent through an electrostatic coalescer, in order to separate the remaining water from the oil. The oil can now be sent to storage.

The gas from the third stage separator is sent through a heat exchanger and the first stage suction drum before being compressed by the first stage low pressure compressor to around 10 barg. After being compressed, the gas is combined with gas from the second stage separator and the Natural Gas Liquids (NGL) splitter. The gas enters a heat exchanger and the second stage suction drum before being compressed by the second stage low pressure compressor to around 30 barg. The gas from the first stage separator is added to the process before the gas enters a heat exchanger and a suction drum. The intermediate pressure compressor raises the pressure to around 50 barg and the gas enters a heat exchanger and a discharge drum.

The gas is typically dried by a TriEthylene Glycol (TEG) facility. After that, the gas is cooled and enters a gas/gas heat exchanger. The gas is sent through a Joule Thompson valve which lowers the pressure and thereby also the temperature of the gas. The fluid enters a NGL knock out drum where the gas and condensed liquid is separated. The liquid is distilled by a NGL splitter and reboiler system, and the gas is sent through the secondary side of the gas/gas heat exchanger. The pressure of the gas is raised to around 120 barg by the high pressure compressor and is cooled further before being exported to shore or used as lift gas in the production.

In summary an offshore oil and gas installation will consist of many different hydrocarbon gas and/or oil inventories of different pressures that in case of loss of containment could lead to a jet and/or pool fire.

2.2.2 Flare system

All pressure vessels containing hazardous hydrocarbons are connected to the flare system. The flare system is an emergency pressure relief system, and is used to dispose of all hazardous inventory from pressure vessels in the case of an emergency.

If the pressure increases too much in a pressure vessel, the flammable gas inventory of the vessel is released in to the flare system, where it is lead to the flare top and burned [11]. The flare system is divided into a low pressure flare system (LP) and a high pressure flare system (HP). The pressure safety valve is connected to the HP flare system, which operates with a high pressure and is also used during blowdown of pressurized vessels.

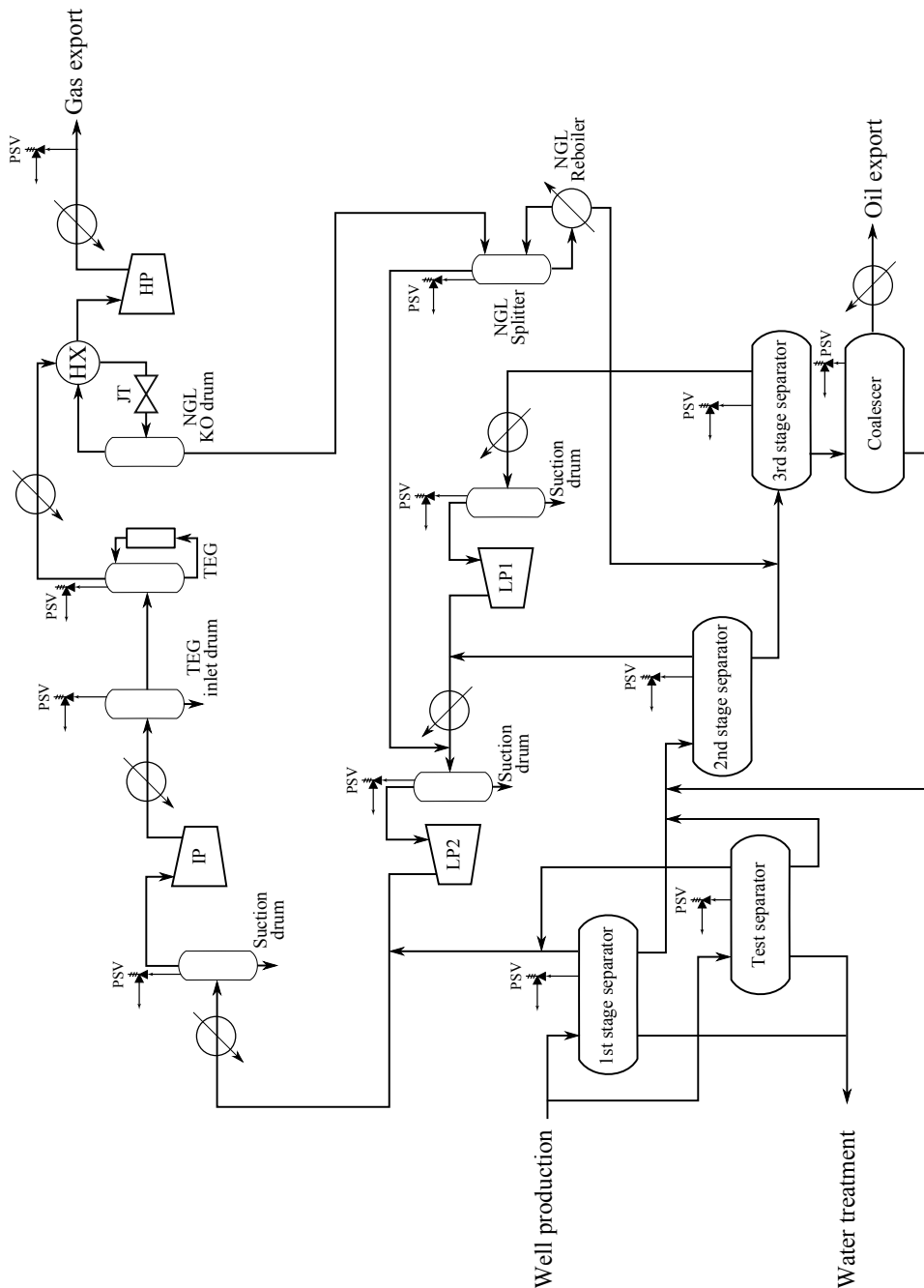


Figure 2.6: Process diagram of an offshore oil and gas production platform.

2.3 Safety design of offshore oil and gas installations

When constructing a platform offshore, several safety barriers are designed to protect personnel, the environment and assets. The process safety design can be divided into a hierarchy of importance and is illustrated in figure 2.7.

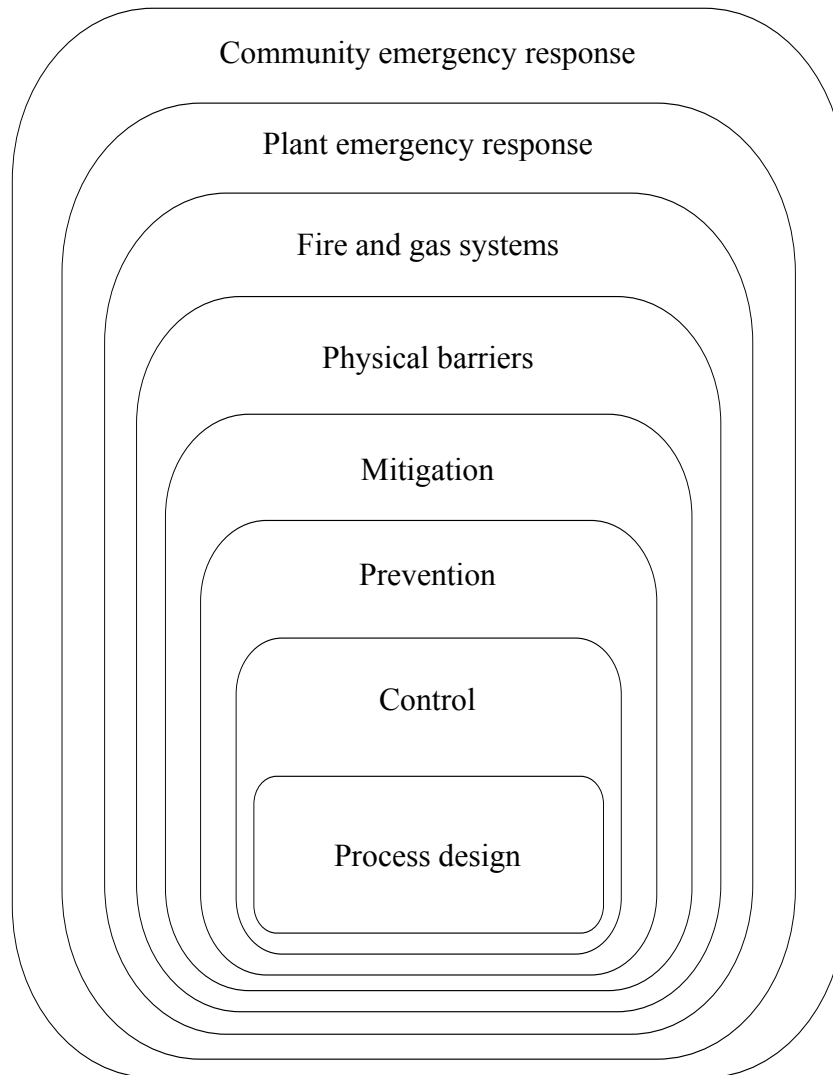


Figure 2.7: Illustration of the process safety level design.

Process design

The first step is to design the equipment, which is at risk of failure, in an inherently safe fashion. This could for instance be achieved by construction of a pressure vessel with adequate wall thickness, in order to withstand even the highest critical temperatures and pressures. In the cases where it is not economically feasible, other methods of protection should be used. A way of ensuring inherently safe

design is to design the process unit with as few parts and pipe connections as possible, in order to limit the risk of failure. Another approach would be to design the layout, in such a way, that when a failure occurs, the surrounding equipment will be protected. This method can be used in some critical cases, and as a general protection and mitigation method, but not as a dedicated protection for each piece of equipment.

Control

The second step in the safety design is the basic control of the process unit. Process alarms are used to ensure that the process does not operate outside design envelope, and is used to shut down the process if an anomaly occurs. Some of the alarms which are used to control the process are pressure alarm low and pressure alarm high (PAL/PAH), temperature alarm low and temperature alarm high (TAL/TAH), and level alarm low and level alarm high (LAL/LAH). The alarms are illustrated in figure 2.8.

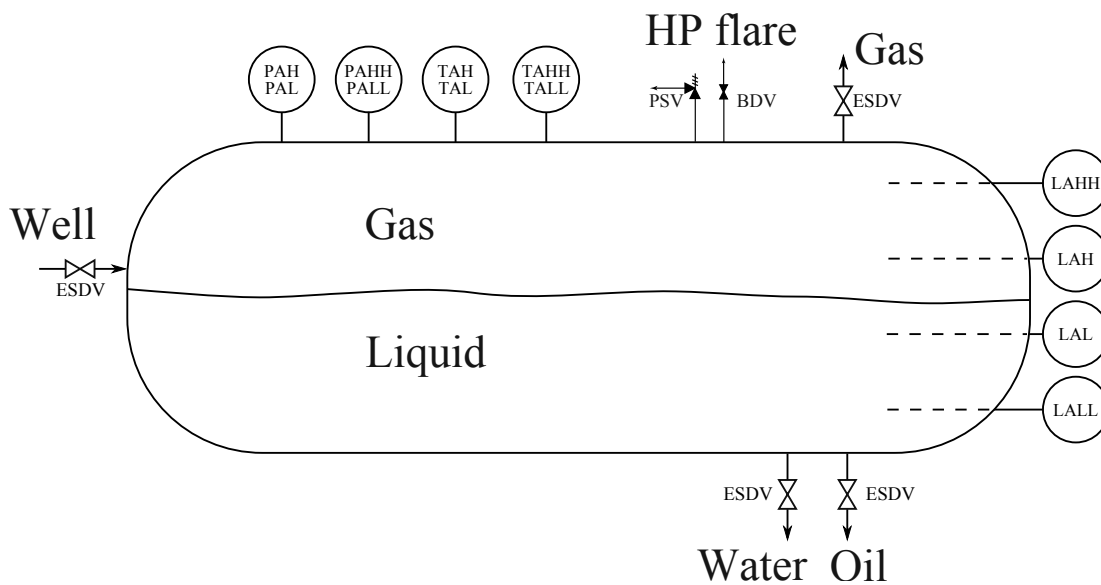


Figure 2.8: Example of a process pressure vessel with ESDVs, process alarms, PSV, and BDV.

Prevention

The next step is prevention, where safety critical process alarms and safety instrumental systems can prevent emergencies from escalating. A trip alarm can be a pressure alarm low low (PALL), pressure alarm high high (PAHH), temperature alarm low low (TALL), temperature alarm high high (TAHH), level alarm low low (LALL), or level alarm high high (LAHH). When a trip alarm is activated, it can

initiate emergency shutdown segregation, using the a Emergency ShotDown Valve (ESDV), which will isolate the process inventory of the pressure vessel. ESDVs are installed on all inlets and outlets as shown in figure 2.8. After the pressure vessel is isolated, a blowdown sequence is initiated, which will depressurize the vessel and evacuate the inventory through a BlowDown Valve (BDV).

Basic controls, safety alarms, and safety instruments are all controlled automatically, by a central control system or independent sensors. This method will also have its limitations, as it is susceptible to sensor errors and is relying on the initial programming set up, which may contain errors or inadequacies. If the system sensors does not respond correctly, either due to sensor error, poor design of cause-effect hierarchy, or lack of sensor extent, a manual override will be the next step of protection. However the personnel on board can not monitor the entire platform manually, and some areas of the platform are rarely directly accessed in the daily operations.

Mitigation

PSVs and rupture discs can be used as a method to mitigate the pressure increase caused by a process upset or a fire emergency. A PSV will relieve the inventory of the pressure vessel if the pressure exceeds a set limit. This will cause the pressure vessel to maintain a relative constant pressure and avoid a rupture due to an abnormally high pressure. This is in contrast to a blowdown procedure which will evacuate the hydrocarbon inventory and decrease the pressure well below the operating pressure.

Physical barriers

When a leakage of hydrocarbons occur, it is generally difficult to contain the gas as it relatively quickly disperses into the atmosphere. The liquid can be contained by bunding, also known as dikes, which will protect the surrounding equipment from flame exposure if the liquid hydrocarbons catch fire. It is not suitable to place the bunding at all possible leakage locations, and is therefore limited in its use.

Fire and gas systems

Fire and gas detection systems are used to raise alarms, which should be acted upon manually, and alarms which will result in automatic actions from the control system. Such actions could be to activate the ESDVs, and initiate isolation of the vessel and begin the blowdown procedure.

Passive Fire Protection (PFP) systems are used to protect equipment and person-

nel from fire, by preventing and slowing the spread of the fire, without the need of activation from the personnel, automatic control system, or independent sensors. PFP could be additional insulation, e.g. expanding foam covering or mineral wool, which will increase the heat resistance of the vessel.

Active Fire Protection (AFP) could be deluge systems, fire sprinkler systems, and fire and gas detection sensors. AFP are characterized by the need to be activated by a certain action, as contrary to PFP.

Plant and community emergency response

When an accident is eminent or in progress, the emergency responses will have to be initiated. First the local plant emergency response is carried out by the personnel, and if necessary the community emergency response is initiated as a secondary aid.

2.4 Fire PSV

As described in the previous section, several safety barriers exist in the offshore oil and gas industry, in order to protect the personnel and process units from fatal damage. Each barrier prevents certain accidents, and a single barrier would be insufficient to cover all safety aspects. This thesis focuses on the use of a PSV as a safety barrier in the case of a fire emergency.

A PSV is a mechanical device actuated by the static pressure in the vessel and a conventional PSV is often used for gas/vapor systems. A conventional PSV is a spring-loaded device which will activate at a predetermined opening pressure, and relieve the vessel pressure until a given reset pressure has been reached. Both the opening pressure and the reset pressure is above the vessel operating pressure, and the PSV will remain closed until the pressure inside the vessel increases to the opening pressure.

The operation of a conventional spring-loaded PSV is based on a force balance. A conventional PSV can be seen in figure 2.9. A spring exerts a force on a disc blocking the inlet of the PSV. When the pressure inside the vessels reaches the opening pressure, the force exerted on the disc by the gas, will be larger than the force exerted by the spring and the PSV will open and allow the gas to flow out of the vessels. The flow of gas out of the vessels will lower the pressure and thereby also the force exerted on the disc. When the pressure in the vessels is reduced to the reset pressure, the PSV will close and the disc will again hinder the gas flow.

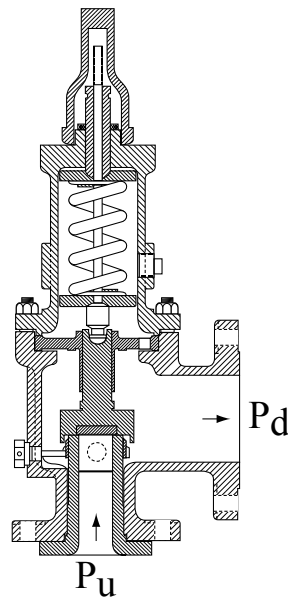


Figure 2.9: Conventional pressure safety valve. The illustration is modified from API 520 [12]. P_u is the upstream pressure and P_d is the downstream pressure.

The opening characteristics of a conventional spring-loaded PSV will be a pop action, which indicates that the PSV will go from closed to fully open in a short period of time. The pop action is illustrated in figure 2.10 which shows the opening and closing hysteresis of the PSV. The opening of the PSV is shown as a function of the pressure.

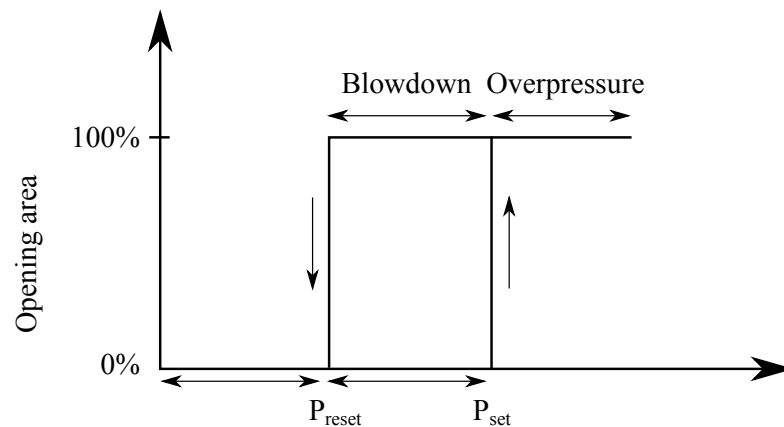


Figure 2.10: Opening and closing hysteresis for a conventional PSV with pop action [12].

It is often a legislative requirement that a PSV is located at the top part or, at the very least, the gas part of most vessels subjected to risk of rupture. Additionally, a

PSV can be placed at the liquid part, in which case sufficient drainage or secondary storage will have to be available, which in turn will lead to economic cost increases and due to the increase material and component cost, and also the additional cost in order to support the added weight offshore. The PSV could be located far from the actual device it protects, which will require additional piping. The area of the piping before the PSV will be increased, which leads to an increased risk of being exposed to a fire.

2.4.1 Fire PSV sizing

When sizing a gas or vapor relief device according to API Standard 520 [12], it is assumed that the pressure volume relationship, following an isentropic path. This is described by equation 2.1.

$$PV^k = c \quad (2.1)$$

- P is the pressure. [kPa]
- V is the volume. [m³]
- k is the isentropic expansion factor, approximated by the heat capacity ratio. [-]
- c denotes a constant.

The k value used in equation 2.1 should be calculated for ideal gas assumptions. The equation may not be applicable for high pressures or if the conditions approach the critical point of the fluid, and ideally the fluid compressibility should be in the region of 0.8 to 1.1 [12].

When a fluid flows through a constriction or opening such as an orifice, the velocity will be affected by conditions upstream and downstream. If the upstream pressure is adequately high, relative to the downstream pressure, the velocity will reach the speed of sound (Ma = 1) and the flow rate obtained will be the critical flow rate. The upstream and downstream pressures are indicated on figure 2.9.

The maximum downstream pressure for the flow to still be sonic (Ma = 1), is when $P_d = P_c$. The ratio of the critical and upstream pressure is defined by equation 2.2.

$$\frac{P_c}{P_u} = \left(\frac{2}{k+1} \right)^{\frac{k}{k-1}} \quad (2.2)$$

- P_c is the critical pressure. [kPa]
- P_d is the downstream pressure. [kPa]
- P_u is the upstream pressure. [kPa]

Typical values of the heat capacity ratio, k , is about 1.1 to 1.6. The pressure ratio found in equation 2.2 will for these values range from 0.50 to 0.58.

For complex molecules with multiple degrees of freedom the heat capacity ratio will tend towards a value of 1. When using a k value of 1 in equation 2.2, a division by zero will occur, and thus no solution exists. When the limit is taken for $k \rightarrow 1$, the right hand side will tend towards a value of 0.61, as indicated in equation 2.3.

$$\lim_{k \rightarrow 1} \left(\left(\frac{2}{k+1} \right)^{\frac{k}{k-1}} \right) = \frac{1}{\sqrt{e}} \approx 0.61 \quad (2.3)$$

Thus, the critical pressure, for the flow to be sonic, will never exceed 61% of the upstream pressure. This relation could be used as a general indicator, of whether a flow rate is sonic or not, if k is unknown.

Four main conditions exists when sizing a PSV through stationary equations as presented in API 520 [12]. These equations are given in the sections below.

Critical gas flow

For sonic flow (critical flow), as indicated in equation 2.2, the effective discharge area of the PSV can be determined by equation 2.4.

$$A = \frac{W}{C \cdot K_d \cdot K_b \cdot K_c \cdot P_1} \sqrt{\frac{T \cdot Z}{M}} \quad (2.4)$$

- A is the effective discharge area. [mm²]
- W is the mass flow through the device. [kg/h]
- C is a coefficient, as a function of k , as defined in equation 2.5.
- K_d , K_b , and K_c are correction factors.
- P_1 is the allowable upstream absolute pressure. [kPa]
- T is the temperature of the inlet gas at relieving conditions. [K]
- M is the molecular mass of the gas at relieving conditions. [kg/kmol]
- Z is the compressibility factor for the gas.

K_d is the effective coefficient of discharge, with a typical value of 0.975, for an installed PSV. K_b is a back-pressure correction factor between 0 and 1. K_c is a correction factor used when a rupture disk is installed upstream, otherwise it is 1.

$$C = 0.03948 \sqrt{k \left(\frac{2}{k+1} \right)^{\frac{k+1}{k-1}}} \quad (2.5)$$

Subcritical gas flow

For subsonic flow (subcritical flow), as indicated in equation 2.2, the effective discharge area of the PSV is determined by equation 2.6.

$$A = \frac{17.9 \cdot W}{F_2 \cdot K_d \cdot K_c} \sqrt{\frac{T \cdot Z}{M \cdot P_1 \cdot (P_1 - P_2)}} \quad (2.6)$$

F_2 is the coefficient of subcritical flow which can be determined from 2.7.

$$F_2 = \sqrt{\left(\frac{k}{k-1}\right) r^{\left(\frac{2}{k}\right)} \left(\frac{1 - r^{\left(\frac{k-1}{k}\right)}}{1 - r}\right)} \quad (2.7)$$

r is the ratio of backpressure to upstream relieving pressure, P_2/P_1 .

The sizing equations for steam relief and liquid relief can be seen in appendix A.

The sizing method applied is a strictly stationary method for which steady state is assumed. The system is in reality a dynamic and coupled system, which will constantly change as pressure is affecting the orifice flow, which in turn affects the pressure. The temperature, energy, and composition also changes and interacts with the flow and pressure.

In the case of a fire scenario it would be necessary to calculate the flow rate from vaporisation. This could be done on the basis of the enthalpy of vaporisation of the mixture, and either a known or assumed heat transfer to the vessel inventory.

The stationary sizing method is thus based on the assumption that the enthalpy of vaporation, at initial conditions, is constant throughout the duration of the fire. Subsequently the heat transfer is also assumed to be constant, and can be estimated for the case of a pool fire using the API fire equation [2], as given in equation 2.8. The equation is based on empirical data from the 1950's, using available pool fire test data at the time.

$$Q = C_{API} \cdot C_E \cdot A^{0.82} \quad (2.8)$$

- Q is the heat generated from the fire. [W]
- C_{API} is an equation coefficient.
- C_E is an environmental factor.
- A is the fire affected area. [m²]

C_{API} is an adjustable coefficient, relating to whether the fire is provided with adequate firefighting and drainage ($C_{API}=43,200$) or if there is inadequate firefighting and drainage ($C_{API}=70,900$). C_E is an environmental factor used to account for insulation or other parameters directly affecting the heat transfer to the vessel. The fire affected area, A , can be assumed to be only the wetted area, as the heat transfer to the gas is considered comparably small.

2.4.2 Problems with the use of fire PSVs offshore

According to API Standard 521 [2], a PSV may not always provide adequate protection, in the case of a fire scenario, if the fire exposure is affecting the unwetted part of the pressure vessel. On the unwetted part of a pressure vessel, the convective heat transfer of the gas is not sufficiently large enough to transfer the heat of the fire away from the vessel wall. This causes a local temperature increase in the wall and thereby lowering the mechanical strength of the wall, which may lead to a rupture of the pressure vessel. According to API Standard 521 [2], it can be appropriate to use other protective measures as an alternative to a PSV, to protect against rupture from a fire exposure, if local jurisdiction permits it. The circumstances for an alternative to a PSV would be if the pressure vessel only contains vapor, the liquid has a high boiling point, or if an engineering analysis indicates that the PSV only serves little value in reducing the likelihood of a vessel rupture.

An alternative protective method of relieving vessel pressure is to perform a blow-down process, in which a BDV is constantly kept open in order to reduce the pressure to a level below the operating pressure. The difference between a PSV and a BDV is illustrated in figure 2.11, by the pressure as a function of time, when a vessel is subjected to a fire. It can be seen that if no safety equipment is installed, the pressure will continue to rise. A PSV will limit the pressure increase to its set limit, while a BDV will lower the pressure of the vessel below the operating conditions.

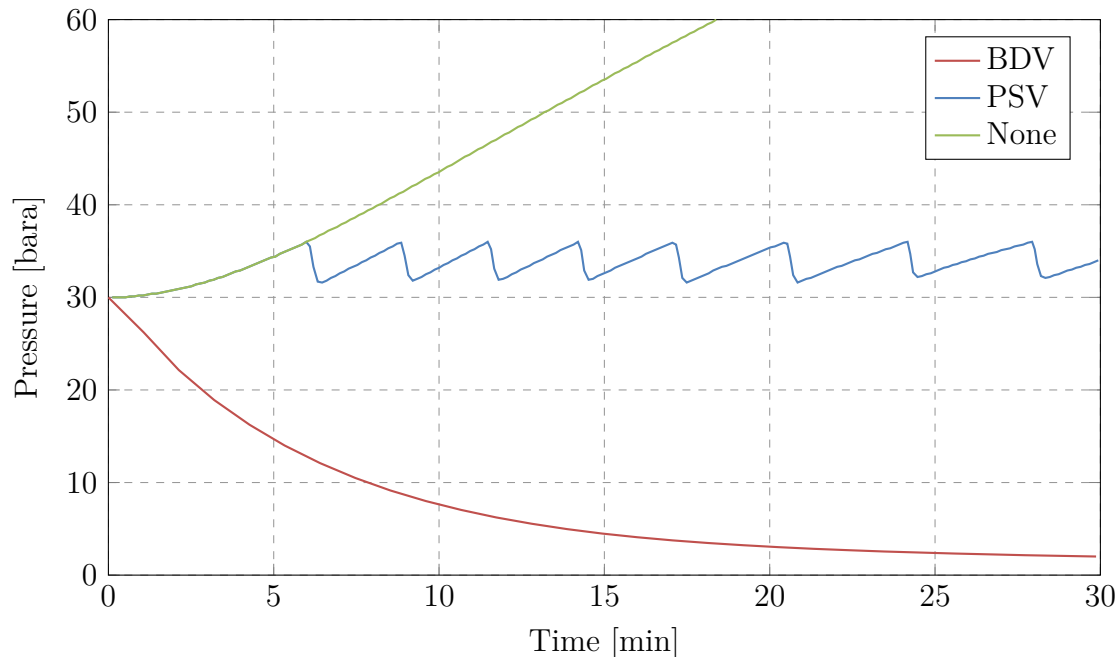


Figure 2.11: Pressure of a vessel subjected to a fire as function of time. The figure illustrates the difference between blowdown, PSV relieving, and no use of either a PSV or BDV.

Correctly sizing of several design parameters can increase the protection against fire. These parameters are flare system capacity, vessel material, insulation, vessel wall thickness, active fire fighting capability, drainage of fire fuel, and PFP initiatives. When passive fire protection, such as insulation and fire retardant material is applied to a vessel, an increased exposure time will be allowable. Subsequently if an accident occurs and the vessel ruptures, could create a jet fire with an extended duration, which may pose a severe risk to other components and vessels in the vicinity [6]. An optimization process should be carried out to ensure the flare system capacity is dimensioned appropriately, as any surplus in available flare capacity could be used in order to reduce the use of PFP equipment. Any insulation of pipes for other purposes than PFP should not be included in any heat transfer calculations. With this additional layer surrounding the vessel comes the risk of corrosion damage, which will not be visible to manual inspection, and therefore poses a safety risk.

When any equipment is added to an environment, in which any accident could escalate very quickly to a large scale destruction, the risk level will increase due to the added complexity of the system. If the added equipment does not adequately reduce the risk in itself, the general risk level of the system will have increased [13].

Several weaknesses are introduced when a PSV is added. For instance, the con-

nection of the pipeline leading to the flare system, which will perforate the vessel wall. The PSV is also sometimes located far from the actual vessel it protects, and thus an accident may cause the evacuation of a vessel not located in the accident zone. As a consequence the accident may inadvertently spread through the system processes. The piping from the vessel to the flare system is also exposing a considerable amount of surface area, which both increases the material cost, and the available area of any impinging flames. The added material of the flare piping is not exclusively the only added cost, but also the necessary increase in structural support will increase the overall budget cost both in initial construction and maintenance.

To reduce the risk of the fire exposure to the flare piping connection, PFP could be added, but this will cause the entire design to stray away from the concept of inherently safe design. This can be exemplified by the thought process of design; that it is necessary to add PFP to protect the flare pipeline, in order to add the PSV, which protects the vessel. To design the system inherently safe the flare piping could be produced using a material with low heat conductivity, or increasing the pipeline wall thickness. A step further would be to design a vessel with such a massive wall thickness that it would not rupture even at the very worst case scenario. Both of these possibilities could increase the cost beyond what is economical feasible. Essentially, the increase in safety risks will produce a feasible design, but this should be done while still keeping the risk as low as reasonable possible.

3 Problem statement

A pressure safety valve protects a vessel if the pressure inside the vessel rises beyond the maximum design pressure. As pointed out by API 521 [2], the pressure safety valve does not always protect the vessel in a fire scenario. This is evident when the flame affects the gas part of the vessel, where the convective heat transfer is low, meaning that the heat is not transported away from the vessel wall. API 521 even states that sometimes a vessel, exposed to a fire on the gas part of the vessel, may rupture before the PSV even lifts, i.e. before any overpressure is generated.

In order to investigate the potential problem with the application of PSVs for fire protection offshore, the phenomenon will be mapped by a detailed case study. The case study will be carried out using a commercial, state of the art software, VessFire, which is capable of simulating the response of a pressure vessel during a fire exposure. Fire cases for different process equipment will be investigated. The vessel will be exposed to a fire on both the liquid and the gas part of the vessel, in order to determine when a PSV can protect the vessel.

Traditionally when a fire PSV is sized the stationary sizing procedure in API 520 [12] is used. API 521 [2] highlights that conventional methods for calculating the relief rates are generally conservative and can lead to overly sized pressure safety valves. This can be due to, underestimation of the latent heat of vaporisation of the liquid inventory. As an alternative, a dynamic calculation can be performed, in order to determine the relief rate of the pressure safety valve. A dynamic model for the sizing of pressure safety valves is developed, and the dynamic results are compared to the stationary sizing results.

The dynamic sizing model is developed in Excel Visual Basic for Applications (VBA), and is based on a thermodynamic module developed by Rambøll. The model should be able to describe the heat transfer to a pressure vessel during a fire emergency, and predict the pressure and temperature conditions in the vessel. The purpose of the dynamic model is:

- 1) To investigate the difference between a traditional steady-state PSV sizing and a rigorous dynamic PSV sizing.
- 2) To make a simple and practical alternative to an expensive commercial software, for PSV sizing.

Initially, a case study of the effectiveness of a PSV is carried out and subsequently a model is described, in order to determine the size of a PSV using a dynamic model.

4 Case study on the effectiveness of a pressure safety valve

A case study is performed in order to investigate for which circumstances a fire PSV provides an adequate safety benefit, on offshore process equipment. The case study is conducted for various fire scenarios for pressure vessels in offshore installations, using VessFire as the simulation tool. The simulations are done with and without a PSV, in order to see if the PSV provides an additional benefit, in terms of a prolonged rupture time of the vessel.

The rupture time is defined as the time, at which rupture occurs. Rupture is defined to occur when the calculated von Mises stress is above the UTS of the vessel wall material. The von Mises stress is proportional to the vessel pressure, and the UTS is a function of wall temperature. It is assumed that rupture is acceptable if the rupture time exceeds 60 min, as all personnel can be evacuated from the process platform in the time period.

The fire scenarios investigated are the standard small jet fire, large jet fire, and pool fire, as defined by the Scandpower guidelines [6]. The three fire scenarios are affecting the wetted as well as the unwetted part of the vessel. The intensity of the fire scenario are described in table 2.1 page 10.

The process equipment used in the simulations are a 1st stage separator, 2nd stage separator, 3rd stage separator, test separator, Intermediate Pressure (IP) suction drum, and Natural Gas Liquid Knock-Out drum (NGL KO drum). The case study is also done for a pressure vessel containing a mixture of propane and n-butane, in order to investigate the effect of a different inventory composition. The dimensions and properties of the pressure vessel can be seen in table 4.1.

The composition of the hydrocarbon inventory can be seen in table B.1 in appendix B. The PSV size is found by sizing the PSV according to API 521 as described in subsection 2.4.1 on page 22. The PSV size is described by a letter, ranging from D to T. The corresponding orifice area of the PSV can be seen in table C.1 in appendix C. The orientation of the vessel is either horizontal (H) or vertical (V). The vessel material is carbon steel with an UTS of 441 MPa, including a 10% safety margin.

VessFire is a tool used to study depressurization scenarios in a process vessel, and can be used to simulate a pressure vessels response to a fire scenario. VessFire solves thermodynamic properties of the inventory, heat transfer, and stress calculations, in a transient model, in order to predict, among others, temperature, pressure and rupture of the pressure vessel.

	Pressure	Temperature	Outer diameter	Length	Wall thickness	Liquid level	Water level	Orientation	PSV size
	[Bara]	[°C]	[m]	[m]	[mm]	[m]	[m]	-	-
1st stage separator	30.0	80	3.058	10.7	32	1.90	1.05	H	K
2nd stage separator	12.0	80	2.632	10.4	32	1.55	0.38	H	L
3rd stage separator	5.0	75	2.532	9.0	16	1.00	0.00	H	K
Test separator	30.0	80	2.150	6.8	25	1.23	0.45	H	J
IP suction drum	32.2	40	1.880	3.5	40	0.95	0.00	V	G
NGL KO drum	62.0	51	1.800	3.1	50	0.77	0.00	V	F
Butane vessel	8.0	40	2.532	9.0	16	1.25	0.00	H	K

Table 4.1: Input data for the vessels used in the case study.

Several cases have been done in the case study. In order to ease the work regarding the input data to VessFire, a code has been developed to easily set up several VessFire cases, and create the VessFire case files needed to run a batch of cases. The code is named CasePlanner and is explained in appendix D. In a similarly fashion, a code named Grapher has been developed in order to easily plot data from VessFire, instead of having to manually plot one case at a time. Grapher is also explained in appendix D.

4.1 Example of VessFire output

An example of the output plots from VessFire is shown in figure 4.1, 4.2, 4.3, and 4.4. The case is for a large jet fire impinging on the gas part of the 1st stage separator.

Figure 4.1 shows a plot of the pressure development as a function of time, together with a plot of the maximum wall temperature. On the pressure plot, it can be seen how the pressure starts at 30 bara, and increases as the vessel is heated. When the pressure reaches 36 bara, the pressure is released through the PSV, and the pressure decreases. Several of these cycles are shown in the plot. The maximum wall temperature starts at its initial condition of 80 °C and rises towards 900 °C, as the peak heat load of the large jet fire affects the wall.

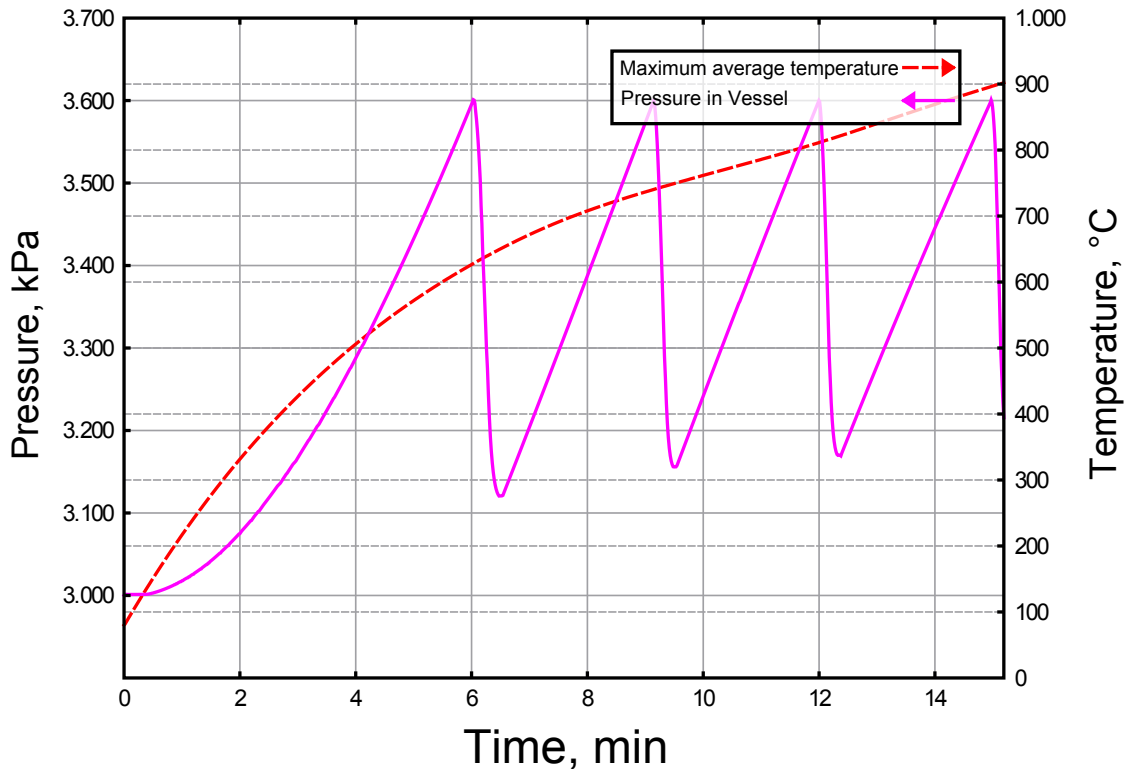


Figure 4.1: VessFire output graph. On the left: Pressure in the vessel as a function of time. On the right: Maximum wall temperature as a function of time.

Figure 4.2 shows a plot of the stresses in the system. Similar to figure 4.1 the maximum wall temperature is also shown. The UTS of carbon steel is temperature dependent, and the plot shows how the UTS decreases when the temperature increases. The maximum longitudinal stress is shown, which together with the circumferential stress is used to calculate the equivalent von Mises stress. Rupture

of the vessel occurs when the UTS intersects with the von Mises stress, as indicated on figure 4.2. The von Mises stress is dependent on the pressure, and it can be seen by comparing figure 4.1 and figure 4.2, that the von Mises stress and pressure follow the same trend. This means, that by reducing the pressure in the vessel, it is possible to limit the von Mises stress and extend the rupture time (assuming that the UTS is decreasing).

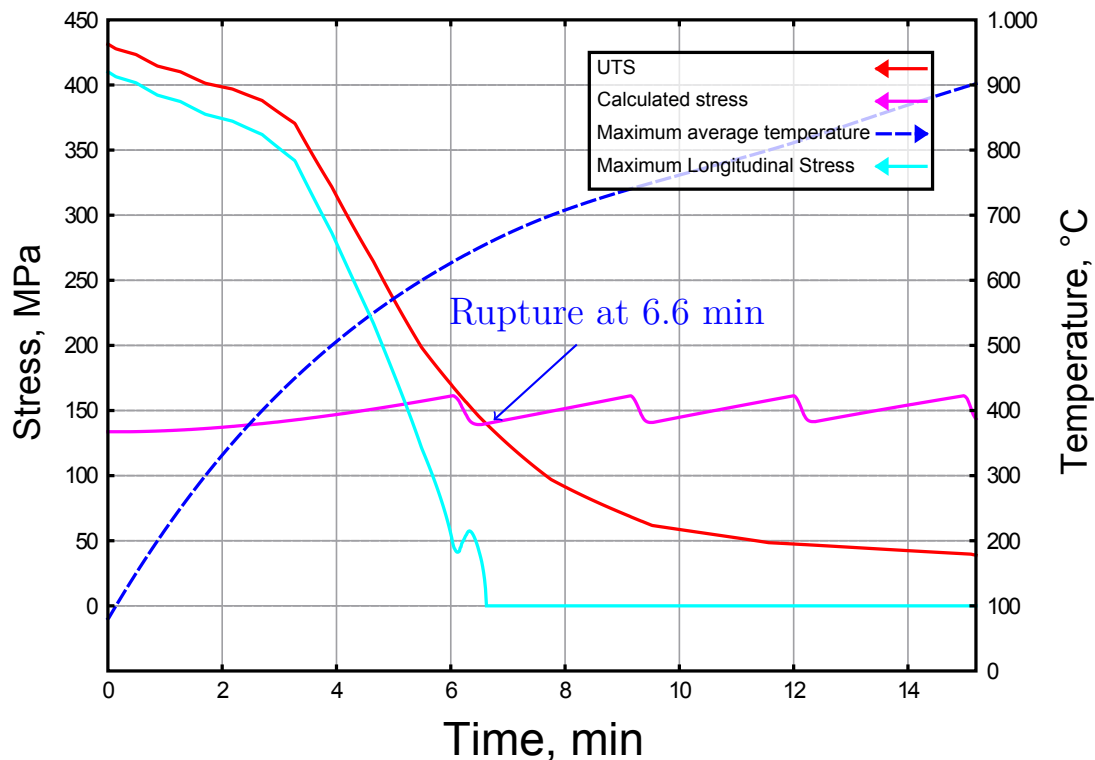


Figure 4.2: VessFire output graph. On the left: UTS, longitudinal, and von Mises stress (calculated stress) of the vessel as a function of time. On the right: Maximum wall temperature as a function of time.

Figure 4.3 shows the fluid temperatures of the vessel. The temperature of the liquid and gas is shown as a function of time. It can be seen that the two phases has different temperatures. The liquid phase has the lowest temperature and rises steadily as the vessel is heated. The gas temperature rises more quickly and is also affected by the opening of the PSV. When the PSV is opened and evacuates the vessel content through the valve, the temperature decreases due to the Joule-Thomson effect.

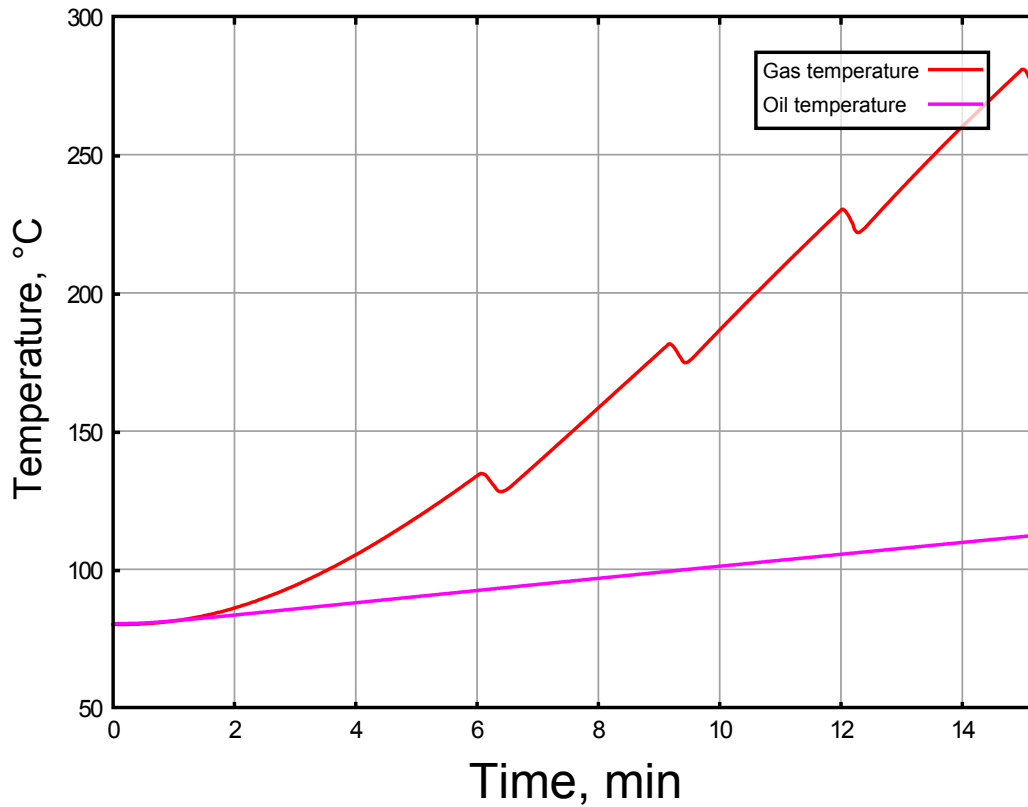


Figure 4.3: VessFire output graph. Fluid temperature of the vessel inventory. The figure shows the gas and liquid (oil) temperatures.

Figure 4.4 shows the PSV release rate as a function of time. It can be seen how the pop-action PSV opens and closes abruptly.

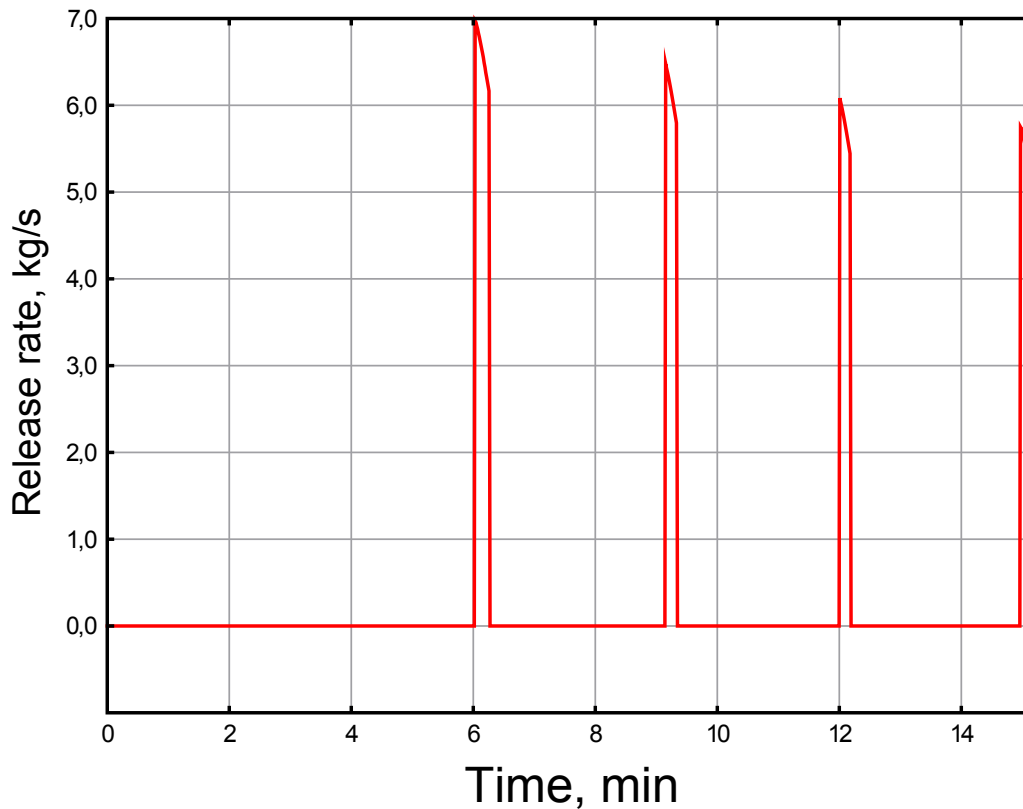


Figure 4.4: VessFire output graph. PSV release rate as a function of time.

4.2 Influence of a PSV on the rupture time for various pressure vessels

The rupture time for various vessels has been found, and the results are shown in the following section.

The 1st stage separator will be explained in details and the other plots will be compared to the 1st stage separator and explained if they differ significantly from the general trend.

Figure 4.5 shows the rupture time of the 1st stage separator exposed to various fire scenarios. A rupture time of 60 min indicates that there is no rupture within the 60 min time limit.

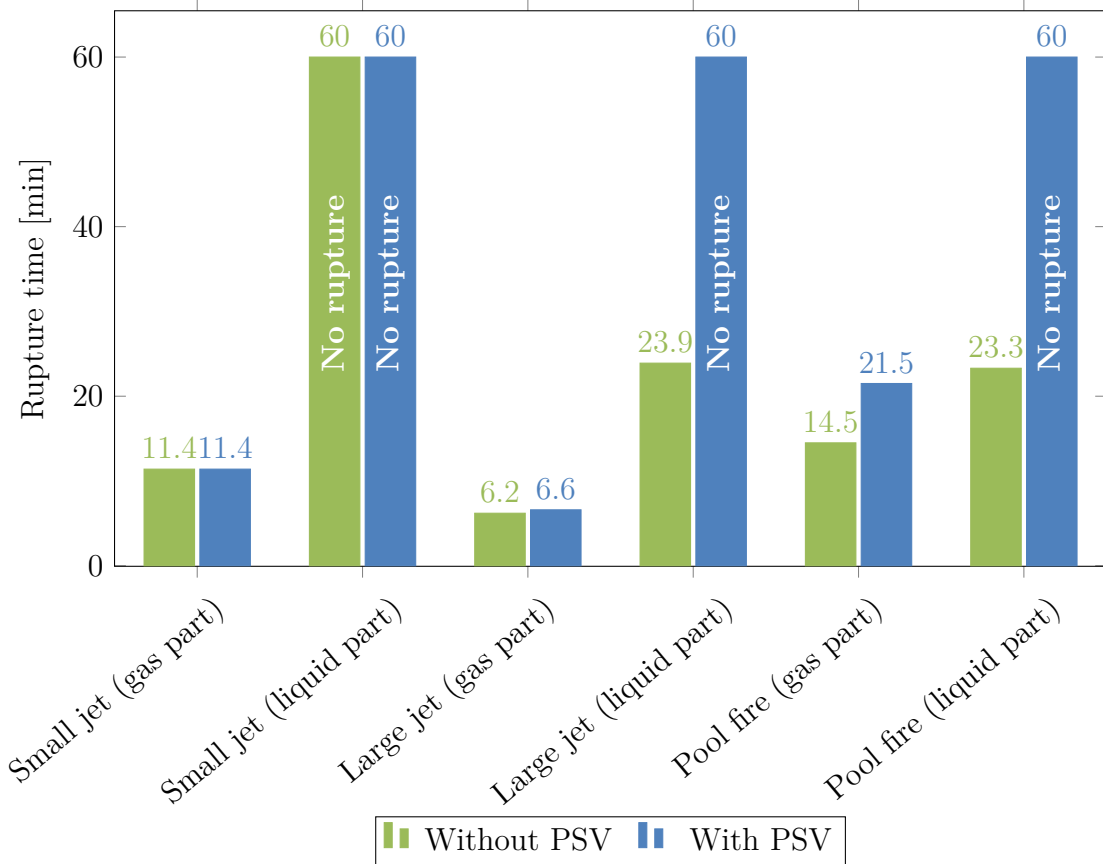


Figure 4.5: Rupture time for the 1st stage separator, with and without a PSV, when exposed to various fire scenarios.

The first bar set on the left shows the rupture time for the 1st stage separator when it is exposed to a small jet fire on the gas part of the vessel. The green bar indicates that rupture time for the vessel without a PSV, and the blue bar indicates the rupture time with a PSV. It can be seen that the PSV does not influence the rupture time. By analysing the VessFire results, it is evident that the peak heat load of the small jet fire is not large enough to influence the inventory of the vessel and cause a pressure increase. In fact, as the vessel temperature is higher than the ambient temperature, the vessel is cooled by natural convection from the ambient air, and the pressure slowly decreases as the temperature decreases. At the same time, the peak heat load affects a local part of the wall, causing a temperature increase, as the convective heat transfer of the gas is not large enough to transport adequate heat away from the wall. This causes the UTS to drop below the von Mises stress, which leads to a rupture after 11.4 min.

The second bar set from the left shows the rupture time for the 1st stage separator when it is exposed to a small jet fire on the liquid part of the vessel. Similarly to the scenario where the flame hits the gas part of the vessel, the pressure does not

increase, and in fact, it decreases a little bit because of a decrease in temperature. The difference in this scenario, is that the flame affects the liquid part of the vessel. The liquid has a high heat transfer coefficient which removes the heat from the wall, keeping the wall relatively cool. The heat from the peak heat load is transferred from the wall to the liquid, and the liquid is then cooled by the ambient conditions, which affects a larger area of the vessel. The vessel enters a state of heat transfer equilibrium, and would therefore be able to withstand this fire exposure indefinitely. It should be noted that the PSV does not have any significance on the outcome of the result.

The third bar set from the left shows the rupture time for the 1st stage separator when it is exposed to a large jet fire on the gas part of the vessel. The green bar indicate a rupture time of 6.2 min, when the vessel is not equipped with a PSV. Similarly to the case where the small jet fire affects the gas part of the vessel, the large jet fire also increase the wall temperature, but as the peak heat load is greater for the large jet fire, the temperature increase occurs more rapidly. The large jet fire also has a background heat load that affects the inventory of the vessel causing the pressure to build up. The combined effect of the faster temperature increase and the pressure build up, means that the UTS and von Mises stress intersects sooner, effectively leading to a shorter rupture time. The blue bar indicate the rupture time when the vessel is equipped with a PSV. This is the VessFire example shown in figure 4.1, 4.2, 4.3, and 4.4. The background heat load of the large jet fire increases the pressure just enough so that the PSV opens just as the UTS and von Mises stress is about to intersect, as shown in figure 4.2. This extends the rupture time with a few seconds, but the peak heat load of the large jet fire is still so large that UTS becomes lower than the von Mises stress leading to a rupture at 6.6 min. A correctly sized PSV is therefore not sufficient to protect the vessel against rupture for a large jet fire on the gas part.

The fourth bar set from the left shows the rupture time for the 1st stage separator when it is exposed to a large jet fire on the liquid part of the vessel. The green bar indicates a rupture time of 23.9 min when a PSV is not equipped. The convective heat transfer of the liquid is high enough to limit the decrease in UTS by the peak heat load, but the background heat load causes the pressure to increase rapidly, causing the von Mises stress to increase and intersect with the UTS. The blue bar indicate that no rupture occurs when a PSV is equipped. In this case, the PSV relieve the pressure from the vessel, and prevents rupture of the vessel. Consequently when a large jet fire affects the liquid part of the pressure vessel, a PSV will prevent a rupture by keeping the pressure below a set limit.

The fifth bar set from the left shows the rupture time for the 1st stage separator when it is exposed to a pool fire on the gas part of the vessel. The green bar indicate a rupture time of 14.5 min when a PSV is not equipped. The rupture time is extended to 21.5 min when a PSV is equipped. This is similar to when the large jet fire affects the gas part, where the peak heat load lowers the UTS of

the wall, and the background heat load increases the pressure of the vessel. The PSV in these cases limits the pressure increase, until the UTS becomes lower than the von Mises stress and rupture occurs. In the case of a pool fire, the PSV has a larger effect on rupture time, than for a large jet fire, as the peak heat load is less, and the UTS therefore decreases more slowly.

The sixth bar set from the left shows the rupture time for the 1st stage separator when it is exposed to a pool fire on the liquid part of the vessel. This case is similar to the case of a large jet fire affecting the liquid part of the vessel, and the only difference is the peak heat load of the flame. In both cases, the vessel will rupture due to a pressure increase if a PSV is not equipped, with rupture times of 23.3 min and 23.9 min respectively. The slight difference in rupture time is due to different peak heat loads for a pool fire and a large jet fire. If a PSV is equipped, then there will be no rupture.

Figure 4.6, 4.7, and 4.8 shows the rupture time of the 2nd stage separator, 3rd stage separator, and test separator exposed to various fire scenarios.

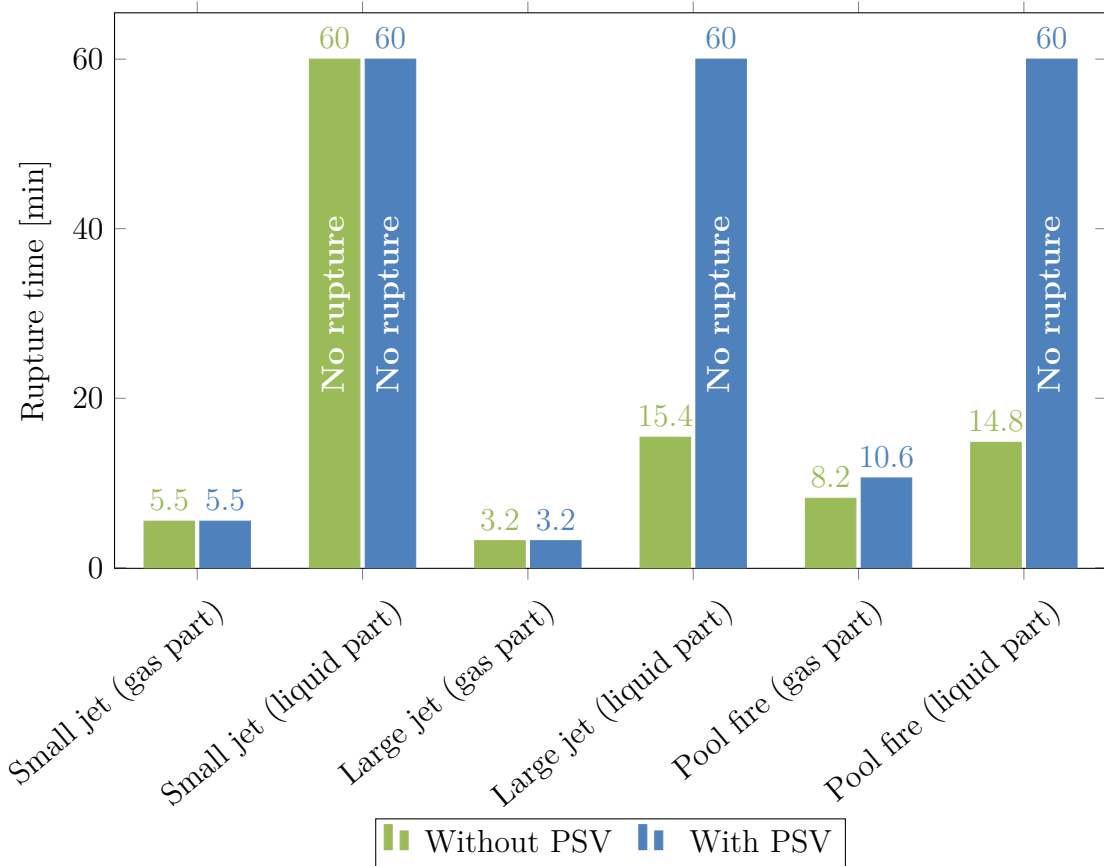


Figure 4.6: Rupture time for the 2nd stage separator, with and without a PSV, when exposed to various fire scenarios.

The general trend for the 2nd stage separator, 3rd stage separator, and test separator is similar to that of the 1st stage separator shown in figure 4.5. The vessels rupture when exposed to a small jet on the gas part, a large jet on the gas part, a large jet on the liquid part without a PSV, a pool fire on the gas part, and a pool fire on the liquid part without a PSV. There is no rupture when the vessels are exposed to a small jet on the liquid part, a large jet on the liquid part with a PSV, and a pool fire on the liquid part with a PSV. The difference between the 1st stage separator and the other separators is time until rupture. The three other separators have shorter rupture times than the 1st stage separator, which is due to a combination of thinner vessel walls and a difference in exerted pressure. These factors affect the UTS of the vessel walls and the von Mises stress, respectively.

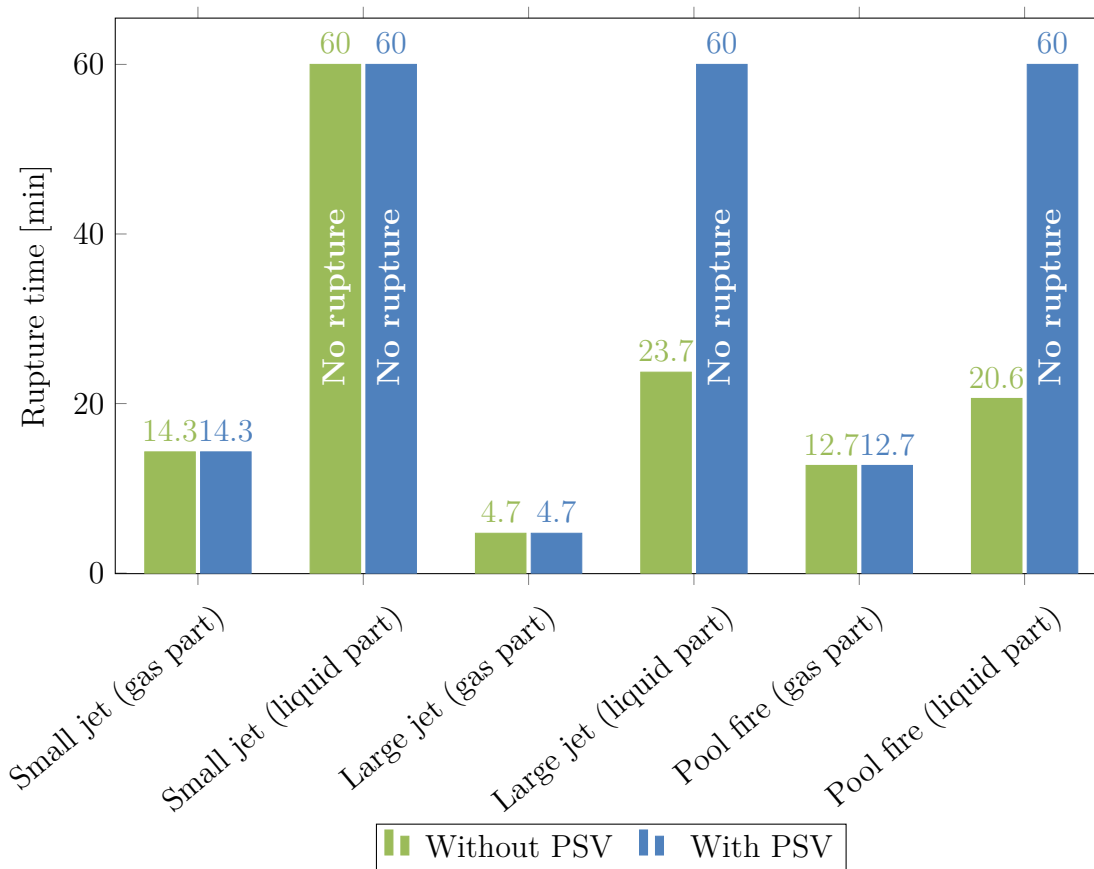


Figure 4.7: Rupture time for the 3rd stage separator, with and without a PSV, when exposed to various fire scenarios.

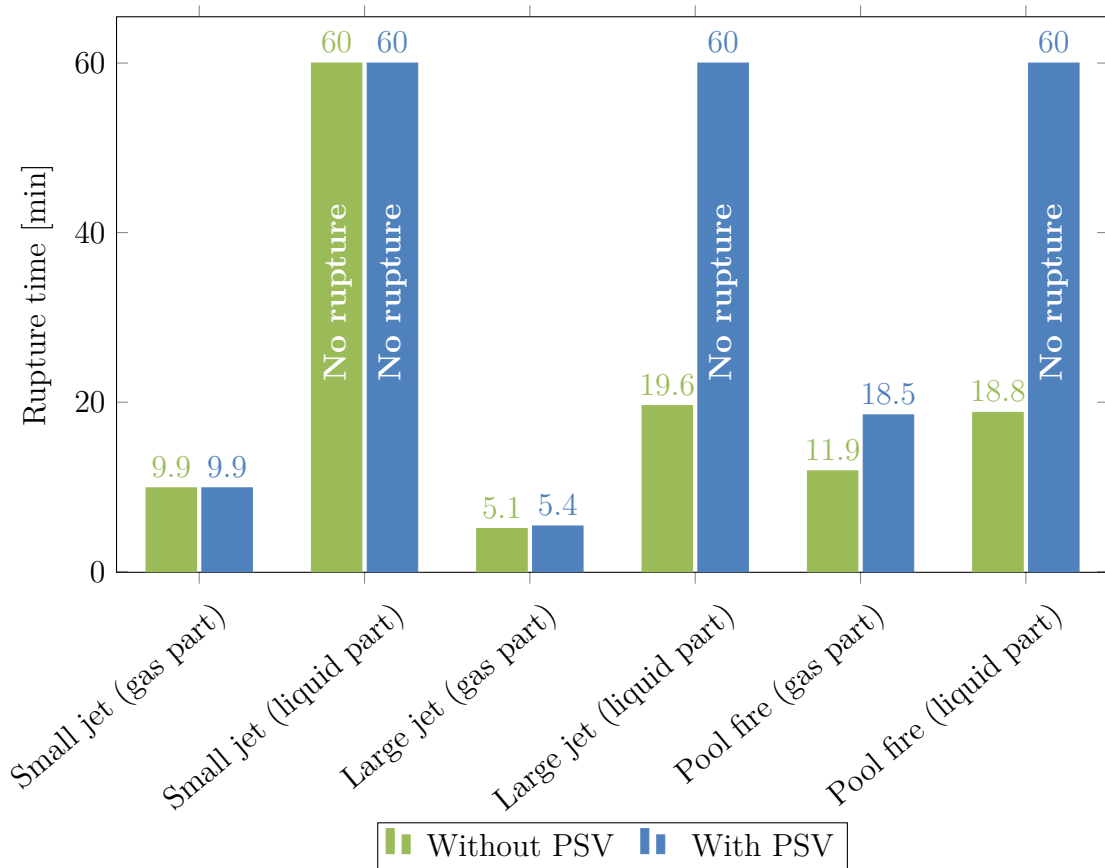


Figure 4.8: Rupture time for the test separator, with and without a PSV, when exposed to various fire scenarios.

Figure 4.9 shows the rupture time of the IP suction drum, exposed to various fire scenarios. The PSV does not affect the rupture time when a small jet fire is on the gas part, and the vessel ruptures after 30.4 min, which is similar to the previous cases. The case of a small jet fire on the liquid part, is also similar to the previous cases presented. The PSV has a small effect in the case of the large jet fire on the gas part. The PSV manages to open a couple of times before rupture occurs, but the extended period is not significant. For the large jet fire on the liquid part, the vessel ruptures when a PSV is not equipped, since the pressure increases until the von Mises stress becomes too large. When a PSV is equipped, the PSV limits the pressure in the vessel, but eventually, the background heat load vaporizes the liquid and the vessel boils dry. This means that the large jet fire can now heat up the vessel wall, which lowers the UTS and leads to rupture at 42.3 min. A pool fire on the gas part of the vessel without a PSV will cause a rupture after 23.4 min. When a PSV is equipped for the same fire scenario, the PSV is able to limit the pressure increase and thus keep the von Mises stress from increasing. The peak heat load is not large enough to weaken the vessel UTS sufficiently to cause a rupture, even though the vessel boils dry after 33 min. This is also the

case for the pool fire when it is affecting the liquid part of the vessel.

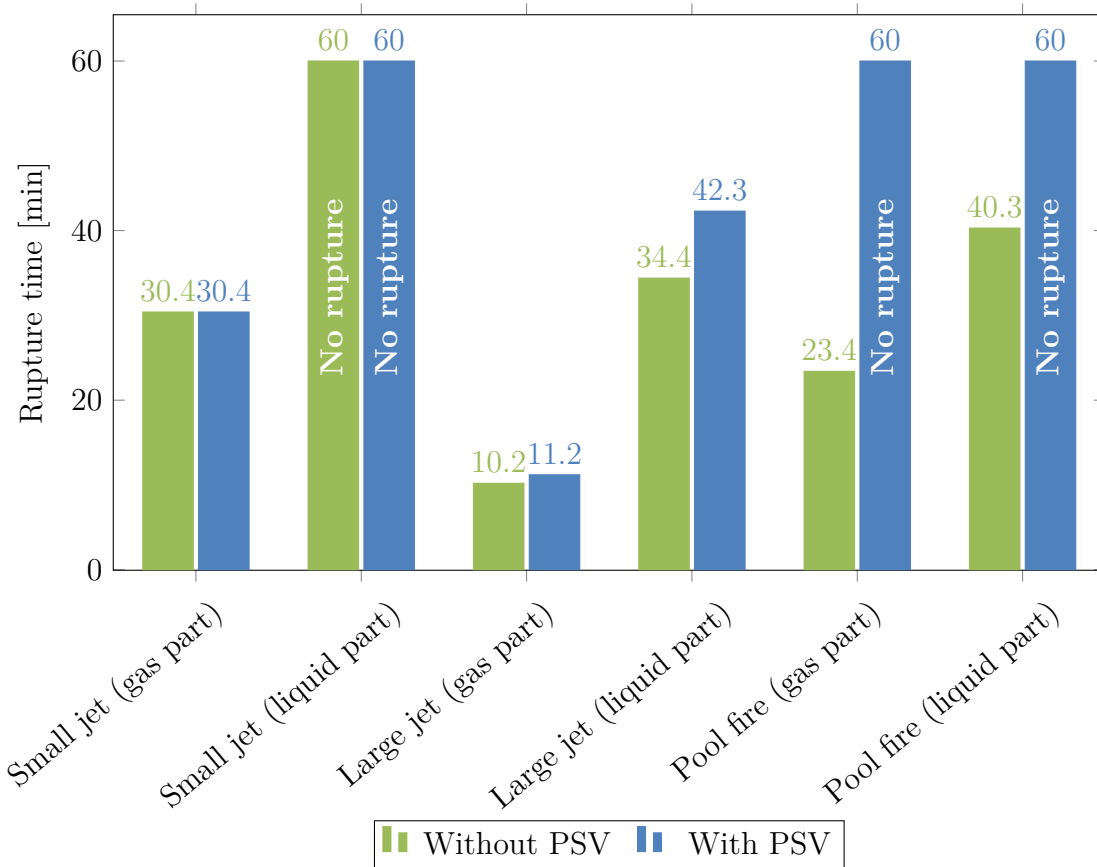


Figure 4.9: Rupture time for the IP suction drum, with and without a PSV, when exposed to various fire scenarios.

Figure 4.10 shows the rupture time of the NGL KO drum exposed to various fire scenarios. The NGL KO drum is at this temperature and pressure completely gas filled, and contains no liquid. This means that the rupture times for the flames affecting the gas part and liquid part will be identical. The small jet fire increases the wall temperature of the vessel, and produces a rupture time of 50.7 min. The PSV has no effect on the outcome. This is the same case for the large jet fire, though with a lower rupture time of 12.4 min. The PSV does have an effect on the pool fire case. The PSV limits the pressure in the vessel for a while and increases the rupture time from 28.9 min to 39.7 min.

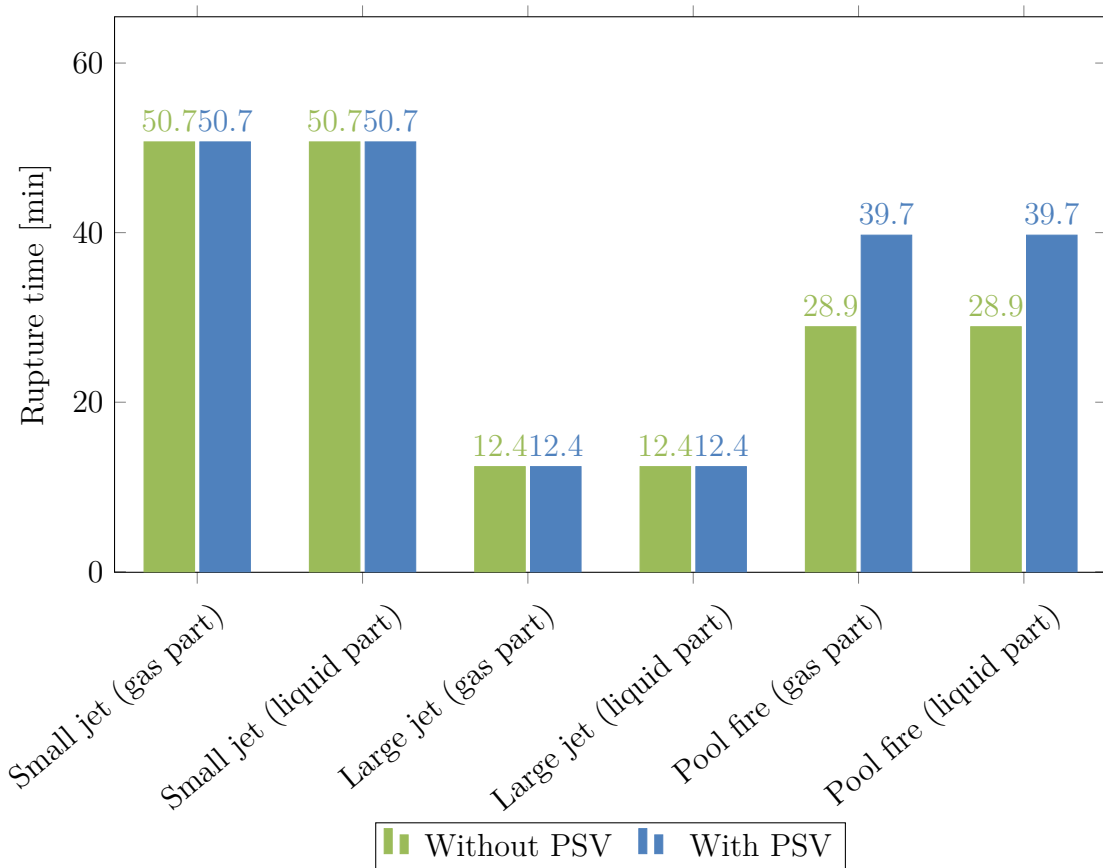


Figure 4.10: Rupture time for the NGL KO drum, with and without a PSV, when exposed to various fire scenarios.

Figure 4.11 shows the rupture of the propane/n-butane tank exposed to various fire scenarios. The case resembles that of the 1st stage separator, but with a few differences, due to the different fluid composition. In the case of the large jet fire hitting the liquid part of the vessel, for which a PSV is equipped, the background heat load causes the liquid to boil off at around 30 min, and the vessel ruptures shortly after at 34 min. This is the same case for the pool fire affecting the liquid part. In general, the PSV seems to be under-sized in the case of the propane/n-butane tank. A properly sized PSV would not affect the results of rupture time much for the case of the propane/n-butane tank. The cases where it would possibly affect the results are for the large jet fire and pool fire affecting the liquid part. In these cases, the tank boils dry and ruptures, which a larger PSV would not be able to prevent. The sizing of the PSV is investigated in section 5.3 page 91.

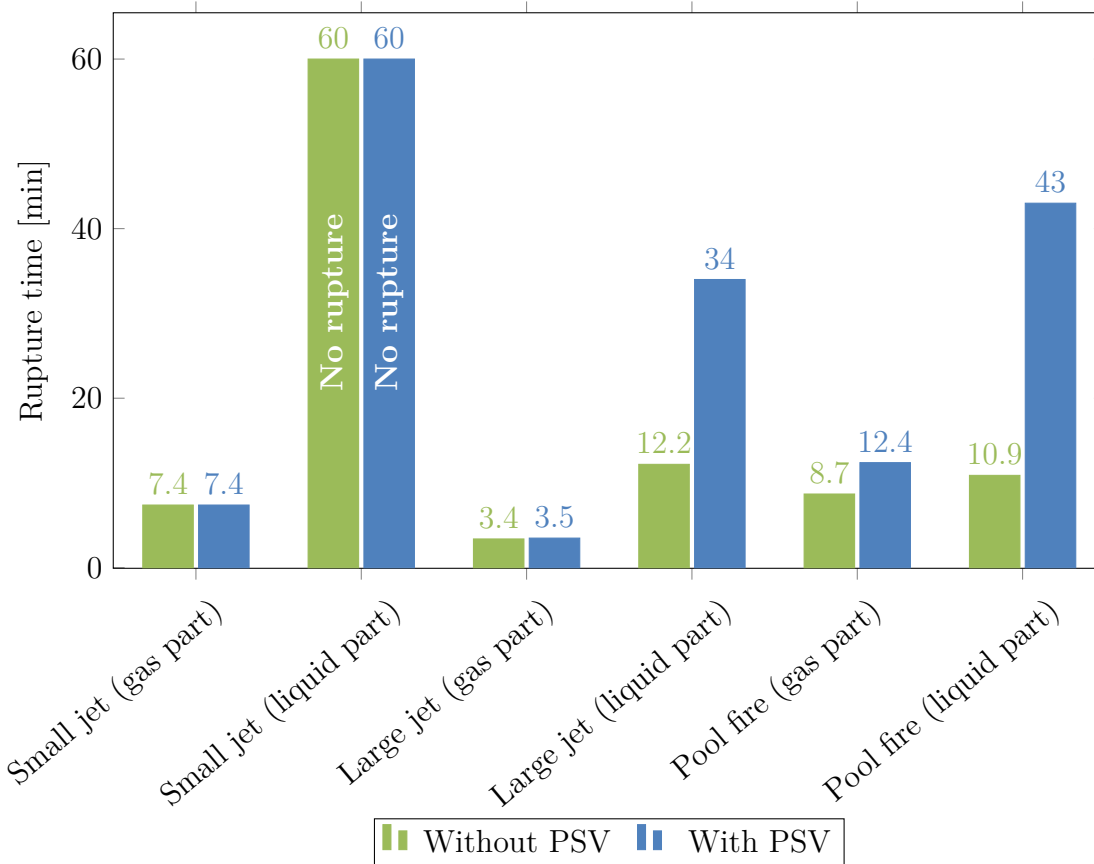


Figure 4.11: Rupture time for the propane/n-butane tank, with and without a PSV, when exposed to various fire scenarios.

4.2.1 Peak heat load and wall thickness

The initial investigation of the separator vessels shows that a peak heat load has an effect on the rupture time, when the flame affects the gas part of the vessel. This is the case for both the small jet fire, large jet fire, and the pool fire. A study is done to investigate what influence the wall thickness and the peak heat load has on the rupture time of a vessel. The 1st stage separator is used as the vessel for the study. The wall thickness of the separator is varied from 10 mm to 50 mm, and the peak heat load to the gas part of the vessel is varied from 0 kW/m² to 500 kW/m². A peak heat load with a value of 500 kW/m² is larger than that of a large jet fire, and is only investigated in order to analyse the trend of increasing peak heat load. There is no background heat load in the simulations. Figure 4.12 shows the rupture time of the 1st stage separator, as a function of different peak heat loads on the gas part of the vessel. It can be seen that the rupture time for each wall thickness approaches a peak heat load value, for which there is no rupture within the 60 min limit. It is also clear that a thicker wall produces a longer rupture time than a thin wall. This is especially relevant at smaller peak

heat loads, and becomes less relevant at higher values.

The effectiveness of increasing the wall thickness to avoid rupture would be limited in the case of a large jet fire with a peak heat load of 350 kW/m^2 . The rupture time is extended by 10-15 min by increasing the wall thickness from 20 mm to 50 mm. This is the same case for a small jet fire with a peak heat load of 250 kW/m^2 . Here, the rupture time would be extended by 20-25 min by increasing the wall thickness from 20 mm to 50 mm. A pool fire has peak heat load of 150 kW/m^2 . In this range it would be possible to extend the rupture time significantly by applying a thicker wall.

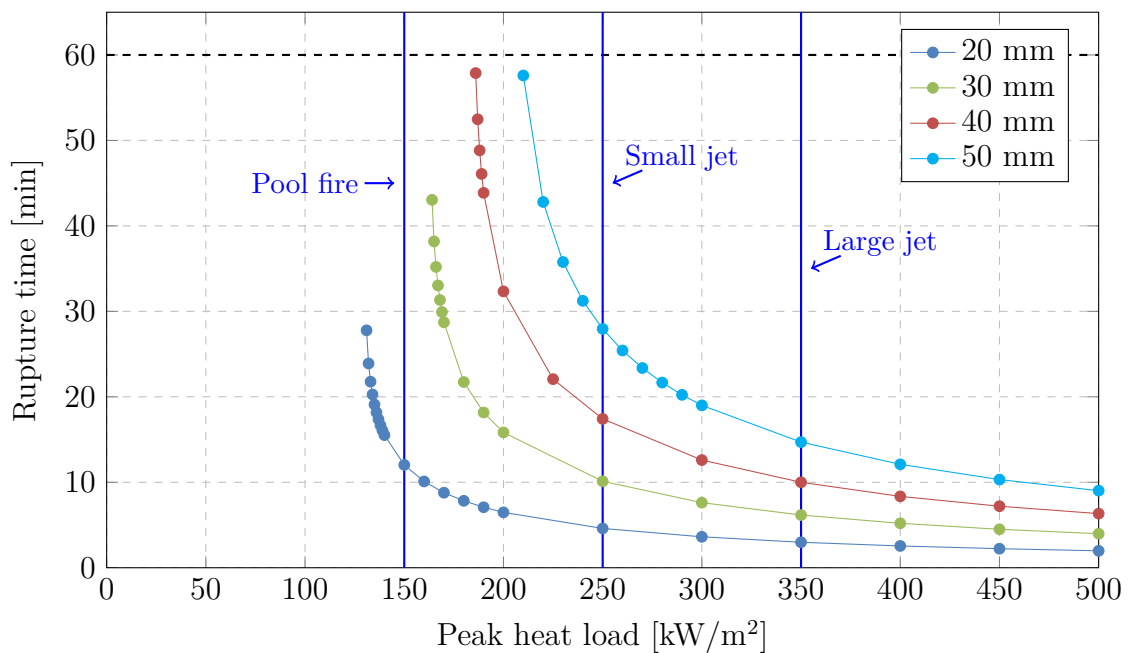


Figure 4.12: Rupture time as a function of peak heat load, to the gas part of a vessel, for 4 different wall thicknesses.

4.2.2 Effect of insulation on rupture time

A study is done in order to determine the effect of PFP on rupture time. A case is done for the 1st stage separator which is insulated with rock wool. Simulations are done for the 1st stage separator with an insulation layer of 50 mm, 100 mm, and 200 mm. The simulations are done for a small jet fire, a large jet fire, and a pool fire on the gas part of the vessel, and also with and without a PSV.

Figure 4.13 shows the rupture time for the 1st stage separator when insulated. The rupture times for the 1st stage separator when not insulated can be seen in figure 4.5. The small jet fire causes a rupture within 11.4 min when the vessel is not insulated. This is for both with and without a PSV. All three insulation levels

prevent a rupture for the small jet fire.

The rupture time for a large jet fire is 6.2 min without a PSV, and 6.6 min with a PSV. An insulation thickness of 50 mm can extend the rupture time to 37 min in both cases, and an insulation thickness of 100 mm can extend the rupture time to 58 min in both cases. The insulation level of 200 mm can prevent a rupture from a large jet fire.

The rupture time for a pool fire is 14.5 min without a PSV and 21.5 min with a PSV. All three insulations levels can prevent the vessel from rupture.

The insulation prevents rupture in the case of a small jet fire or a pool fire. The insulation is able to delay the rupture for a large jet fire.

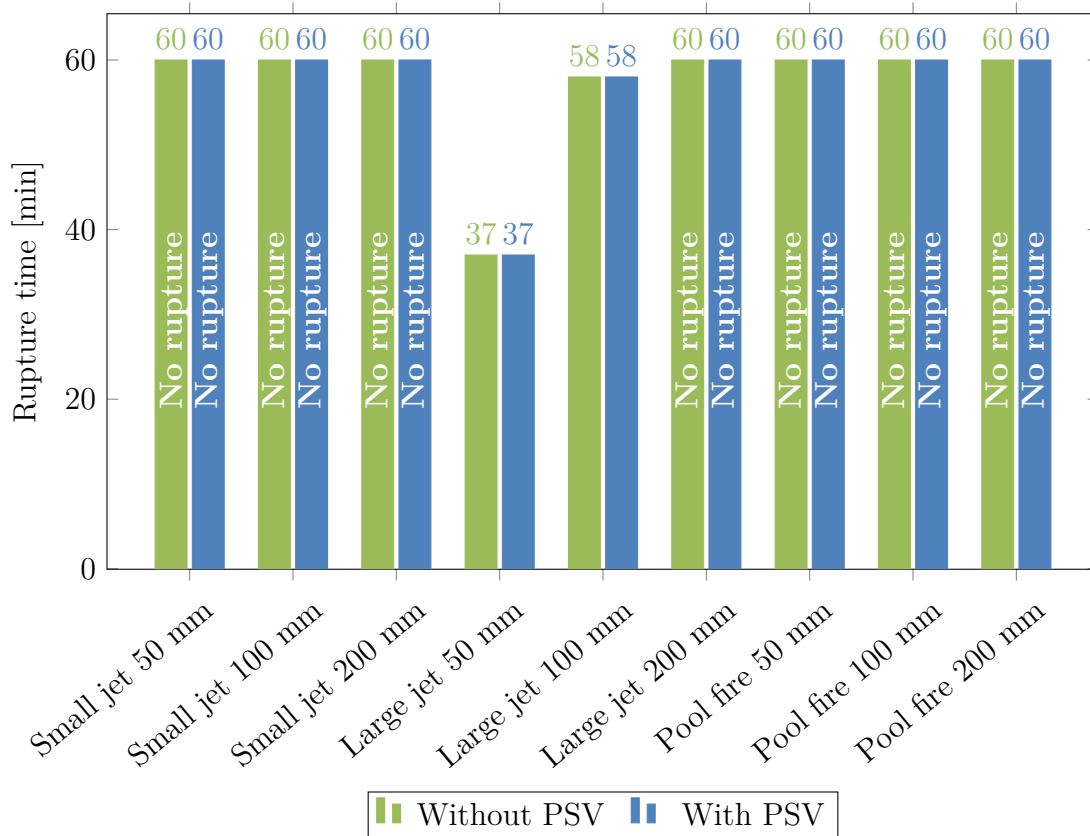


Figure 4.13: Rupture time for the 1st stage separator, with and without a PSV, when exposed to various fire scenarios on the gas part and insulated with rock wool.

4.2.3 Rupture time for blowdown cases

A blowdown valve can be used as an alternative to a PSV to protect a vessel. A case study is done, in which the 1st stage separator is affected with different fire

scenarios and a BDV is used to lower the pressure of the vessel. The BDV has a orifice diameter of 35 mm and is open from the start of the simulation. Figure 4.14 shows the rupture time and blowdown time of the 1st stage separator. The blowdown time is when the pressure reaches 50% of the initial pressure. The initial pressure of the 1st stage separator is 30 bara, and the blowdown requirement is therefore 15 bara. Blowdown was able to avoid rupture for all the cases except for the large jet fire on the gas part. Blowdown lowers the pressure of the vessel and thereby also the von Mises stress. This makes it possible for the UTS to decrease considerably before intersecting with the von Mises stress. Only the large jet fire has a high enough peak load to cause the UTS to decrease enough and cause a rupture.

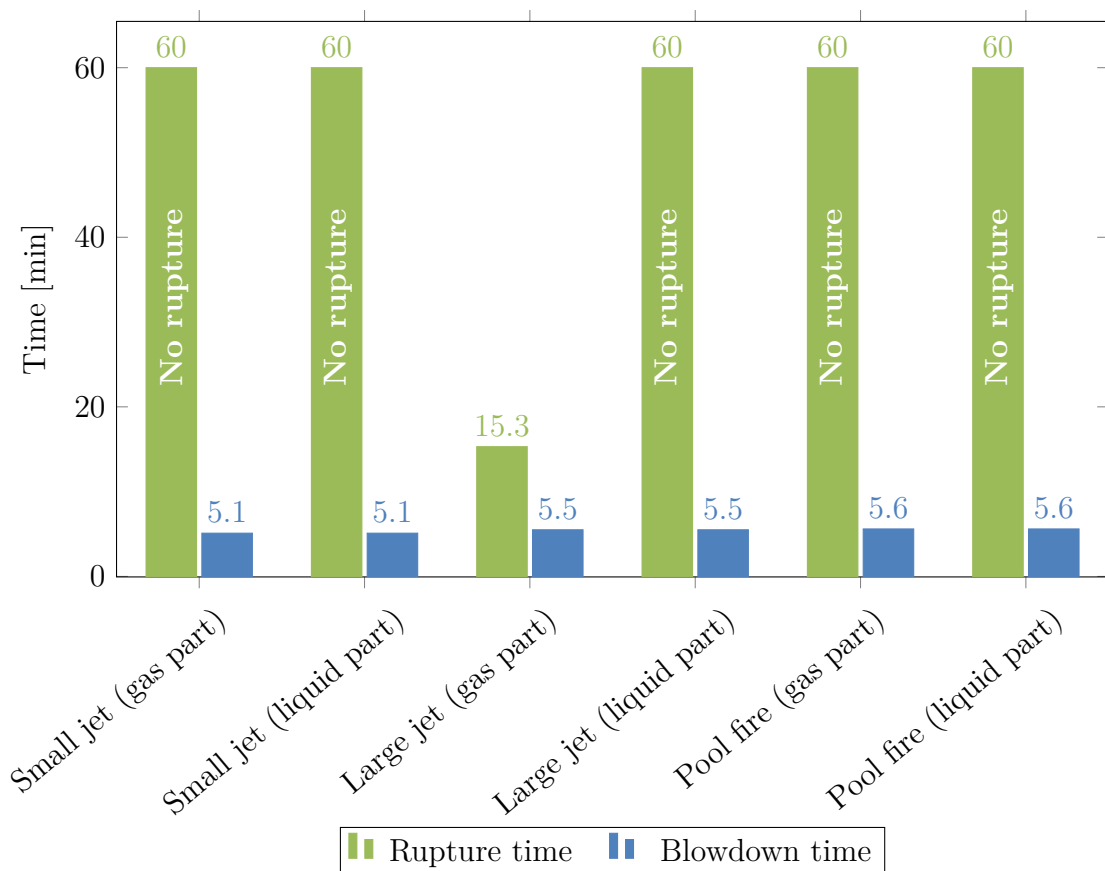


Figure 4.14: Rupture time and blowdown time for a 35 mm BDV, at different fire types.

4.3 Comparison of case study results

The results from the case study show that when a vessel is affected by a fire on the liquid part of the vessel, the PSV is able to relieve the pressure, as long the the vessel contains liquid. The convective heat transfer coefficient of the liquid

is high enough to limit the wall temperature and therefore prevent rupture. The PSV is not able to prevent rupture, when the fire affects the gas part of the vessel. The peak heat load causes a local temperature increase, which causes the UTS to decrease rapidly, which leads to rupture of the vessel.

The thickness of the wall determines how long the vessel can be exposed to a peak heat load before it ruptures. It is possible to extend the rupture time by increasing the wall thickness of a vessel, when the vessel is exposed to low peak heat loads.

Blowdown was able to prevent rupture of the 1st stage separator in all but one case, which was for the large jet fire affecting the unwetted part of the vessel. This shows that in a majority of the fire scenarios, blowdown can be an effective way of depressurizing the vessel, in order to prevent rupture.

Similarly, PFP was able prevent rupture for all fire scenarios, except for a large jet fire affecting the unwetted part of the vessel. This indicates that PFP can be a way to avoid rupture in a majority of the fire scenarios.

When a large jet fire affects the unwetted part of the 1st stage separator, both a PSV, a BDV, and PFP was unable to protect the tank from rupture within a 60 min limit. The rupture times indicate that a PSV offers very little additional protection compared with a vessel which does not have any protection. A blowdown process does not prevent rupture, but it does extend the rupture time, which means when the large jet fire causes a rupture, the pressure of the vessel will be lower than that of a PSV, and any rupture will subsequently be less catastrophic. PFP is able to significantly extend the rupture time, and by applying a thick enough layer of insulation, it is possible to avoid rupture within the 60 min limit.

API 521 [2] highlights that a high momentum jet fire is able to erode the insulation material and degrade the quality of the insulation. This is not part of the simulations in VessFire.

4.4 Variables influence on rupture time

The case study shows that the PSV does not protect the vessel from rupture when a vessel is exposed to a fire on the gas part of the vessel. However, the PSV does, in some cases, increase the rupture time and therefore offer some additional protection.

A further investigation is done, in order to clarify which variables of the vessel influences the rupture time when a PSV is installed. A fictive vessel is used, where parameters of the vessel is varied. The variables investigated are the length, pressure, diameter, liquid level, water level, peak heat load, and background heat load. The heat loads correspond to a range between a small jet fire and a large jet fire.

In order to limit the number of possible variations, the design of experiment theory is utilized, where a central composite design (CCD) is chosen. The CCD limits the number of simulations needed to observe a response from multiple variables [14]. Instead of simulating all possible combinations of the variables, the CCD utilizes a limited number of points, which are the factorial points, the axial points, and the center point. An illustration of the central composite design for three variables are given in figure 4.15.

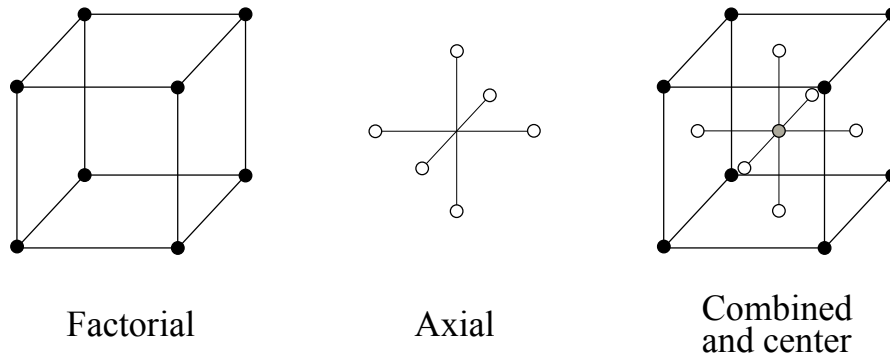


Figure 4.15: Central composite design for a three level design with three variables. The analysis is done with seven variables which results in a CCD in seven dimensions.

Each variable in the design of experiment is assigned a three level value, +1, 0, and -1. The value for the three levels for each of the seven variables are shown in table 4.2.

Variable	X1	X2	X3	X4	X5	X6	X7
	Length	Diameter	Pressure	Liquid level	Water level	Peak	Back
	[m]	[m]	[bara]	[m]	[m]	[kW/m ²]	[kW/m ²]
High (+1)	12	4	60	1.9	1	350	100
Mid (0)	9	3.25	35	1.475	0.5	300	50
Low (-1)	6	2.5	10	1.05	0	250	0

Table 4.2: Three level value range for the central composite design for all seven variables used in the analysis.

The wall thickness of the vessel is calculated for each variable combination. The wall thickness calculation is given in appendix E.

The CCD of the design of experiment results in 128 factorial points, 14 axial points and one center point, with a total of 143 simulations. The simulation plan

is shown in appendix F. The simulation plan is done twice, both with and without a PSV, in order to determine what effect a PSV has on the rupture time, which gives a total number of simulations of 286.

4.4.1 Rupture times with and without a fire PSV

Figure 4.16 shows the rupture time for a vessel with a PSV, plotted as a function of the rupture time without a PSV. Each point is a different case of the 143 cases from the simulation plan. A straight line would indicate that there is no difference in rupture. A deviation from a straight line indicates that the PSV has an effect on the rupture time. The results show that the PSV does not affect the rupture time in most of the cases. The PSV manages to extend the rupture time in a few cases, but the rupture time is only extended with a few minutes, and thus the effect of the PSV is limited.

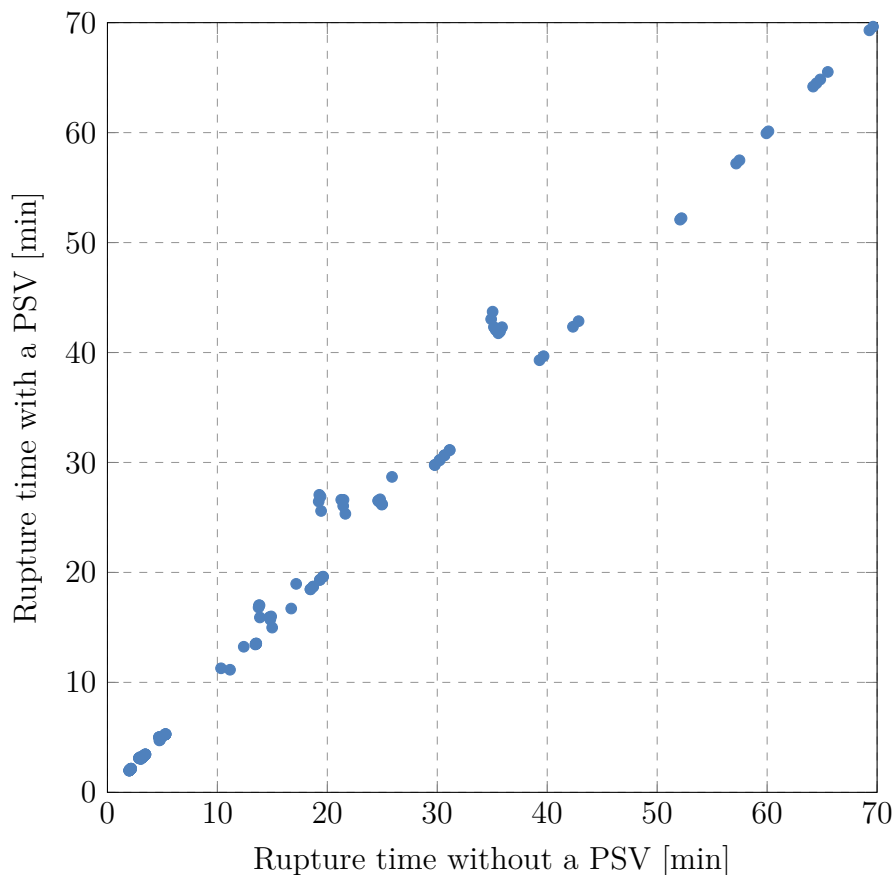


Figure 4.16: Rupture time with and without a PSV, for cases studied by design of experiment theory.

This shows that the PSV does not have a major effect on the rupture time, when

a jet fire affects the gas part of a vessel, and that the parameters of the vessel is of little importance for the outcome of this result.

5 Dynamic sizing of fire pressure safety valves

As indicated by API 521 [2], the conventional stationary sizing equations is generally conservative and would therefore oversize the PSV. As an alternative it would be advantageous to use a dynamic model, based on a detailed simulation package, capable of modeling multiple phenomena such as fluid mechanics, thermodynamics of hydrocarbon mixtures, and detailed heat transfer including radiation, convection and conduction.

A comprehensive software package, such as a CFD simulation package, would extend beyond the necessary capabilities and scope of the problem, and thus, as a compromise, a generally simpler model could suffice.

A model for this purpose is developed and described in the following section. The model will predict the heat transfer from a flame surrounding the vessel, to the vessel inventory of a gas and liquid mixture. The methods of heat transfer will be conduction, radiation, and convection. The heat transfer to the inventory will result in a change in pressure of the vessel, and temperature of the fluid. The heat transfer from the flame causes the vessel wall to increase in temperature, and thus a rupture model should be used to predict a rupture time.

For simplification, a 1-D heat transfer model in the radial direction is used for the background heat load, and a 3-D model is used for the peak heat load, which inherently has a smaller area of affect, and thus the number of control volumes is less than in the case of a full 3-D model of the entire vessel. The model is created in the Excel VBA programming language, and an excel spreadsheet is used as the user interface. The thermodynamic calculations is based on available code supplied by Rambøll, and is utilised in the general problem solving techniques.

In order to determine the effect of using a detailed dynamic model for PSV sizing, the model will be compared to the stationary sizing equations. The cases of comparison will be based on existing installations in the North Sea sector, and will thus be representative of reality.

5.1 Design of dynamic model for fire pressure safety valves

The computational algorithm for the model is described by a flowchart in figure 5.1. Each square box indicates variables to be calculation, and each rhombus indicates choices, deciding which variables to further calculate. The parallelogram indicates the initial variables defined by the user, from the Excel interface.

After initial conditions have been set and calculated, the flame temperature is

calculated. The flame temperature is kept constant throughout the calculations, and the heat load from the flame to the vessel can thus be defined as a function of time. See section 5.1.1 for further description.

The algorithm will loop through each time iteration and update all relevant variables. The heat transfer from the surroundings to the surface of the vessel will be calculated, and the heat conduction through the wall. Three separate scenarios exist, the liquid covered wall, the gas covered wall, and the wall affected by the peak heat load. See section 5.1.2, and 5.1.3.

The temperatures through the wall is calculated, and the peak temperature is used to determine whether rupture has occurred or not in the rupture model. See section 5.1.8.

The vessel wall temperature will determine the net heat transfer to the gas phase and the liquid phase. See section 5.1.5 and 5.1.5.

The added heat to each phase is used in the equilibrium calculations, indicated in figure 5.1 by "PV and TH iteration", and the mass and energy balances. PV is a pressure-volume iteration and TH is a temperature-enthalpy iteration. See section 5.1.6. The algorithm procedure for "PV and TH iteration" is illustrated in figure 5.2.

If the vessel pressure has increased above the PSV set pressure, the mass flow rate of the PSV is calculated, and further equilibrium calculations are performed. See section 5.1.7.

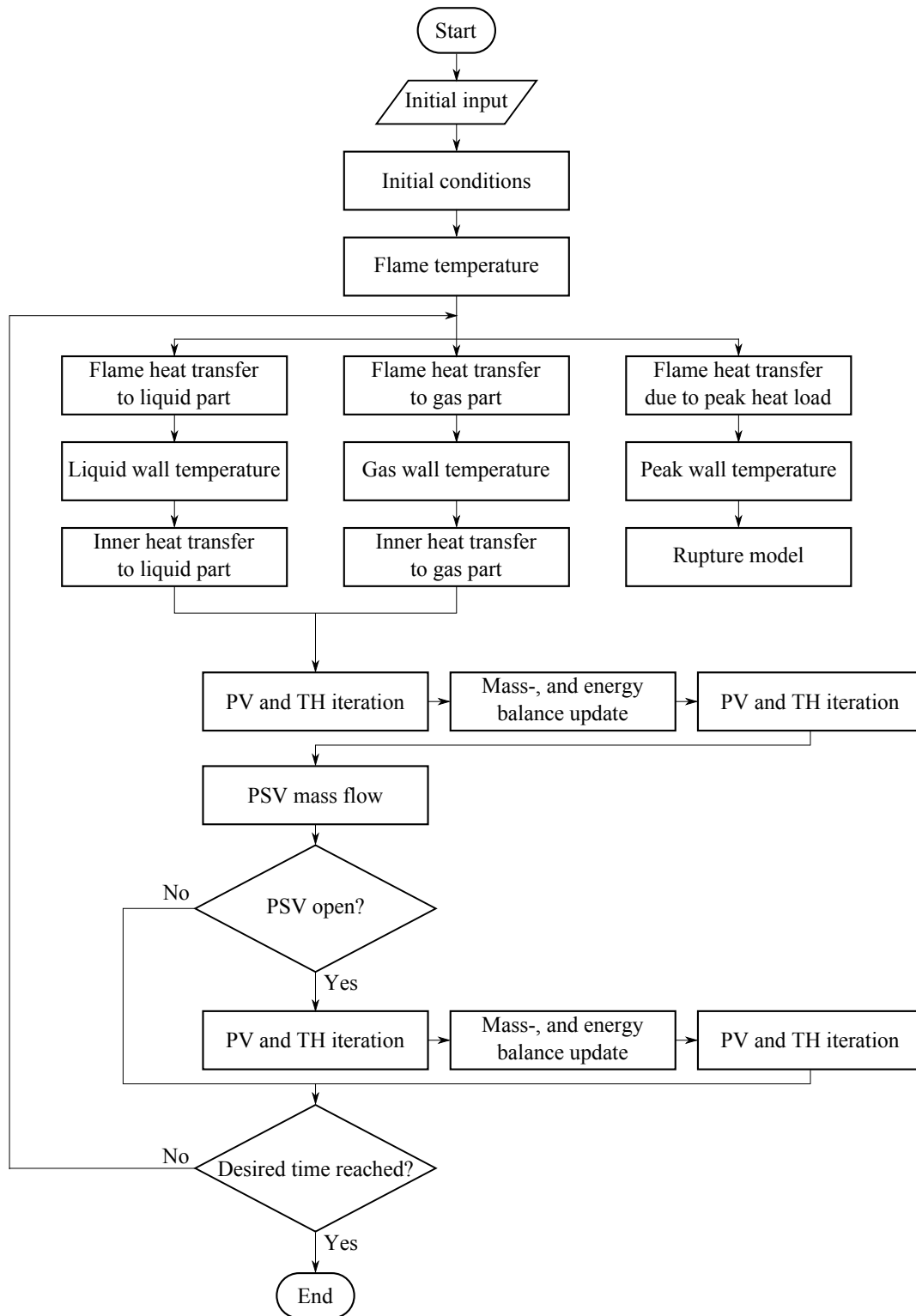


Figure 5.1: Flowchart of the model calculation algorithm.

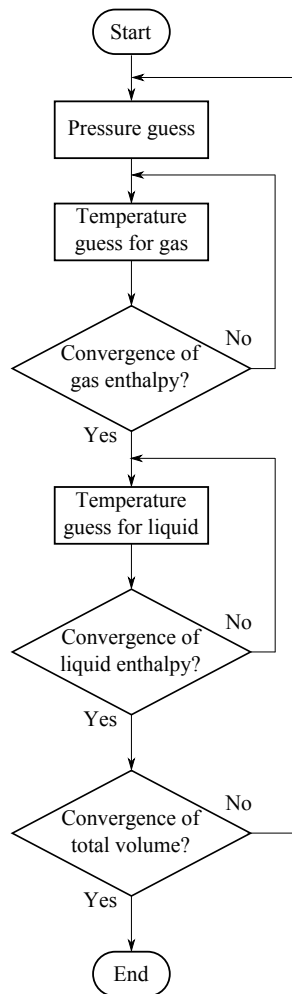


Figure 5.2: Illustration of the algorithm procedure "PV and TH iteration".

Figure 5.2 illustrates the algorithm procedure "PV and TH iteration". It is the main algorithm used to update the pressure and temperature of the gas and liquid phases, by using the constraints of constant volume and enthalpy. Initially the pressure is set as a guess, and then each phase temperature is iterated. The temperature is iterated towards the enthalpy of each phase by a secant iteration method, a variant of Newton's method of iteration. As the phase temperatures are independent of each other, the sequence of calculation has no influence on the result, within the convergence criteria. When the temperatures have been updated, the total volume is computed to define whether the pressure has converged or not. If it is not converged, a new pressure guess will be updated and the iteration of temperatures will be carried out again.

5.1.1 Flame heat flux model

The heat transfer from the flame to the shell is modelled using the recommended approach from Scandpower [6]. The heat transfer from the flame to the vessel shell is divided into radiation, convection and reradiation as seen in equation 5.1.

$$q_f = \underbrace{\alpha_s \cdot \varepsilon_f \cdot \sigma \cdot T_f^4}_{\text{Radiation}} + \underbrace{h_f \cdot (T_f - T_s(t))}_{\text{Convection}} - \underbrace{\varepsilon_s \cdot \sigma \cdot T_s(t)^4}_{\text{Reradiation}} \quad (5.1)$$

- q_f is the flame heat flux. [W/m^2]
- α_s is the vessel surface absorptivity. [-]
- ε_f is the flame emissivity. [-]
- σ is the Stefan-Boltzmann constant, $\sigma = 5.67 \cdot 10^{-8}$ [$\text{W}/\text{m}^2 \cdot \text{K}^4$]
- T_f is the flame temperature. [K]
- h_f is the convection heat transfer coefficient between the flame and the surface. [$\text{W}/\text{m}^2 \cdot \text{K}$]
- $T_s(t)$ is the time dependent surface temperature. [K]
- ε_s is the surface emissivity. [-]

This model assumes that the pressure vessel is fully engulfed by the flame. This means that the view factor for the radiation is unity and is therefore not taken into consideration. The convective heat transfer coefficients for a jet fire and a pool fire, and recommended values for the emissivity and absorptivity, are given by Scandpower as [6];

- $h_{jet \ fire} = 100$ [$\text{W}/\text{m}^2 \cdot \text{K}$]
- $h_{pool \ fire} = 30$ [$\text{W}/\text{m}^2 \cdot \text{K}$]
- $\alpha_s = 0.85$
- $\varepsilon_s = 0.85$
- $\varepsilon_f = 1.0$ (optical thick flames, thickness > 1 m)

The flame temperature is found by solving equation 5.2 for the incident heat flux in relation to the ambient conditions. The flame temperature is kept constant throughout the simulation.

$$q_{total} = \sigma \cdot T_f^4 + h_f \cdot (T_f - T_{amb}) \quad (5.2)$$

- q_{total} is the incident flame heat flux as given in table 5.1. [W/m^2]
- T_{amb} is the ambient temperature ≈ 293 K (20 °C)

The heat flux used to calculate the flame temperature is given in table 5.1.

	Small jet fire [kW/m ²]	Large jet fire [kW/m ²]	Pool fire [kW/m ²]
Peak heat load	250	350	150
Background heat load	0	100	100

Table 5.1: Incident heat fluxes for various fire scenarios given by Scandpower [6].

5.1.2 Transient 1-D conductive heat transfer model for shell wall

The heat transfer through the vessel wall is modelled as a 1-D heat transfer problem through a cylinder wall. The cylindrical wall is divided into volume elements and is represented in cylindrical coordinates. An illustration of the wall discretisation is shown in figure 5.3.

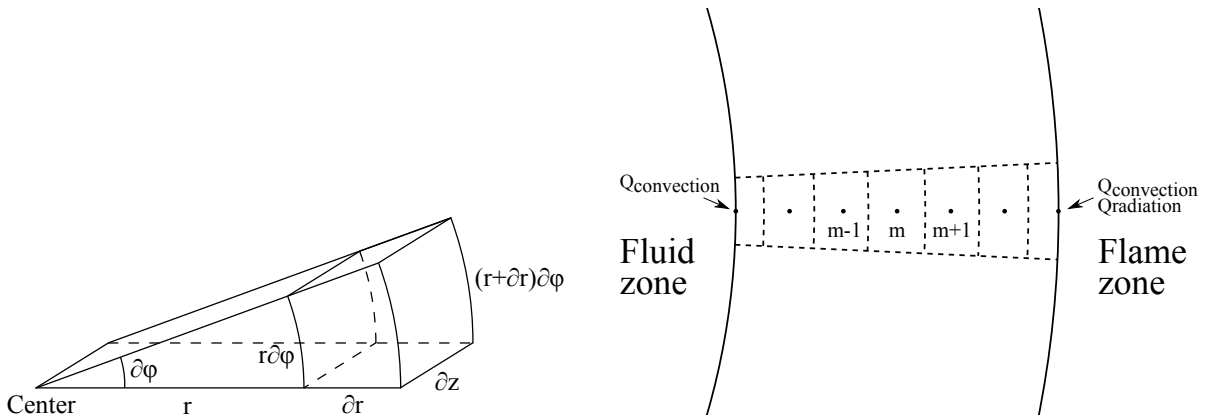


Figure 5.3: Left: Illustration of a 3-D discretisation volume element. Right: Illustration of the volume elements and nodes in the 1-D cylindrical heat transfer model.

For simplicity the 1-D transient heat transfer model is used for the background heat load, effectively assuming an infinitely long cylinder with uniform temperature distribution and heat load in the circumferential direction.

Transient heat conduction equation in the interior nodes

The 1-D transient heat transfer equation is based on an energy balance for the volume elements as shown in equation 5.3.

$$\frac{\partial E_{acc}}{\partial t} = \dot{E}_{in} - \dot{E}_{out} \tag{5.3}$$

- \dot{E}_{in} is the energy into an element. [J/s]
- \dot{E}_{out} is the energy out of an element. [J/s]
- $\frac{\partial E_{acc}}{\partial t}$ is the change in accumulated sensible energy. [J/s]

The energy terms in equation 5.3 can be rewritten in cylindrical coordinates, as given in equation set 5.4. The energy flow into an element volume is determined from Fourier's law of heat conduction. The net energy flow of an element must be equal to its change of energy in the element. The accumulated energy in the element is determined from the change in sensible heat as a function of time.

$$\dot{E}_{in} = Q_r = -k \cdot \frac{\partial T}{\partial r} r \partial \varphi \partial z \quad (5.4a)$$

$$\dot{E}_{out} = Q_{r+\partial r} = Q_r + \frac{\partial Q_r}{\partial r} \partial r \quad (5.4b)$$

$$\frac{\partial E_{acc}}{\partial t} = \rho \cdot c_P \cdot \frac{\partial T}{\partial t} \partial r r \partial \varphi \partial z \quad (5.4c)$$

- Q_r is the heat flow into the element. [J/s]
- $Q_{r+\partial r}$ is the heat flow out of the element. [J/s]
- k is the conductive heat transfer coefficient. [W/m·K]
- T is the temperature of the element. [K]
- ρ is the density of the wall. [kg/m³]
- c_P is the heat capacity of the wall. [J/kg·K]
- ∂r is the change in radial direction. [m]
- $r \partial \varphi$ is the change in angular direction. [m]
- ∂z is the change in longitudinal direction. [m]
- ∂t is the change in time. [s]

Equation 5.5 is simplified by combining equation set 5.4 and equation 5.3.

$$\rho \cdot c_P \cdot \frac{\partial T}{\partial t} \partial r r \partial \varphi \partial z = -\frac{\partial Q_r}{\partial r} \partial r \quad (5.5)$$

Equation 5.6 is found by combining equation 5.4a and 5.5.

$$\rho \cdot c_P \cdot \frac{\partial T}{\partial t} \partial r r \partial \varphi \partial z = \frac{\partial}{\partial r} \left(k \cdot r \cdot \frac{\partial T}{\partial r} \right) \partial r \partial \varphi \partial z \quad (5.6)$$

Equation 5.6 is divided with the elements volume ($\partial r r \partial \varphi \partial z$) and result in the 1-D heat equation for a hollow cylinder wall in the radial direction as shown in equation 5.7.

$$\rho \cdot c_P \cdot \frac{\partial T}{\partial t} = \frac{1}{r} \frac{\partial}{\partial r} \left(k \cdot r \cdot \frac{\partial T}{\partial r} \right) \quad (5.7)$$

Two main methods of time iteration of a differential equation can be applied in the solution, which are the implicit method and the explicit method. The explicit method uses values already determined from the previous time iteration, to determine the variable values of the new iteration. The methods are described in equation set 5.8. E.g. the differential function, $f(n)$, to be solved is given in equation 5.8a. Q is the variable to be solved, in the time iteration n , using the time step Δt .

$$\frac{dQ(n)}{dt} = f(n) \quad (5.8a)$$

$$Q(n+1) = Q(n) + \Delta t \cdot f(n) \quad \text{Explicit method} \quad (5.8b)$$

$$Q(n+1) = Q(n) + \Delta t \cdot f(n+1) \quad \text{Implicit method} \quad (5.8c)$$

The explicit method can be solved directly, hence the designation of explicit, while the time step stability criteria needs to be obeyed. Alternatively, the implicit method will need to be solved, and larger time steps can be employed. For the purpose of the model programming the explicit method is applied, as a great deal of dependent variables would need to be calculated at each implicit iteration. In order to model the variable gradients with low error, the time step should also be kept adequately low, which would be counterproductive to the implicit method, while it would coincide with the stability criterion of the explicit method.

Equation 5.7 can be written in its explicit numerical formulation as equation 5.9, for which the temperature of the new iteration is calculated.

$$T_m^i = T_m^{i-1} + \frac{t^i - t^{i-1}}{\rho \cdot c_P} \left(\frac{-k \cdot r_{m-\frac{1}{2}} \left(\frac{T_m^{i-1} - T_{m-1}^{i-1}}{r_m - r_{m-1}} \right) + k \cdot r_{m+\frac{1}{2}} \left(\frac{T_m^{i-1} - T_{m+1}^{i-1}}{r_m - r_{m+1}} \right)}{r_m \cdot (r_{m+\frac{1}{2}} - r_{m-\frac{1}{2}})} \right) \quad (5.9)$$

- m indicates the position of the node.
- i indicates the iteration.

Outer node boundary condition

The outer boundary condition of the 1-D heat transfer model is where the shell surface is in contact with the engulfing flame. The outer boundary condition is modelled as a Neumann boundary condition with a heat flux as the output to the boundary volume element. The energy balance is shown in equation set 5.10. Note that the boundary volume is only half the size of the interior volumes, so the volume is divided by two, as illustrated in figure 5.3.

$$\frac{\partial E_{acc}}{\partial t} = \dot{E}_{in} - \dot{E}_{out} \quad (5.10a)$$

$$\dot{E}_{in} = -k \cdot \frac{\partial T}{\partial r} r \partial \varphi \partial z \quad (5.10b)$$

$$\dot{E}_{out} = \dot{q} \cdot r \partial \varphi \partial z \quad (5.10c)$$

$$\frac{\partial E_{acc}}{\partial t} = \rho \cdot c_P \cdot \frac{\partial T}{\partial t} \frac{\partial r r \partial \varphi \partial z}{2} \quad (5.10d)$$

- \dot{q} is the flame heat flux given in equation 5.1 page 54. [W/m²]

Equation 5.11 is given by combining equation set 5.10.

$$\rho \cdot c_P \cdot \frac{\partial T}{\partial t} \frac{\partial r r \partial \varphi \partial z}{2} = -k \cdot \frac{\partial T}{\partial r} r \partial \varphi \partial z - \dot{q} \cdot r \partial \varphi \partial z \quad (5.11)$$

Equation 5.11 is divided by the volume of the outer boundary element $\left(\frac{\partial r r \partial \varphi \partial z}{2}\right)$, which results in equation 5.12.

$$\rho \cdot c_P \frac{\partial T}{\partial t} = \frac{2}{\partial r} \left(-k \frac{\partial T}{\partial r} - \dot{q} \right) \quad (5.12)$$

Equation 5.12 is written in its explicit numerical formulation and solved for the current temperature of the node as shown in equation 5.13.

$$T_m^i = T_m^{i-1} + \frac{2 \cdot (t^i - t^{i-1})}{\rho \cdot c_P} \left(\frac{-r_{m+\frac{1}{2}} \cdot k \left(\frac{T_m^{i-1} - T_{m-1}^{i-1}}{r_m - r_{m-1}} \right) - r_m \cdot \dot{q}}{r_{m+\frac{1}{4}} (r_{m+\frac{1}{2}} - r_{m-\frac{1}{2}})} \right) \quad (5.13)$$

Inner node boundary condition

The inner boundary condition of the 1-D heat transfer model is where the shell surface is in contact with the fluid inventory. The inner boundary condition is

modelled as a Neumann boundary condition with the convective heat transfer from the fluid as the input to the boundary volume element. The energy balance is shown in equation set 5.14. Note that the boundary volume is only half the size of the interior volumes, consequently the volume is divided by two, as illustrated in figure 5.3.

$$\frac{dE_{acc}}{dt} = \dot{E}_{in} - \dot{E}_{out} \quad (5.14a)$$

$$\dot{E}_{in} = -h(T_s - T_\infty)r\partial\varphi\partial z \quad (5.14b)$$

$$\dot{E}_{out} = -k \cdot \frac{\partial T}{\partial r} r\partial\varphi\partial z \quad (5.14c)$$

$$\frac{dE_{acc}}{dt} = \rho \cdot c_P \cdot \frac{\partial T}{\partial t} \frac{\partial rr\partial\varphi\partial z}{2} \quad (5.14d)$$

- h is the convective heat transfer coefficient between the fluid and the wall as found in subsection 5.1.5 page 66. [$\text{W}/\text{m}^2\cdot\text{K}$]
- T_s is the surface temperature of the vessel wall. [K]
- T_∞ is the temperature of the fluid. [K]

Equation 5.15 is found by combining equation set 5.14.

$$\rho \cdot c_P \cdot \frac{\partial T}{\partial t} \frac{\partial rr\partial\varphi\partial z}{2} = k \cdot \frac{\partial T}{\partial r} r\partial\varphi\partial z - h(T_s - T_\infty)r\partial\varphi\partial z \quad (5.15)$$

Equation 5.15 is divided by the volume of the inner boundary element $\left(\frac{\partial rr\partial\varphi\partial z}{2}\right)$. This reduction results in equation 5.16.

$$\rho \cdot c_P \frac{\partial T}{\partial t} = \frac{2}{\partial r} \left(k \frac{\partial T}{\partial r} - h(T_s - T_\infty) \right) \quad (5.16)$$

Equation 5.16 is written in its explicit numerical formulation and solved for the current temperature of the node as shown in equation 5.17.

$$T_m^i = T_m^{i-1} + \frac{2 \cdot (t^i - t^{i-1})}{\rho \cdot c_P} \left(\frac{r_{m+\frac{1}{2}} \cdot k \left(\frac{T_m^{i-1} - T_{m+1}^{i-1}}{r_m - r_{m+1}} \right) - r_m \cdot h(T_m^{i-1} - T_{fluid}^{i-1})}{\left(r_{m+\frac{1}{4}} \right) \left(r_{m+\frac{1}{2}} - r_{m-\frac{1}{2}} \right)} \right) \quad (5.17)$$

Stability criterion

The explicit numerical method is not unconditionally stable, and temperature in the nodes may oscillate wildly and diverge from an accurate solution if a too large time step is used. The numerical model must satisfy the stability criterion to avoid this problem. Each node type has a unique equation which set a restriction for the time step. The criterion with the most restrictive time step should be used to ensure stability [15]. Boundary conditions which include convective and/or radiation has more restrictive time steps than interior nodes [15]. The stability criterion is satisfied if the coefficients for T_m^{i-1} in the T_m^i expression is greater than or equal to zero in all nodes [15].

The stability criterion for the interior nodes can be derived to be as shown in equation 5.18,

$$1 - 2 \cdot \tau_r \geq 0 \quad (5.18)$$

where τ_r is defined as the dimensionless mesh Fourier number as given in equation 5.19,

The derivation is given in detail in appendix G.

$$\tau_r = \frac{\alpha \cdot \Delta t}{\Delta r^2} \quad (5.19)$$

and α is defined in equation 5.20.

$$\alpha = \frac{k}{\rho \cdot c_P} \quad (5.20)$$

- Δt is the time step. [s]
- Δr is the radial step size between the nodes. [m]

Δt can be solved from equation 5.18, 5.19, and 5.20, in order to determine the maximum time step applicable for the interior nodes.

The stability criterion for the inner wall boundary conditions, with convective heat transfer, can be derived to be as shown in equation 5.21,

$$1 - 2\tau_r \left(\frac{r_m + \frac{1}{2}\Delta r}{r_m + \frac{1}{4}\Delta r} \right) - 2\tau_r \frac{h}{k} \Delta r \left(\frac{r_m}{r_m + \frac{1}{4}\Delta r} \right) \geq 0 \quad (5.21)$$

The derivation is given in detail in appendix G.

Δt can in a similarly fashion be solved from equation 5.21, 5.19, and 5.20, in order to determine the maximum time step applicable for the inner boundary condition.

It is problematic to formulate an expression for the outer wall boundary condition, as the heat input to the node which is nonlinear in regards to the flame temperature, $Q(T_f^4)$. The time step can be adjusted manually if the model shows signs of oscillation, but that have not been the case in this project. If it becomes necessary to deal with the outer wall boundary condition, then Milton et al [16] discusses how to formulate an approximate boundary condition criterion for a boundary node with convection and radiation.

5.1.3 Peak temperature of shell wall using 3-D heat transfer

To more precisely predict the temperature distribution in the vessel wall due to the peak heat load, a 3-D model is applied. The 3-D model is only applied to the gas-wall interface, as it is assumed that the liquid adequately cools the vessel wall, such that it does not reach a critical temperature for rupture to occur.

The governing equation for the heat transfer in cylindrical coordinates is given in equation 5.22. The terms are in units of heat flow per volume.

$$\rho \cdot c_P \frac{\partial T}{\partial t} = \frac{1}{r} \frac{\partial}{\partial r} \left(r \cdot k \frac{\partial T}{\partial r} \right) + \frac{1}{r^2} \frac{\partial}{\partial \varphi} \left(k \frac{\partial T}{\partial \varphi} \right) + \frac{\partial}{\partial z} \left(k \frac{\partial T}{\partial z} \right) \quad (5.22)$$

The area of the vessel wall is modelled within the area defined by the peak heat load. The area affected by the peak heat load is defined by an angle span (0° to 360°) and longitudinal span (0% - 100% of vessel length), which corresponds to a set of discrete volumes, for which the 3-D model should be applied.

The boundary in the angular and longitudinal direction is defined by a Neumann boundary condition. The boundary value is defined as the temperature of the vessel, which is calculated by the 1-D heat transfer model, corresponding to the effect of the background heat load. For each time step, the temperature of the vessel wall is calculated and thus the boundary condition for the 3-D model is also updated. The boundary conditions is expressed in equation set 5.23.

The boundary conditions in the radial direction is the same as the 1-D model (fluid convection and flame radiation and convection), and is recalculated to apply for the new vessel wall temperature from the 3-D model.

The Neumann boundary condition for the 3-D model is illustrated in equation set 5.23 and figure 5.4. The equations apply for all values of radius, r , and for varying

values of circumferential length $r\varphi$, and longitudinal length z .

$$T(r, \varphi, z_{min}) = T_{gas}(r) \quad \text{for } \varphi_{min} < \varphi < \varphi_{max} \quad (5.23a)$$

$$T(r, \varphi, z_{max}) = T_{gas}(r) \quad \text{for } \varphi_{min} < \varphi < \varphi_{max} \quad (5.23b)$$

$$T(r, \varphi_{min}, z) = T_{gas}(r) \quad \text{for } z_{min} < z < z_{max} \quad (5.23c)$$

$$T(r, \varphi_{max}, z) = T_{gas}(r) \quad \text{for } z_{min} < z < z_{max} \quad (5.23d)$$

Each equation corresponds to a surface in the 3-D illustration in figure 5.4. Increasing the number of mesh divisions in the radial direction will decrease the maximum time step.

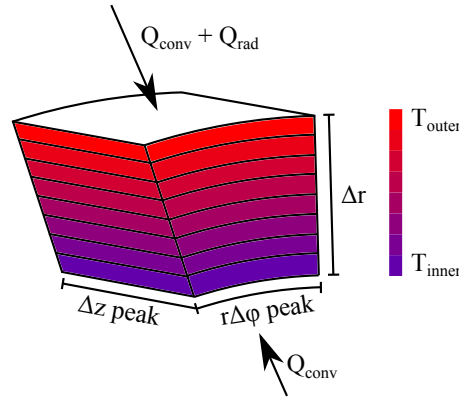


Figure 5.4: Illustration of the vessel wall segment for the 3-D model of peak heat load.

The stability criterion for the numerical modelling in 3-D is given in equation 5.24, with a modified value of τ , as indicated in equation 5.25.

$$1 - 2\tau_{r;z;\varphi} \geq 0 \quad (5.24)$$

$$\tau_{r;z;\varphi} = \alpha \Delta t \cdot \left(\frac{1}{\Delta r^2} + \frac{1}{\Delta z^2} + \frac{1}{(r_m \Delta \varphi)^2} \right) \quad (5.25)$$

The derivation is given in detail in appendix G.

The stability criterion for the 3-D model at the gas-wall interface is given in equation 5.26.

$$1 - 2\tau_r \left(\frac{r_m + \frac{1}{2}\Delta r}{r_m + \frac{1}{4}\Delta r} \right) - 2\tau_r \frac{h}{k} \Delta r \left(\frac{r_m}{r_m + \frac{1}{4}\Delta r} \right) - 4\tau_\varphi - 4\tau_z \geq 0 \quad (5.26)$$

The derivation is given in detail in appendix G.

The definition of the dimensionless mesh Fourier numbers τ_r , τ_z , and τ_φ are as given in equation 5.27.

$$\tau_r = \frac{\alpha \Delta t}{\Delta r^2} \quad \tau_z = \frac{\alpha \Delta t}{\Delta z^2} \quad \tau_\varphi = \frac{\alpha \Delta t}{(r_m \Delta \varphi)^2} \quad (5.27)$$

5.1.4 Thermodynamic properties for the wall

The thermodynamic properties of the steel wall are dependent of the temperature of the wall. Properties of interest are the density, the heat capacity, and the conductive heat transfer coefficient. The specific heat of steel is a fit of the properties for steel taken from Eurocode [17] as seen in equation set 5.28.

$$\begin{aligned} &\text{for } 20 \text{ }^\circ\text{C} \leq T < 600 \text{ }^\circ\text{C} \\ c_P &= 425 + 7.73 \cdot 10^{-1} \cdot T - 1.69 \cdot 10^{-3} \cdot T^2 + 2.22 \cdot 10^{-6} \cdot T^3 \end{aligned} \quad (5.28a)$$

$$\begin{aligned} &\text{for } 600 \text{ }^\circ\text{C} \leq T < 735 \text{ }^\circ\text{C} \\ c_P &= 666 + \frac{13,002}{738 - T} \end{aligned} \quad (5.28b)$$

$$\begin{aligned} &\text{for } 735 \text{ }^\circ\text{C} \leq T < 900 \text{ }^\circ\text{C} \\ c_P &= 545 + \frac{17,820}{T - 731} \end{aligned} \quad (5.28c)$$

$$\begin{aligned} &\text{for } 900 \text{ }^\circ\text{C} \leq T \leq 1,200 \text{ }^\circ\text{C} \\ c_P &= 650 \end{aligned} \quad (5.28d)$$

- c_P is the heat capacity for steel. [J/kg·°C]
- T is the temperature of the steel. [°C]

Equation set 5.28 for the heat capacity of steel is plotted in figure 5.5. The peak in heat capacity around $T=730 \text{ }^\circ\text{C}$, is caused by the heat of transformation when the steel structure changes from ferrite to austenite, as described by Umino [18]. The peak in heat capacity means that, the rate of the temperature increase will slow down when the temperature approaches this temperature. The change in temperature (and therefore also time step) needs to be sufficiently small to resolve the peak in heat capacity.

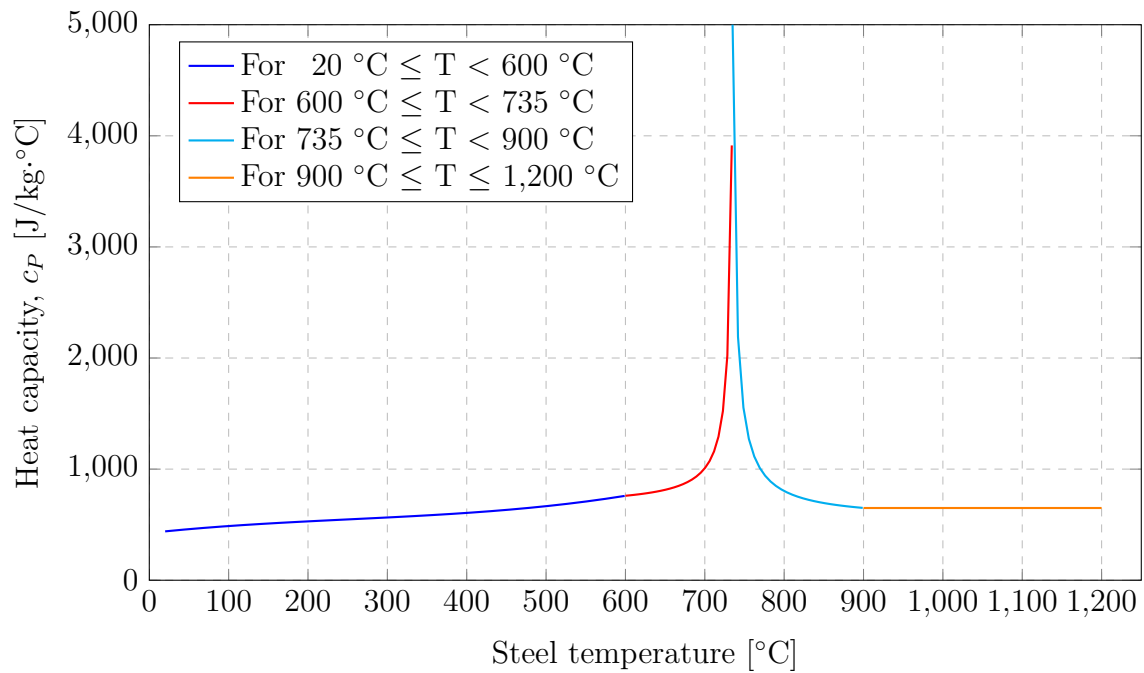


Figure 5.5: Heat capacity of steel as a function of temperature.

The conductive heat transfer coefficient is modelled from equation set 5.29, as found by Eurocode [17], and plotted in figure 5.6.

$$\begin{aligned} &\text{for } 20 \text{ }^\circ\text{C} \leq T < 800 \text{ }^\circ\text{C} \\ &k = 54 - 3.33 \cdot 10^{-2} \cdot T \end{aligned} \quad (5.29a)$$

$$\begin{aligned} &\text{for } 800 \text{ }^\circ\text{C} \leq T \leq 1,200 \text{ }^\circ\text{C} \\ &k = 27.3 \end{aligned} \quad (5.29b)$$

- k is the conductive heat transfer coefficient for steel. [W/m·°C]

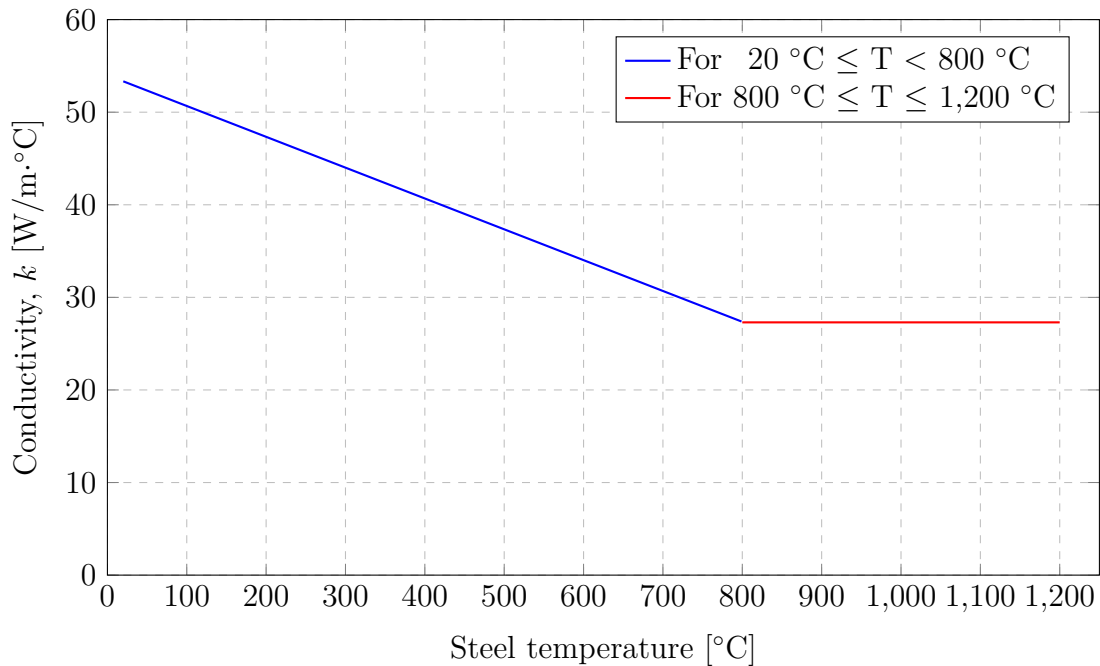


Figure 5.6: Conductive heat transfer coefficient of steel as a function of temperature.

The density of the wall is modelled by equation set 5.30. The density dependency is taken from Engineering Equation Solver (EES) for carbon steel in a temperature range of 273.15 K to 1,500 K.

$$\begin{aligned} &\text{for } 273.15 \text{ K} \leq T < 1,000 \text{ K} \\ &\rho = -0.34233 \cdot T + 7,952.33 \end{aligned} \quad (5.30a)$$

$$\begin{aligned} &\text{for } 1,000 \text{ K} \leq T \leq 1,500 \text{ K} \\ &\rho = 7,610 \end{aligned} \quad (5.30b)$$

- ρ is the density of carbon steel. [kg/m³]

Equation 5.30 for the density of carbon steel is plotted in figure 5.7.

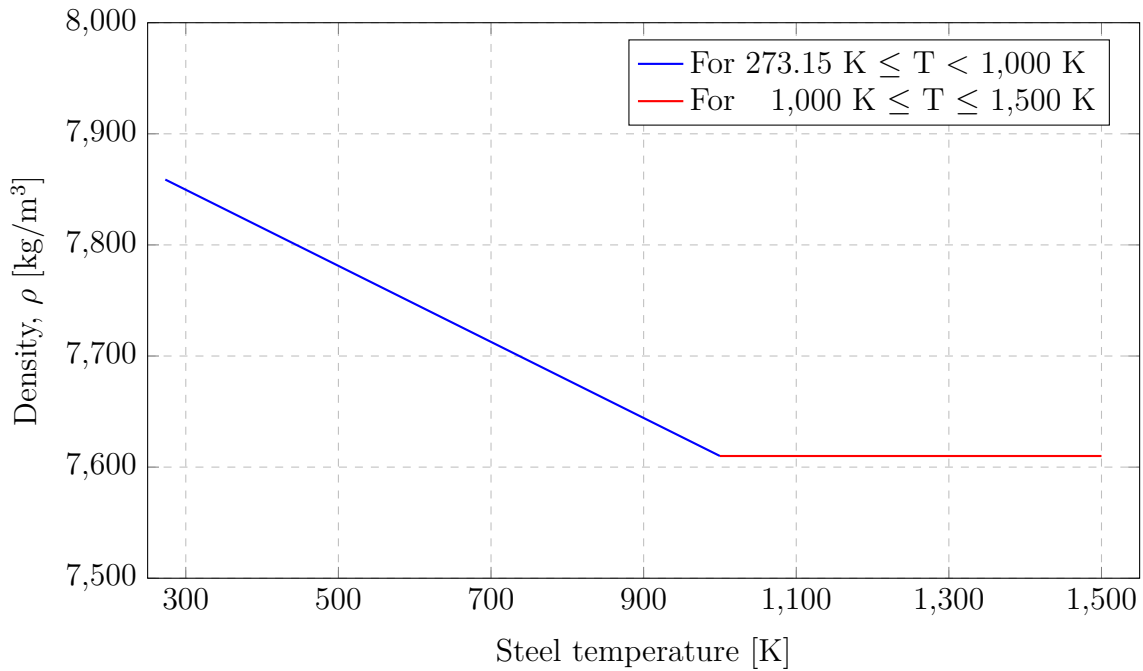


Figure 5.7: Density of carbon steel as a function of temperature.

5.1.5 Convective heat transfer coupling of fluid and wall

The convective heat transfer from the vessel wall to the fluid is categorised into two scenarios. The first scenario is heat transfer from the vessel wall to the gas phase, and the second scenario is heat transfer from the vessel wall to the liquid phase. Convective heat transfer between the gas and liquid phase is also considered. The heat transfer between the gas and the wall is that of natural convection, and the heat transfer between the liquid and the wall is either natural convection or a boiling phenomena. Typical values for the convective heat transfer coefficient for fluids are shown in table 5.2.

Type of convection	h [W/m ² ·K]
Free convection (gas)	2-25
Free convection (liquids)	10-1,000
Forced convection (gas)	25-250
Forced convection (liquids)	50-20,000
Boiling	2,500-100,000

Table 5.2: Typical values for the convective heat transfer coefficient [15].

It is evident from the values in table 5.2, that the heat transfer coefficient between

the gas and the wall, is much lower than the heat transfer coefficient between the liquid and the wall. This comparatively insulates the wall segment exposed to the gas volume, while the wall segment exposed to the liquid part will experience more cooling effects. Thus a heat load on the gas part of the vessel increases the risk of rupture, due to material weakening.

Gas-wall interface

To determine the heat transfer for the gas-wall interface, Newton's law of cooling is applied, as given in equation 5.31.

$$\frac{dQ}{dt} = -hA(T_s - T_{gas}) \quad (5.31)$$

- dQ is the change in thermal energy due to convective heat transfer. [J]
- dt is the change in time during the heat transfer. [s]
- h is the convective heat transfer. [$\text{W}/\text{m}^2 \cdot \text{K}$]
- A is the area normal to the direction of the heat transfer. [m^2]
- T_s is the surface temperature of the geometry. [K]
- T_{gas} is the temperature of the surrounding gas. [K]

Equation 5.31 indicates the heat transfer to the surface of any geometry such as a plate or cylindrical wall, by means of heat convection from its surroundings [15].

The convective heat transfer will need to be estimated for the the gas-wall interface, by the use of empirical relations for the Nusselt number. The Nusselt number describes the ratio of convective heat transfer to conductive heat transfer, normal to a surface area, as given in equation 5.32.

$$Nu = \frac{hL}{k} \quad (5.32)$$

- Nu is the Nusselt number. [-]
- h is the convective heat transfer. [$\text{W}/\text{m}^2 \cdot \text{K}$]
- L is a characteristic length of the geometry. [m]
- k is the thermal conductivity of the gas. [$\text{W}/\text{m} \cdot \text{K}$]

The characteristic length L used is the height of the gas volume, i.e. from the liquid level to the top of the vessel. The thermal conductivity of the wall material varies as a function of temperature, and will need to be re-calculated at every new temperature condition as described in subsection 5.1.4.

The empirical correlations used to calculate the Nusselt number of the gas-wall interface is a function of the Rayleigh number, which can be defined by the Grashof number and Prandtl number, as in equation 5.33.

$$Ra = Gr \cdot Pr \quad (5.33)$$

- Ra is the Rayleigh number. [-]
- Gr is the Grashof number. [-]
- Pr is the Prandtl number. [-]

The Grashof number is a dimensionless number which approximates the ratio of the buoyancy forces to viscous forces, as given in equation 5.34. The Prandtl number is a dimensionless number defined as the ratio of the momentum diffusivity to thermal diffusivity, as given in equation 5.35.

$$Gr = \frac{\beta g \rho^2 L^3 \Delta T}{\mu^2} \quad (5.34)$$

$$Pr = \frac{c_p \mu}{k} \quad (5.35)$$

- β is the coefficient of volume expansion. [1/K]
- g is the standard acceleration of gravity. [m/s²]
- ρ is the gas density. [kg/m³]
- L is the characteristic length. [m]
- ΔT is the temperature difference of the surface and gas. [K]
- μ is the dynamic viscosity. [kg/m·s]
- c_p is the heat capacity of gas. [J/kg·K]
- k is the thermal conductivity of gas. [J/m·K]

In order to estimate the convective heat transfer of the gas-wall interface, the Nusselt number is calculated for the vessel part exposed to the gas phase. No applicable information have been found for the calculation of the Nusselt number of an internal cylinder, and thus assumptions have been made, by the use of empirical correlations for both vertical and horizontal plates [15].

To fulfill this assumption, the geometry is divided into assumed stepwise linear pieces, as illustrated in figure 5.8.

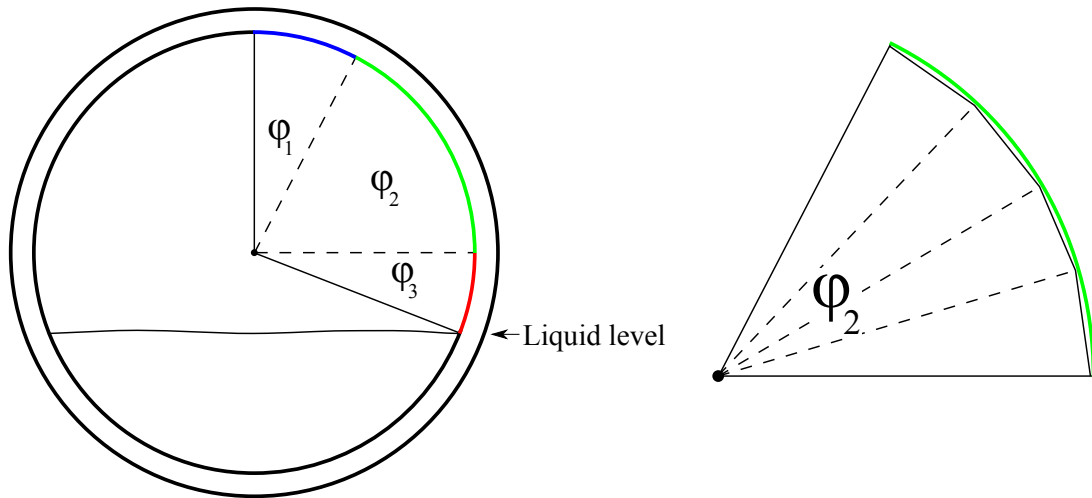


Figure 5.8: Left: Illustration of angles used to determine the Nusselt number of the gas-wall interface. The angle reference is from the vertical line at φ_1 , with clock-wise positive direction. Right: Illustration of the stepwise deviation of the vessel wall, in the φ_2 arc length.

The angle from the vertical reference to the liquid level will be $\omega = \varphi_1 + \varphi_2 + \varphi_3$, for which the maximum value of φ_1 is 30° , φ_2 is 60° , and φ_3 is 90° .

For the arc length of the vessel wall given by the angle φ_3 , in figure 5.8, the vertical plate correlations are used to determine the Nusselt number, as given in equation set 5.36.

$$Nu = 0.59 \cdot Ra^{\frac{1}{4}} \quad \text{for } 10^4 < Ra < 10^9 \quad (5.36a)$$

$$Nu = 0.1 \cdot Ra^{\frac{1}{3}} \quad \text{for } 10^{10} < Ra < 10^{13} \quad (5.36b)$$

For practical reasons the limits of the Rayleigh number have been adjusted to simply be $Ra < 10^9$, for equation 5.36a, and $Ra > 10^9$ for equation 5.36b. The extension of the range of equation 5.36b, to also apply for $10^9 < Ra < 10^{10}$ is illustrated in figure 5.9.

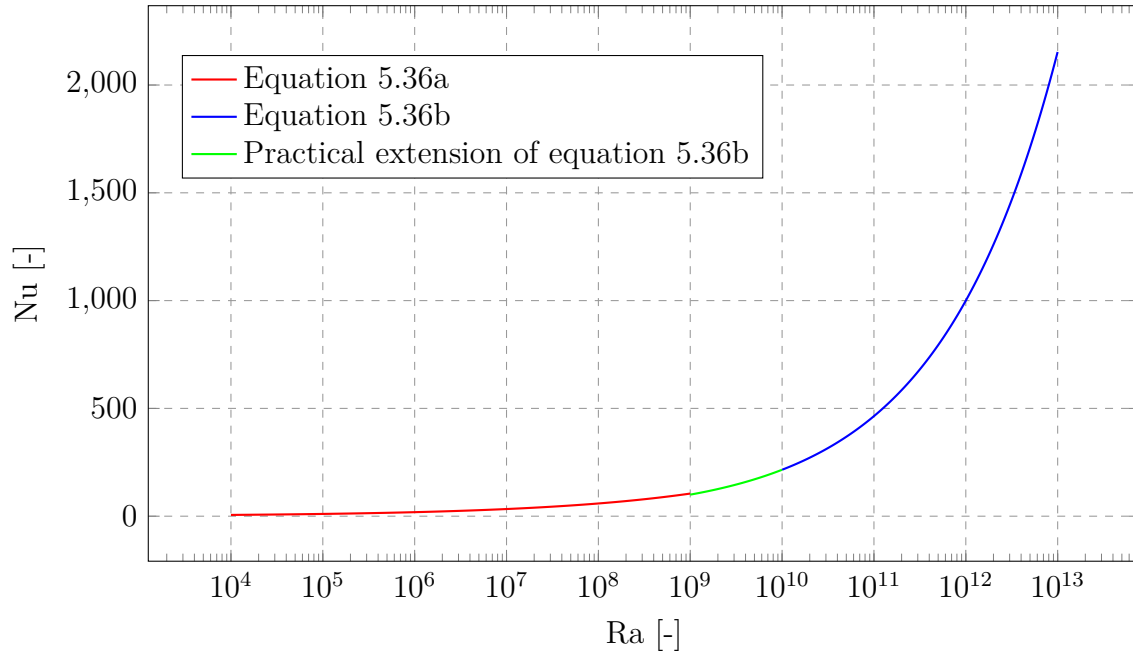


Figure 5.9: The Nusselt number for the vertical plate correlations as a function of the Rayleigh number.

The Nusselt number in the arc length, defined by the angle φ_2 , as illustrated in figure 5.8, is estimated by modifying the equation set 5.36, which is applicable for vertical plates.

As the Grashof number is a function of, g , the standard acceleration of gravity, the equation set can be modified to take into account the angle between the plate and the direction of gravity [15].

The modified version of the Grashof number is given in equation 5.37, with the transformation from the angle reference used by Çengel [15], to the reference used in figure 5.8. The applicability range for this modification is from 90° to 30° , using the reference system of figure 5.8. This can be related to an angle range between the plate and the direction of gravity from 0° to 60° .

$$Gr_{mod} = Gr \cdot \sin(\varphi) \quad (5.37)$$

- Gr_{mod} is the modified Grashof number to account for change in direction of gravity.
- φ is any angle within the range of φ_2 in figure 5.8.

The Nusselt number for the top part of the vessel, defined by the arc length of φ_1 , is determined using a horizontal plate equation, from Çengel [15], as given by equation 5.38.

$$Nu = 0.27 \cdot Ra^{\frac{1}{4}} \quad \text{for} \quad 10^5 < Ra < 10^{11} \quad (5.38)$$

To determine an average Nusselt number for the entire arc length for the gas phase, a weighted summation of the individually determined Nusselt numbers is used as given in equation 5.39.

$$Nu_{gas} = (Nu_{\varphi_1} \cdot l_{\varphi_1} + Nu_{\varphi_2} \cdot l_{\varphi_2} + Nu_{\varphi_3} \cdot l_{\varphi_3}) / (l_{\varphi_1} + l_{\varphi_2} + l_{\varphi_3}) \quad (5.39)$$

- Nu_{gas} is the average Nusselt number for the gas-wall interface.
- Subscript 1, 2, and 3 indicate the angle segments in figure 5.8.

The sum of the stepwise linear part of the arc length of φ_2 is given in equation 5.40.

$$Nu_{\varphi_2} = \frac{1}{l_{\varphi_2}} \cdot \sum_{i=1}^n (Nu_i \cdot l_i) \quad (5.40)$$

- Nu_{φ_2} is the Nusselt number of the arc length defined by φ_2 . [-]
- l_{φ_2} is the arc length defined by φ_2 . [m]
- Nu_i is the Nusselt number as a function of the angle by the use of the modified Grashof number, at the angle node i . [-]
- l_i is arc length of the stepwise linear node i . [m]

Liquid-wall interface

The heat transfer between the vessel wall and the liquid is a boiling phenomena. Boiling occurs at the wall-liquid interface, when the liquid is in contact with the wall, and the wall temperature is sufficiently above the saturation temperature of the liquid [15]. The boiling heat flux is described as a form of convective heat transfer as shown in equation 5.41.

$$\dot{q}_{boiling} = h \cdot (T_s - T_{sat}) \quad (5.41)$$

- $\dot{q}_{boiling}$ is the boiling heat flux. [W/m²]
- h is the convective heat transfer coefficient for boiling. [W/m²·K]
- T_s is the surface temperature. [K]
- T_{sat} is the saturation temperature of the liquid. [K]

Boiling is divided into four boiling regimes, which is distinguished by the temperature difference between the wall surface and the saturation temperature. The four boiling regimes are natural convection boiling, nucleate boiling, transition boiling, and film boiling. The four boiling regimes are shown in the boiling curve

in figure 5.10. The boiling curve in figure 5.10 is for water at 1 atm, and shows the relationship between the boiling heat flux and the temperature difference, ΔT , between the surface temperature and the saturation temperature. Even though the illustrated boiling curve is for water, the general shape for the boiling curve remains the same for different liquids [15].

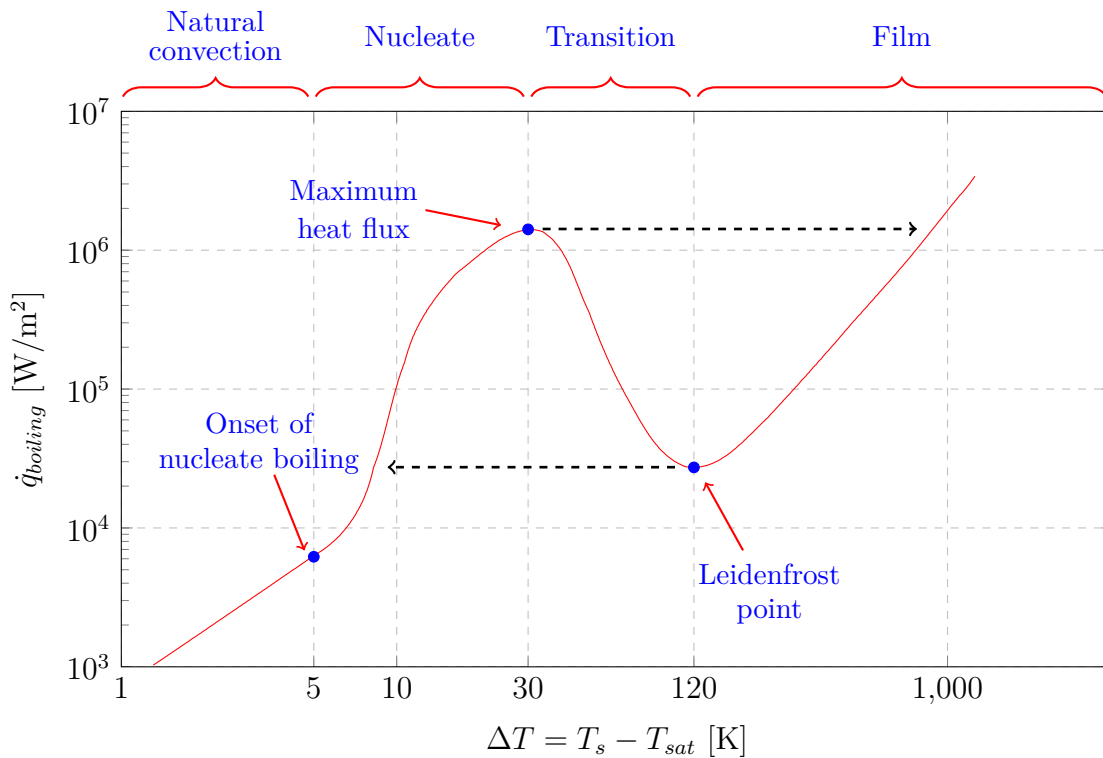


Figure 5.10: Illustration of the boiling curve regimes of water, based on description from Çengel [15].

The natural convection regime is when ΔT is low (2-5 °C for water). In this regime the water is slightly superheated, but there is no bubble formation. The superheated water rises to the surface of the pool, by means of natural convection, and evaporates at the free surface of the liquid.

The nucleate boiling regime initiates after the natural convection regime at around $\Delta T = 5^\circ\text{C}$ for water. Bubbles form from the nucleation sites on the wall surface and rises to the liquid surface. The rising bubbles increases the turbulence in the vicinity of the wall surface. The agitation and stirring is the main reason behind the increased heat transfer coefficient with nucleate boiling [15].

At a certain ΔT , the amount of bubbles formed becomes so large, that the heat transfer reaches a maximum, as the water can not wet the wall surface fast enough to transfer all the heat flux. The transition boiling starts at this point, and is a mixture of nucleate boiling and film boiling.

At a higher ΔT the nucleate boiling phenomenon disappears and the boiling regimes becomes film boiling. At this regime there is a film layer of vapor which covers the wall surface and insulates the surface from most of the convective heat transfer and the boiling is caused by radiation heat transfer from the wall surface.

Experiments made by Birk et al [19] investigate the heat transfer and rupture of a 500 gallon propane tank exposed to a pool fire. The temperature measurements indicate that the wall temperature is about 10 °C above the liquid temperature near the wall. In an experiment made by Berge et al [20], a water tank was heated and the wall and liquid temperatures was measured. It was found that the wall temperature was close to the water temperature, with a temperature difference of 3 K, when the tank was heated with approximately 60 kW/m². Based on these cases, it is assumed that the boiling phenomena is limited to the natural convection regime and nucleate boiling regime, since ΔT does not increase enough to initiate transitional or film boiling. This is the case for both water and propane in a heated vessel, which is representative for this type of application.

The heat transfer in the natural convection regime is based on natural convection in the liquid. The convective heat transfer coefficient is calculated from the Nusselt number as described in equation 5.32 page 67. The correlation used for the Nusselt number is for the upper surface of a hot plat [15], and is shown in equation set 5.42.

$$Nu = 0.54 \cdot Ra^{\frac{1}{4}} \quad \text{for } 10^4 < Ra < 10^7 \quad (5.42a)$$

$$Nu = 0.15 \cdot Ra^{\frac{1}{3}} \quad \text{for } 10^7 < Ra < 10^{11} \quad (5.42b)$$

The heat transfer in the nucleate boiling regime is difficult to predict as it depends on the nucleation site on the surface and bubble formation [15]. It is therefore necessary to use a empirical correlation in order to predict the heat transfer during nucleate boiling. The most widely used correlation to predict heat transfer in nucleate boiling is proposed by Rohsenow (1951) [21] and is shown in equation 5.43.

$$\dot{q}_{boiling} = \mu_l \cdot h_{fg} \left(\frac{g(\rho_l - \rho_v)}{\sigma} \right)^{\frac{1}{2}} \left(\frac{c_{Pl}(T_s - T_{sat})}{C_{sf} \cdot h_{fg} \cdot Pr_l^n} \right)^3 \quad (5.43)$$

- $\dot{q}_{boiling}$ is the nucleate boiling heat flux. [W/m²]
- μ_l is the viscosity of the liquid. [kg/m·s]
- h_{fg} is the enthalpy of vaporisation. [J/kg]
- g is the acceleration of gravity. [m/s²]

- ρ_l is the density of the liquid. [kg/m³]
- ρ_v is the density of the vapor. [kg/m³]
- σ is the surface tension of the liquid-vapor interface. [N/m]
- c_{pl} is the heat capacity of the liquid. [J/kg·K]
- T_s is the surface temperature. [K]
- T_{sat} is the saturation temperature of the liquid. [K]
- C_{sf} is an experimental constant that depends on the surface-fluid combination.
- Pr_l is the Prandtl number of the liquid.
- n is an experimental constant that depends on the fluid.

From equation 5.43 it can be seen that nucleate boiling is a complicated phenomena with many variables, which is also stated by Cengel et al [15]. Some of the variables needed for this empirical correlation, such as the surface tension, would be difficult to obtain for a multicomponent hydrocarbon system. Based on these findings, it is assessed that an empirical expression for the nucleate heat transfer is beyond the scope of this project, and therefore an assumption is made regarding the boiling heat transfer.

The nucleate boiling heat transfer is assumed to dominate the wall temperature with a high heat transfer coefficient, keeping the wall temperature close to the saturation temperature of the liquid. It is therefore assumed, that if the temperature difference between the wall temperature and the saturation temperature exceeds a limit, the innermost control volume of the wall will not increase in temperature, but instead, the energy, that enters the control volume, will transfer directly to the liquid. This will effectively control the temperature of the wall to not exceed a temperature difference limit. The temperature difference limit is in the model set to 1 K. The equivalent nucleate boiling heat transfer coefficient can afterwards be calculated based on the heat transfer and the temperature difference. If the temperature difference is below the temperature limit, the natural convective heat transfer coefficient will be used to calculate the heat transfer.

The purpose of the model is to predict the dynamic of the fluid inventory and the rupture time of the vessel. The importance of the heat transfer to the liquid is to predict the evaporation rate of the liquid. The total amount of energy and the rate of heat transfer is only little affected by the above assumption. In regards to the rupture time, it is not expected that the vessel will rupture when the liquid part of the vessel is exposed to a fire since the heat transfer coefficient is expected to be sufficiently large to avoid a high temperature. This means that the altered wall temperatures, introduced by the assumption, is not of concern for this model.

Gas-liquid interface

The convective heat transfer between the gas and the liquid phase is determined from Newtons law of cooling as described in equation 5.31 page 67. The temper-

ature difference is determined as the difference between the gas and liquid, and the area is taken as the gas-liquid interface area. The Nusselt correlation used, depends on the direction of the heat transfer.

If $T_{gas} > T_{liquid}$ then the Nusselt number is calculated for the lower surface of a hot plate by equation 5.44 [15], and properties from the liquid is used for Rayleigh number which is described in equation 5.33 page 68.

$$Nu = 0.27 \cdot Ra^{\frac{1}{4}} \quad \text{for } 10^5 < Ra < 10^{11} \quad (5.44)$$

If $T_{gas} < T_{liquid}$ then the Nusselt number is calculated for the upper surface of a hot plate by equation 5.45 [15], and properties from the gas is used for the Rayleigh number.

$$Nu = 0.54 \cdot Ra^{\frac{1}{4}} \quad \text{for } 10^4 < Ra < 10^7 \quad (5.45a)$$

$$Nu = 0.15 \cdot Ra^{\frac{1}{3}} \quad \text{for } 10^7 < Ra < 10^{11} \quad (5.45b)$$

The convective heat transfer coefficient is determined from equation 5.32.

5.1.6 Pressure vessel inventory conditions

To calculate various conditions of the vessel inventory, the existing code base developed by Rambøll is utilised. The code base allows for the use of two different equations of state (EOS), either a Peng-Robinson (PR EOS), or Soave-Redlich-Kwong (SRK EOS). The equations of state calculates the vapor-liquid equilibrium equations, and the results are used to determine various state variables such as the phase fractions, mole fractions, compressibility, enthalpy, entropy, molar weight of phases, density, heat capacity, and heat capacity ratio.

For simplification, only mass and heat transfer are taken into account, while chemical processes and mechanical forces are omitted.

The viscosity property for water and each phase of hydrocarbons is calculated based on existing code base from Rambøll. The gas hydrocarbon viscosity is calculated based on the Lee Gonzales correlation, the liquid hydrocarbon viscosity is based on a corresponding states viscosity model, and the water viscosity is an empirical correlation fitted within a range of temperatures.

The conductivity for the three phases is defined based on fitted function from the program Engineering Equation Solver (EES). The fitted functions are described in appendix H.

When calculating the pressure and temperature inside the vessel, the basic function described as the "EOS_flash" function in the code, is utilised as the basis of iteration.

In order to solve the two unknown variables temperature, T , and pressure, P , two constraints are needed. These are conservation of total volume and conservation of enthalpy. The total volume of the phases are more affected by pressure than temperature, and therefore the pressure is solved using the total volume as a constraint. The total volume will be iterated towards the vessel volume. Equally, the enthalpy is more affected by temperature than the pressure, and thus the enthalpy is used as a constraint for the calculation of temperature.

The gas phase is regarded as being a uniquely separate phase, while the liquid hydrocarbon and water phases are regarded as being a uniformly mixed phase, described as the liquid phase. This entails the calculation of a vessel pressure, and two separate temperatures, one for the gas phase, and one for the liquid phase.

The mole fractions and phase fractions calculated by the "EOS_flash" function can be exploited to calculate mass flow, due to evaporation and condensation. Equation 5.46 describes the mass balance used, and equation 5.47 describes the energy balance used for the vessel inventory.

$$m_{liq} = m_{liq;0} + m_{gas;lig} - m_{lig;gas} \quad (5.46a)$$

$$m_{gas} = m_{gas;0} - m_{gas;lig} + m_{lig;gas} - m_{vent} \quad (5.46b)$$

- m_{liq} is the calculated mass of liquid at the new iteration. [kg]
- m_{gas} is the calculated mass of gas at the new iteration. [kg]
- $m_{liq;0}$ is the mass of liquid at the previous iteration. [kg]
- $m_{gas;0}$ is the mass of gas at the previous iteration. [kg]
- $m_{gas;lig}$ is the mass of gas condensed into liquid. [kg]
- $m_{lig;gas}$ is the mass of liquid evaporated to gas. [kg]
- m_{vent} is the mass flow through the vent, assumed only to be gas. [kg]

$$H_{liq} = H_{liq;0} + H_{gas;lig} - H_{lig;gas} + Q_{liq} + Q_{interface} \quad (5.47a)$$

$$H_{gas} = H_{gas;0} - H_{gas;lig} + H_{lig;gas} - H_{vent} + Q_{gas} - Q_{interface} \quad (5.47b)$$

- H_{liq} is the enthalpy of liquid at the new iteration. [J]
- H_{gas} is the enthalpy of gas at the new iteration. [J]
- $H_{liq;0}$ is the enthalpy of liquid at the previous iteration. [J]
- $H_{gas;0}$ is the enthalpy of gas at the previous iteration. [J]
- $H_{gas;lig}$ is the enthalpy of gas condensed into liquid. [J]
- $H_{lig;gas}$ is the enthalpy of liquid evaporated to gas. [J]
- H_{vent} is the enthalpy of the mass flow through the vent, assumed only to be gas. [J]
- Q_{gas} is the net heat transfer from the vessel wall to the gas phase. [J]
- Q_{liq} is the net heat transfer from the vessel wall to the liquid phase. [J]
- $Q_{interface}$ is the heat transfer from the gas phase to the liquid phase, due to temperature differences. [J]

5.1.7 PSV and mass flow calculations

In order to calculate the mass flow rate through an orifice equation 5.49 is used based on literature from *the Committee for the Prevention of Disasters* [22]. It is assumed that only gas exits the orifice, as the PSV is positioned on the top of the vessel.

If the pressure differential across the orifice opening is adequate it will cause the flow to become choked, meaning the fluid velocity has reached the speed of sound, Mach 1, and can thus not increase any further due to the pressure differential.

When a fluid is choked the mass flow will solely be dependent on the upstream conditions.

To account for the difference in choked and non-choked flow a set limit pressure is introduced as in equation 5.48. If the downstream pressure, P_{down} , is below the pressure limit, P_{limit} , then the flow is choked, and the pressure used, P_{used} , in equation 5.49 should be the pressure limit, P_{limit} . Otherwise if the downstream pressure, P_{down} , is greater than or equal to the pressure limit, P_{limit} , the flow is no longer choked and the pressure used should be the downstream pressure, P_{down} [22].

$$P_{limit} = P_{up} \cdot \left(\frac{2}{k+1} \right)^{\frac{k}{k-1}} \quad (5.48)$$

$$\dot{m}_{flow} = C_d \cdot A \cdot \sqrt{\left(\frac{2k}{k-1} \right) \cdot P_{up} \cdot \rho \cdot \left(\frac{P_{used}}{P_{up}} \right)^{\frac{2}{k}} \left(1 - \left(\frac{P_{used}}{P_{up}} \right)^{\frac{k-1}{k}} \right)} \quad (5.49)$$

- ρ is the density of the gas upstream. [kg/m^3]
- P_{limit} is the pressure limit of the upstream absolute pressure. [bara]

- P_{up} is the absolute pressure upstream of the orifice. [bara]
- k is the ratio of the heat capacities at constant pressure, C_p , and at constant volume, C_v .
- P_{down} is the absolute pressure downstream of the orifice. [bara]
- P_{used} is the pressure used in the mass flow equation based on choked or non-choked conditions. [bara]
- \dot{m}_{flow} is the mass flow through the orifice. [kg/s]
- C_d is the discharge coefficient of the orifice opening. [-]
- A is the cross sectional area of the orifice. [m^2]

In the majority of cases of calculating pressure relief by the use of a PSV, in offshore installations, the subsonic phenomena will not be of great significance.

5.1.8 Calculation of exerted stress and prediction of rupture

The rupture time of the vessel can be estimated by calculating the stresses in the vessel wall, and by determining the allowable stress in the wall. If the calculated stress is larger than the allowable stress, then rupture occurs.

The maximum allowable strength can be defined either as the yield strength or the UTS. Figure 5.11 depicts an illustrative stress-strain curve of a metal material such as steel. The first linear part is the elastic region, for which the material will not permanently deform. The following section is the plastic region, in which the material will permanently deform, until it reaches the UTS.

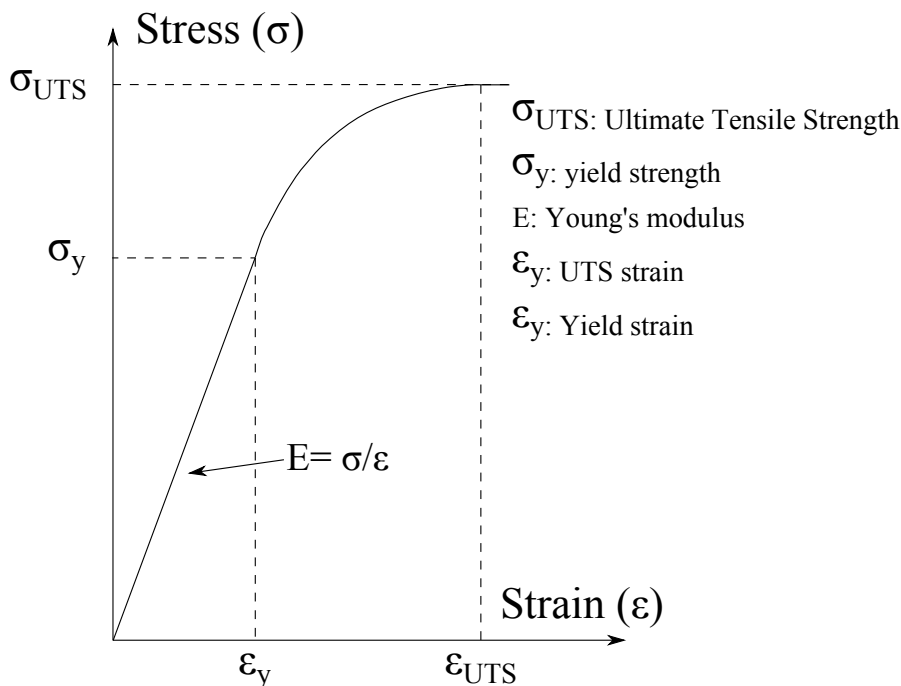


Figure 5.11: Illustrative stress-strain curve, with elastic and plastic regions.

The stress exerted by the pressure from the interior fluid, is calculated as the von Mises stress. Equation set 5.50 describes the procedure to obtain an equivalent stress, the von Mises stress, in the vessel wall material, by taking into account the longitudinal and circumferential stresses. As the cylinder wall thickness is less than one twentieth of the radius, the stress in the radial direction can be neglected [23].

$$\sigma_l = \frac{P - P_0}{\left(\frac{R_o}{R_i}\right)^2 - 1} \quad (5.50a)$$

$$\sigma_c = \frac{(P - P_0)(R_i + \Delta R)}{b} \quad (5.50b)$$

$$\Delta R = \frac{PR_iR_o}{bE} \quad (5.50c)$$

$$\sigma_e = \sqrt{\sigma_l^2 + \sigma_c^2 - \sigma_l\sigma_c} \quad (5.50d)$$

- σ_e is the calculated equivalent tension based on the von Mises hypothesis. [Pa]
- σ_l is the calculated stress in the longitudinal direction. [Pa]
- σ_c is the calculated stress in the circumferential direction. [Pa]
- P is the vessel pressure. [Pa]
- P_0 is the atmospheric pressure. [Pa]
- R_o is the outer vessel radius. [m]
- R_i is the inner vessel radius. [m]
- ΔR is the change in radius due to the stresses applied to the vessel. [m]
- b is the thickness of the vessel wall. [m]
- E is Young's modulus of the wall material [Pa]

The allowable stress in the vessel wall material can be defined in various manners, but is for simplicity defined as the yield strength.

In order to model the yield stress of the wall material as function of temperature, the concept of reduction factor is applied, as defined in equation 5.51.

The reduction factor is defined as a set of values for given temperatures, and for intermediate values a linear interpolation will be adequate. The reduction factor illustrated in figure 5.12 is only applicable for carbon steel, as indicated by Eurocode [17].

Similarly, reduction factors for Young's modulus of the material are described in equation 5.52 and figure 5.12, from Eurocode [17].

$$k_y(T) = \frac{\sigma_y}{\sigma_{y;20}} \quad (5.51)$$

- $k_y(T)$ is the reduction factor of the yield strength as function of material temperature, T . [-]
- σ_y is the yield strength at the material temperature, T . [Pa]
- $\sigma_{y;20}$ is the yield strength of the material at a reference temperature of 20°C. [Pa]

$$k_E(T) = \frac{E}{E_{y;20}} \quad (5.52)$$

- $k_E(T)$ is the reduction factor of Young's modulus as function of material temperature, T . [-]
- E is Young's modulus at the material temperature, T . [Pa]
- $E_{y;20}$ is Young's modulus of the material at a reference temperature of 20°C. [Pa]

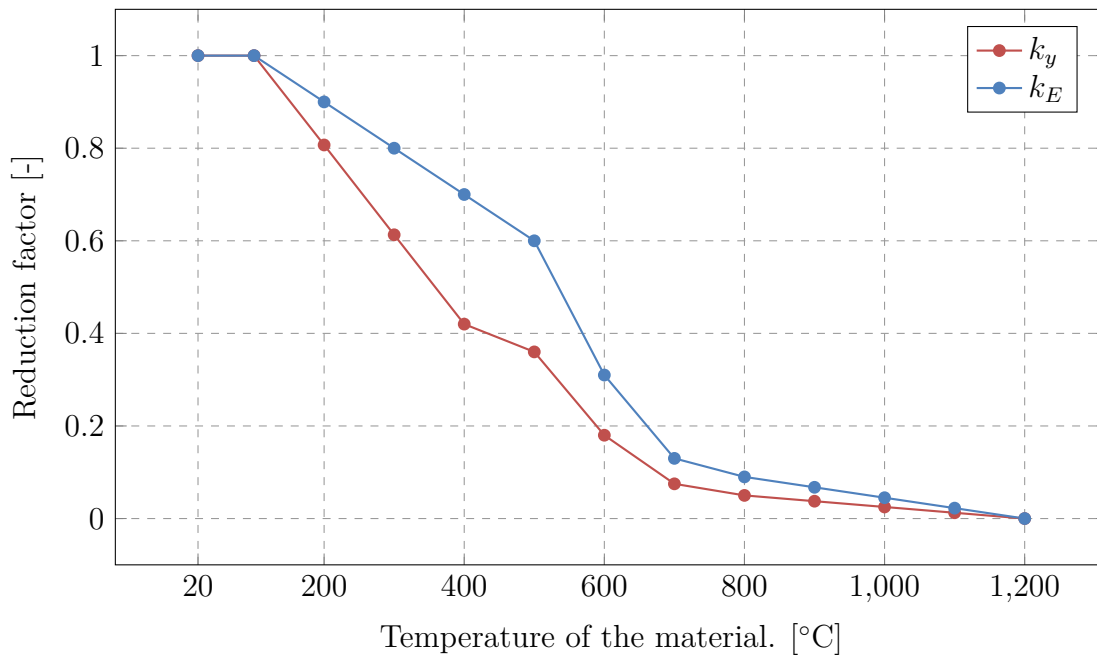


Figure 5.12: The reduction factor of the yield strength, k_y , and Young's modulus, k_E , as function of material temperature [17].

If the temperature is outside the range for the reduction factor functions in figure 5.12, the reduction factor is assumed to be either 1 or 0, for temperatures below 20°C and above 1200°C, respectively.

5.2 Model validation

Validation of the model is done by comparing results obtained from the model, with results from experiments, and from similar cases in VessFire.

Experiment by Moodie et al

The first validation experiment was conducted by Moodie et al in 1988 [24], where a 5 tonne horizontal cylindrical Liquefied Petroleum Gas (LPG) tank was exposed to an engulfing kerosene pool fire. The LPG was filled with commercial propane and test was conducted for fill levels between 22% and 72%. The validation comparison is done for the 22% fill level test. Table 5.3 shows the test conditions which is used as input data for the model and VessFire. The tank has round heads at each end, and the length of the vessel is therefore adjusted to a pseudo length, while keeping the diameter and volume as in the experiment. The composition of the inventory is in the model and VessFire set as 95% propane, 4% n-butane, and 1% nitrogen. The tank is fitted with two PSV's of the same size.

Operation pressure	5.5 bara
Operation temperature	5.7 °C
Outer diameter	1.7 m
Pseudo length	4.64 m
Wall thickness	11.85 mm
Liquid height (22% fill level)	0.4668 m
PSV area (single PSV)	$8.87 \cdot 10^{-4} \text{ m}^2$
PSV set pressure	14.3 bara
PSV reset pressure	11.0 bara

Table 5.3: Test conditions for experiment 1, which are used as input data for the model and VessFire.

The background heat flux used is shown in figure 5.13. A fitted function of the heat flux was found from the experimental values and used in the model. The heat flux used in VessFire was adjusted in intervals to fit the experimental values.

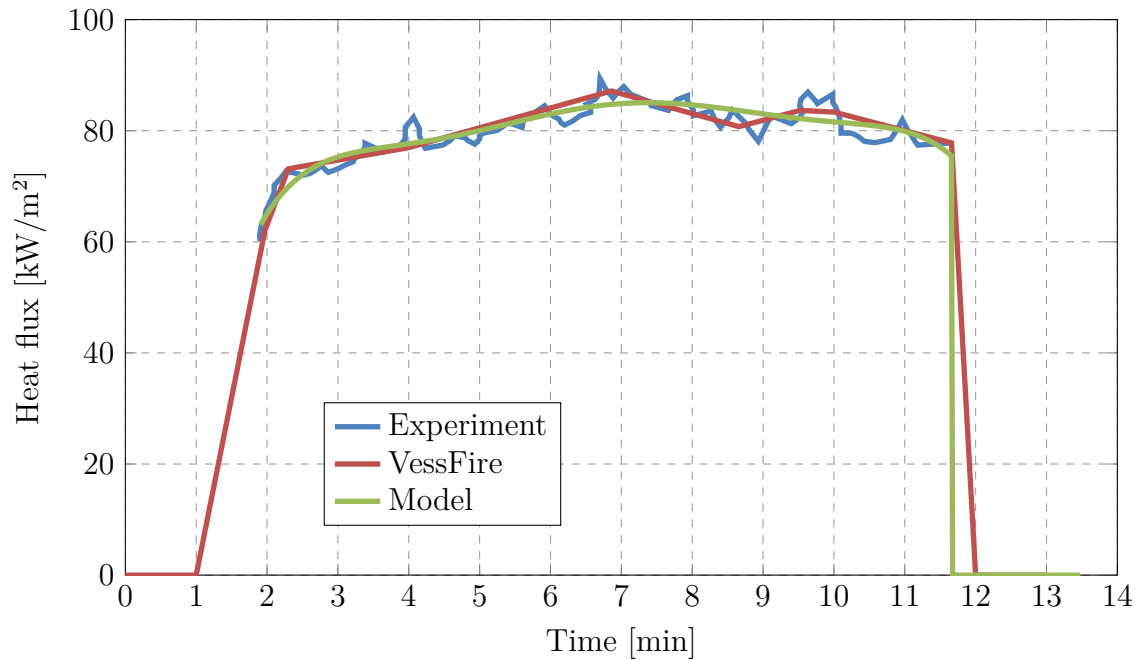


Figure 5.13: Heat flux measured in the experiment and heat flux used in the model and VessFire.

Figure 5.14 shows the pressure measured in the experiment, calculated by the model, and from VessFire. The pressure obtained by the model resembles the pressure from both the experiment and VessFire, until the PSV opens after 6 min. Both the pressure from the model and VessFire deviates from the experiment after the PSV opens. This is possibly due to how the dynamics of the PSV is modelled. The model and the VessFire simulation is done with a PSV using a square opening characteristics, while the PSV dynamic of the experiment is unknown. It is suspected that the experiment uses a PSV with a triangular opening characteristic. The PSV used in the experiment does not seem to open at a consistent pressure for the entire duration. This could indicate varying dynamics of the PSV, due to heating or mechanical wear, which would be difficult to predict. The results from the model and VessFire seems to be similar with some small variation in the duration of the pressure increase.

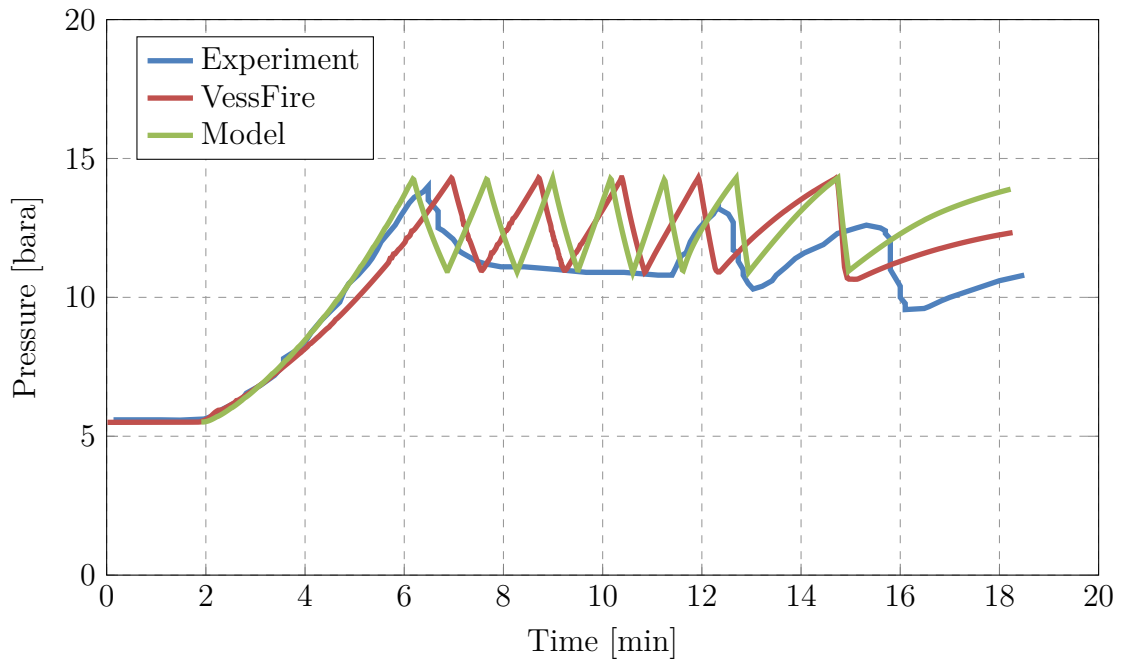


Figure 5.14: Pressure measured in the experiment and pressure calculated by the model and VessFire.

Figure 5.15 shows the gas temperature measured in the experiment, calculated by the model, and from VessFire. The temperature in the experiment is measured at different points in the gas volume as shown on the drawing in figure 5.15. The dashed line shows the division between the gas and liquid phase. The temperature in the experiment indicates some stratification of the gas temperature, while the model and VessFire calculates the temperature as an average. Figure 5.16 shows the temperature of the liquid from the experiment, the model, and VessFire. The experimental setup used thermocouples to measure all temperatures throughout the tank wall and fluid inventory. The placement of the thermocouples are indicated in relevant figures such as figure 5.15, including the 22% fill level (FL).

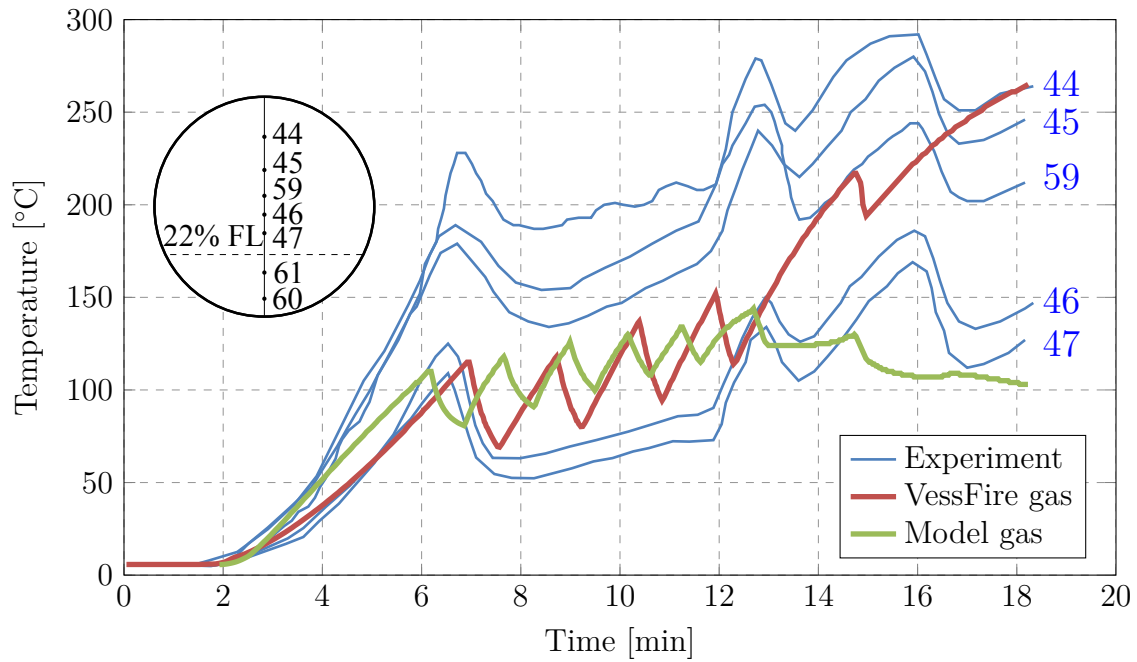


Figure 5.15: Gas temperatures measured in the experiment and gas temperature calculated by the model and VessFire.

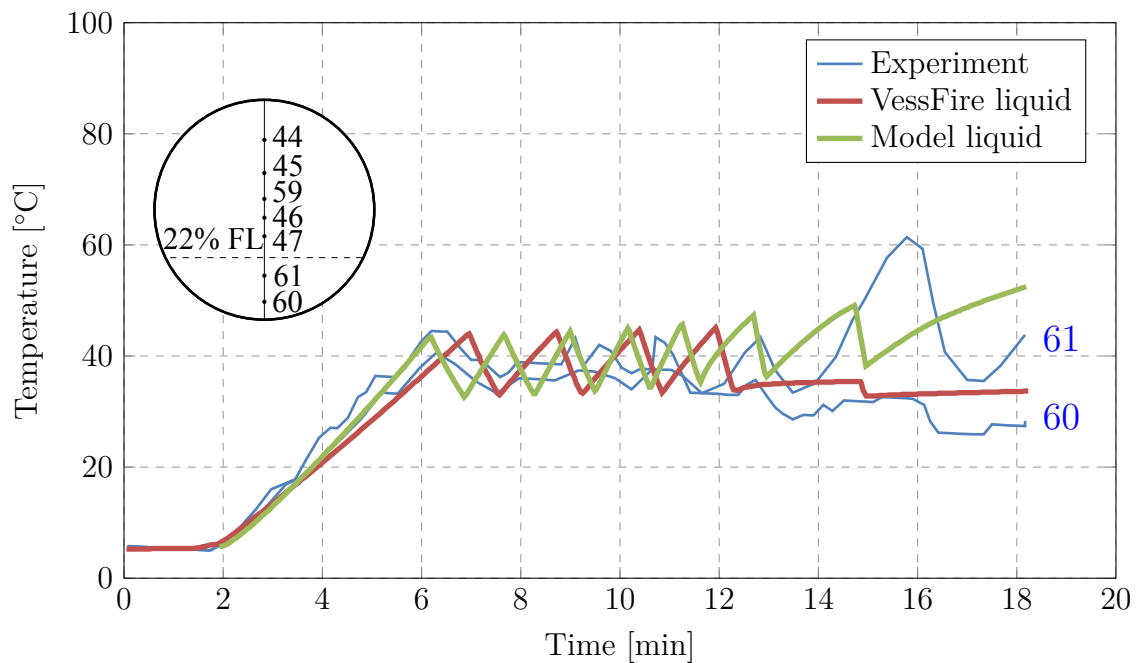


Figure 5.16: Liquid temperatures measured in the experiment and liquid temperature calculated by the model and VessFire.

The difference in maximum and minimum gas temperatures in figure 5.15 ranges

from 100-200°C, within a vessel of diameter of 1.7m. No further explanation is given in Moodie et al [24] to the difference in gas temperatures, except this would indicate stratification of the gas due to lack of proper mixing or frothing. The thermocouples used in the experiment are sheathed, and should therefore not be affected by any change in parameters such as the view factor of each thermocouple.

The temperature measured by thermocouple 61 in figure 5.16, suddenly deviates from the general trend of thermocouple 60 and the model data. This is sought to be explained by Moodie et al by the splashing effects of the liquid, and other factors such as poor mixing in the longitudinal direction.

Figure 5.17 shows the peak wall temperature from the experiment and the calculated peak wall temperature from the model, and from VessFire. The peak wall temperature are in the model and VessFire calculated with a peak heat flux on a small wall area. The heat contribution from the peak heat flux is, due to the small area of the wall, not large enough to affect the inventory of the vessel, and is only used to calculate the maximum wall temperature that can occur with a peak heat flux. The peak heat flux is set to 150 kW/m², which corresponds to a pool fire, as described in table 2.1 page 10.

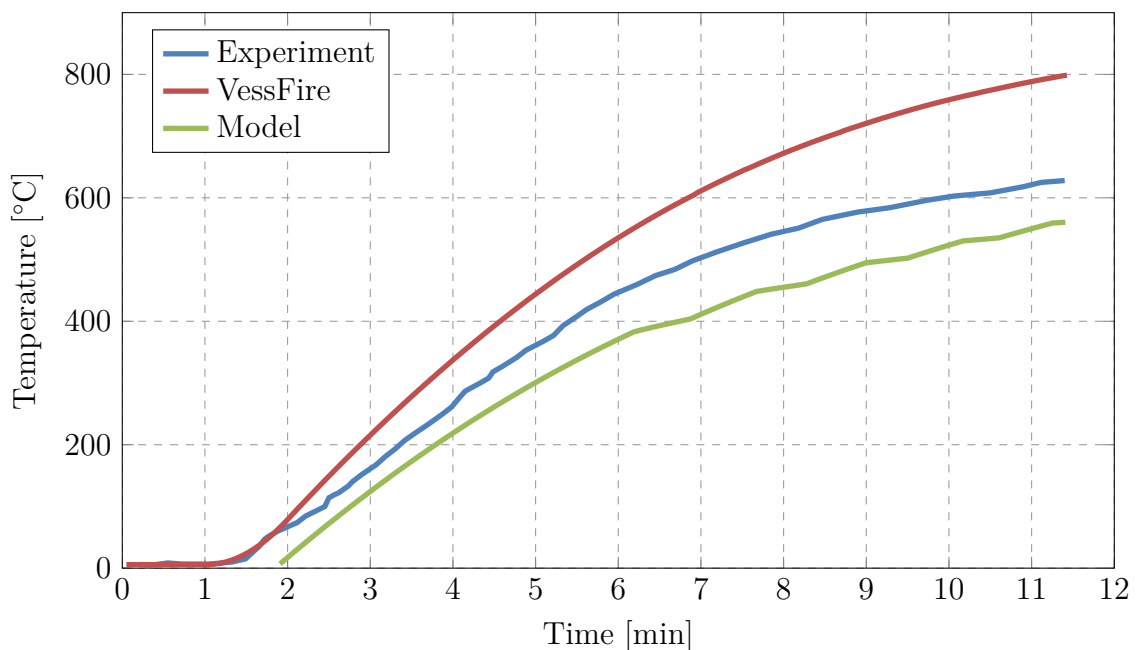


Figure 5.17: Peak wall temperatures measured in the experiment and peak wall temperature calculated by the model and VessFire.

Figure 5.18 shows the mass loss from the experiment and the calculated mass loss from the model, and from VessFire. The mass loss is the accumulated mass flow from the PSV. The difference between the model and VessFire is due to the duration, and the frequency the PSV openings.

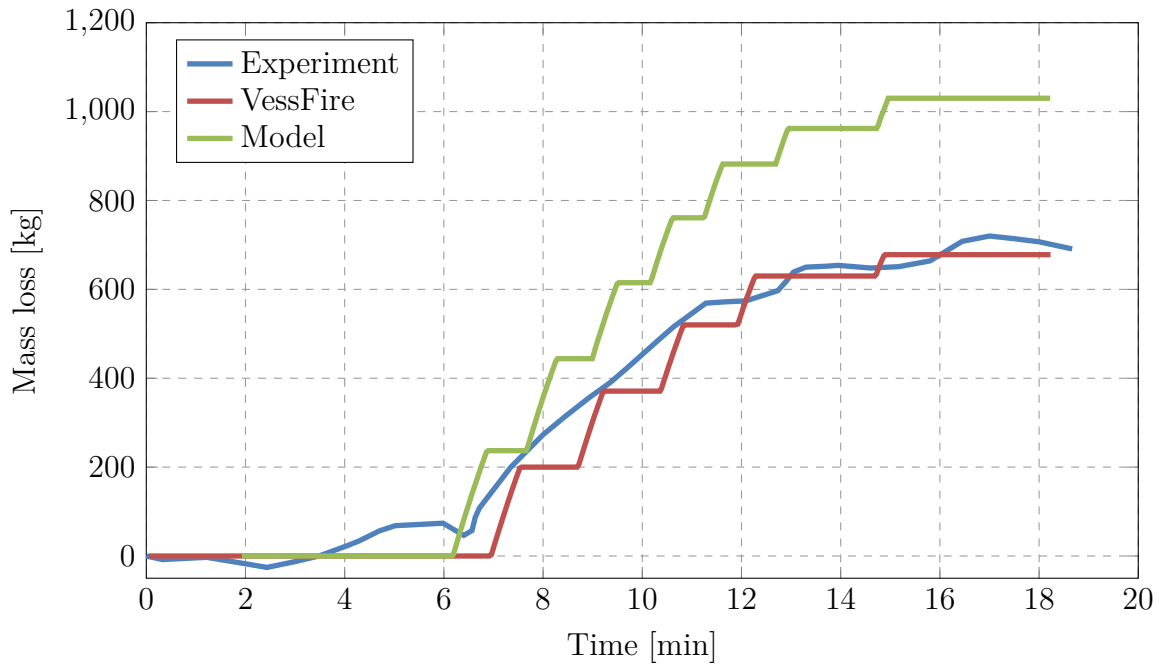


Figure 5.18: Mass loss measured in the experiment and mass loss calculated by the model and VessFire.

The mass loss, indicated by the experimental results by Moodie et al, decreases below zero and varies through the initial time period. According to Moodie et al, the tank was placed on four supports, in order to weigh the total system mass throughout the duration of the experiment. The weighing system is reported to have an overall accuracy of ± 10 kg, and will also be affected by the thrust produced by the PSV opening. No further explanation is given by Moodie et al to account for the experimental results.

Experiment by Birk et al

The second validation experiment was conducted by Birk et al in 2005 [19], where a 500 gallon propane tank was subjected to a 25% engulfing hydrocarbon fire. The fire was designed to simulate a pool fire which affects both the gas and liquid area of the tank. Rupture of the tank occurs after 8 minutes in the experiment. The validation comparison is done for a fill level of 80%. Table 5.4 shows the test conditions which is used as input data for the model and VessFire. The composition in the model is set to 50% propane, 49% n-butane, and 1% nitrogen.

The data for the background and peak heat load used in the experiment are not accessible, as the heat load in the experiment was highly affected by the wind conditions. The experiment set out to achieve a heat load corresponding to 25% of a fully engulfing pool fire. Therefore, the heat load should be close to a fourth

Operation pressure	7.8 bara
Operation temperature	14 °C
Outer diameter	0.953 m
Length	3.07 m
Wall thickness	7.4 mm
Liquid height (80% fill level)	0.71 m
PSV area	$1.77 \cdot 10^{-4} \text{ m}^2$
PSV set pressure	27.3 bara
PSV reset pressure	24.9 bara

Table 5.4: Test conditions for experiment 2, which are used as input data for the model and VessFire.

of the normal value of a pool fire (100 kW/m^2). The heat load in the model is adjusted such that the pressure increase in the model fits that of the experiment. The modelled heat load is found to be 39 kW/m^2 . Fluid and wall temperature of the experiment are compared with the model predictions, based on this heat load assumption.

Figure 5.20 shows the pressure measured in the experiment and the adjusted model pressure.

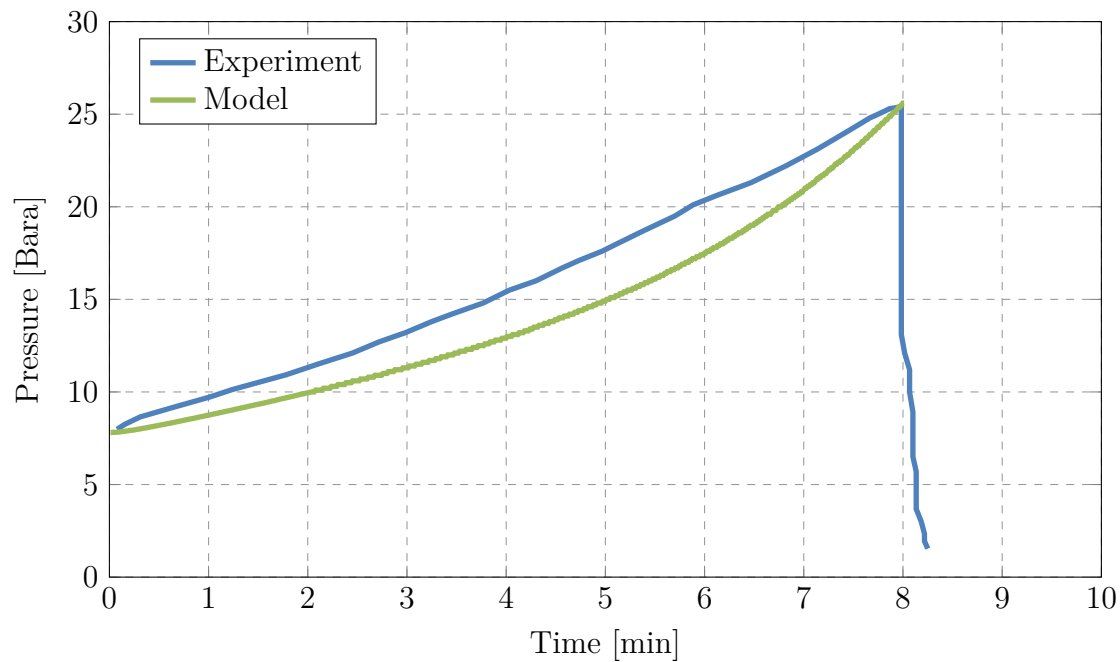


Figure 5.19: Pressure measured in the experiment and pressure calculated by the model.

The heat load is not known from the experiment, and in order to fit the pressure curve properly, the heat load as function of time would be needed to iterate through. As an alternative, the heat load is set constant and the temperature results from the experiment is compared to that of the model predictions.

Figure 5.20 shows the measured fluid temperature from the experiment and the fluid temperatures calculated by the model. The gas temperature is in the experiment measured with a single thermocouple, and the liquid temperature is measured with a range of 15 thermocouples placed at different depths. The thermocouples are in the experiment referred to as ladings.

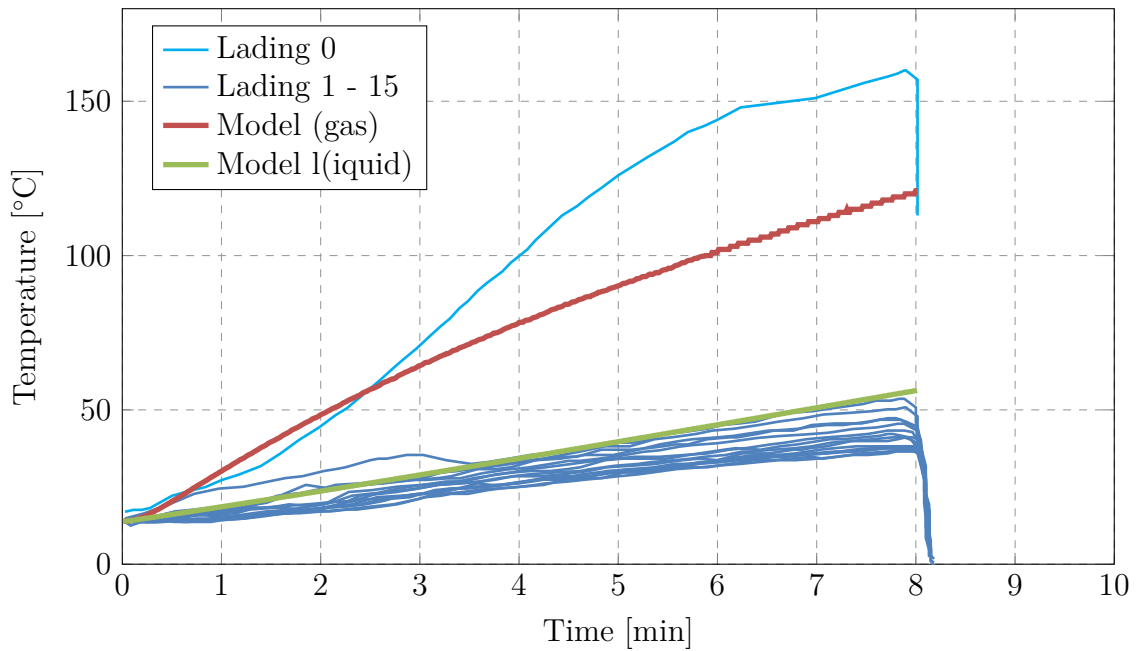


Figure 5.20: Fluid temperatures measured in the experiment and fluid temperatures calculated by the model.

The temperatures in figure 5.20 are within the same range, except significant deviations in the prediction of the gas temperature beyond 3 minutes. The gas temperature is only measured by one thermocouple at a single location, which may not give a fulfilling reflection of reality. If stratification have occurred, as previously illustrated in figure 5.15, this could indicate that the modeled gas temperature more closely resembles an accurate average of the temperature.

Figure 5.21 shows the measured wall temperatures from the experiment and the wall temperature calculated by the model. The wall temperatures are in the experiment measured for a range of thermocouples on the wall of the gas phase, and for a range of thermocouples on the wall of the liquid phase.

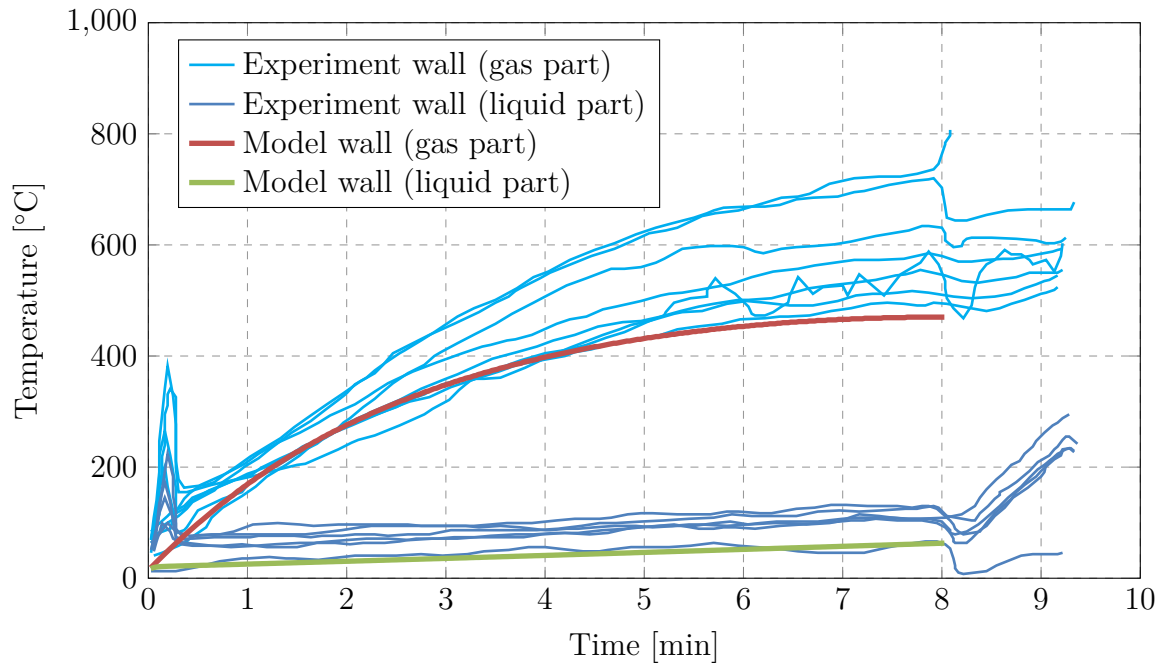


Figure 5.21: Wall temperatures measured in the experiment by Birk et al, and wall temperatures calculated by the model.

As the peak heat load was not given by Birk et al, the heat load used in the model is that of pool fire of 150 kW/m^2 . The temperatures modelled is in the lower range of those given by the experiment. The heat load is not given, and could vary in time, and more information about the vessel material should be implemented in the model, in order to more accurately predict the wall temperatures.

The model also predicts a rupture time, but the calculations are based on the yield strength of the material, which is not given in the experiment. The model can predict a rupture time of 8 min, if the yield strength is set to 350 MPa. Many of the factors involved in the rupture prediction is not present, and more care should be taken before validating the rupture prediction.

Overall, the model is judged to fit the experimental data well, and the model is able to predict the pressure increases, fluid temperatures, and wall temperature to a certain extent. The precision of the model could be improved upon by performing more rigorous calculations or resolve more of the physical phenomena, to achieve more detailed predictions of system variables, such as pressure, temperature, and heat transfer. The validation process could be improved by validating against a wider range of operating conditions. Experiments that can be used for validation of this type of application are sparse, and more experiments should be done on offshore pressure vessels with hydrocarbons.

5.3 Comparison of stationary and dynamic sizing for pressure safety valves

According to the API 520 standard [12], the sizing of a PSV should be done by the steady state sizing equations, as described in section 2.4.1 page 22.

Using the stationary equation, see equation 2.4 page 23, and equation 2.8 page 24, the heat transfer could be incorrectly determined, and consequently it could be advantageous to apply a detailed and dynamic model to fire scenario problems.

The advantage of using a dynamic model is the incorporation and coupling of various variables, all influencing the required release rate. The disadvantage is the need of time and computational resources, and an increased level of complexity. Additionally not all data might be available to perform a detailed modelling, and in those cases the stationary equation might be adequate or simply the only possible choice. Two type of errors is possible when applying the stationary sizing equation, either the PSV size is overestimated or underestimated. Initially the worst error would be to underestimate the size, and thus risking a rupture. If the PSV size is overestimated, it would lead to increased cost in installation, maintenance, and the additionally required infrastructure, such as increased flare capacity, or unwanted operation characteristic such as chatter.

Table 5.5 illustrates different PSV sizes obtained by stationary sizing equations, and dynamic modelling. The presented cases have been selected as representative of typical offshore installations. The data have been supplied by Rambøll, and is thus valid solutions in reality.

Cases 1-5 are based on vessels in table 4.1 page 30. Case 1 is the "2nd stage separator", case 2 is the "3rd stage separator", case 3 is the "Test separator", case 4 is the "Butane vessel", and case 5 is the "1st stage separator". Cases 6-11 are based on case 5, with variations in length, diameter and pressure. Case 6 have increased length by 50%, and case 7 by 100%. Case 8 have increased diameter by 50%, and case 9 by 100%. Case 10 have increase pressure by 50%, and case 11 by 100%. Case 12 has the same vessel dimensions as case 5, and the composition consists of the 5 light hydrocarbons, methane, ethane, propane, n-butane, and n-pentane.

When a case scenario is modelled, in order to determine whether a given PSV size is adequate or not, it will be necessary to predefine a "properly sized" criterion. The criterion is, in the cases presented, met when the PSV is sized such that the vessel pressure is kept below the given maximum set pressure, for the duration of 60 minutes. The criterion may be set differently and consequently increase or decrease the necessary PSV size, according to the dynamic sizing method.

Case no.	Vessel	Stationary	Dynamic
1	2nd stage separator	L	L
2	3rd stage separator	K	G
3	Test separator	J	H
4	Propane/n-butane tank	K	P
5	1st stage separator	K	E
6	1st stage separator (L+50%)	L	E
7	1st stage separator (L+100%)	M	F
8	1st stage separator (D+50%)	L	G
9	1st stage separator (D+100%)	L	K
10	1st stage separator (P+50%)	K	G
11	1st stage separator (P+100%)	J	E
12	1st stage separator (light hydrocarbons)	J	N

Table 5.5: PSV sizes based on stationary sizing equations, and dynamic modelling, in letter designations.

The data in table 5.5 is presented by the equivalent area in figure 5.22. The area relating to a designated category letter is indicated in table C.1 appendix C.

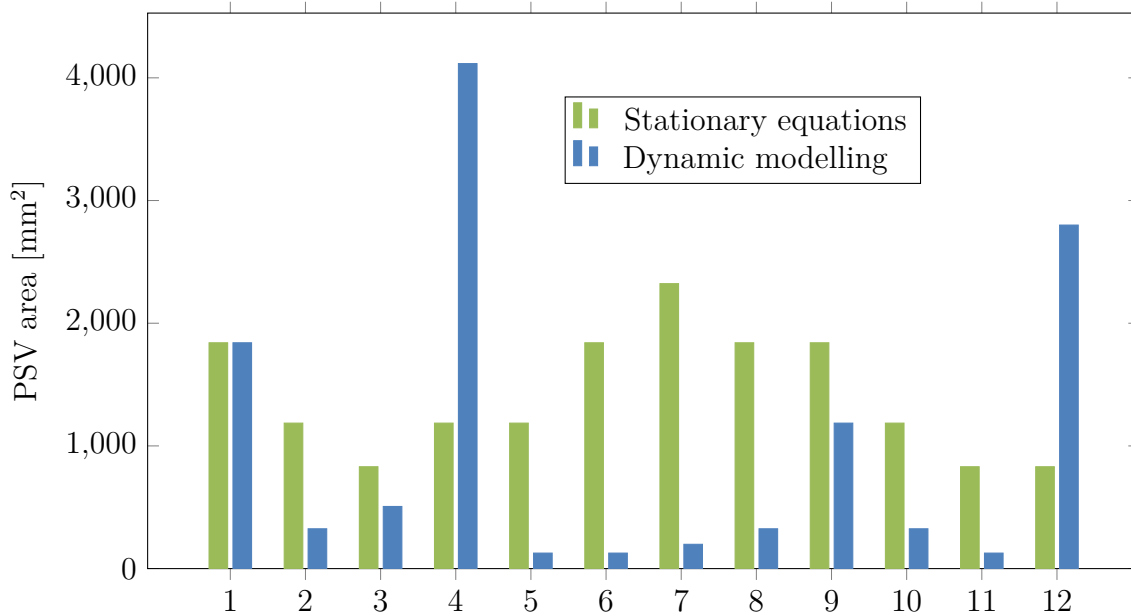


Figure 5.22: PSV sizes based on stationary sizing equations, and dynamic modelling.

In the majority of cases represented in figure 5.22 the PSV size is oversized by the stationary equations, while only two are undersized, and one is sized appropriately, when comparing stationary and dynamic sizing methods. As the PSV sizes are categorized in letter designations, case 1 may in reality differ in the required PSV orifice area, as predicted by the two methods.

The two cases 4, and 12 indicate that the stationary sizing equations underestimate the required PSV size. The main difference of cases 4, and 12, in regards to the other cases presented, are the compositions, which mainly consist of light hydrocarbons.

No clear tendency is present in the differences of estimations by the stationary sizing equations and dynamic sizing method. Some of the cases have been underestimated, and as such the stationary sizing equations can not exclusively be used as conservative estimation methods. Care should thus be taken when a conservative estimate is needed. Multiple variables influence the PSV sizing and thus the exact scenarios in which the stationary sizing equations will predict PSV sizes conservatively can not be established.

6 Conclusion

The project sets out to investigate the effectiveness of a PSV, when a fire affects the gas part of an offshore pressure vessel. The effect of a PSV can be limited in this scenario, as pointed out by API 521 [2]. The investigation was done by conducting a case study of simulations to map the effect of a PSV as fire protection. If a PSV is required on a vessel, then it needs to be properly sized. The sizing of a fire PSV was investigated by developing a dynamic model, which can be used to determine the maximum relief rate.

6.1 Case study

The case study is based on simulations done for six pressure vessels located on an offshore production platform, and a propane/n-butane tank. The results of the case study is therefore not universal for all pressure vessel, and care should be taken before applying the conclusions for different types of vessels.

VessFire was used as a tool to conduct the simulations for the case study. The results of VessFire have been validated by other authors [25]. It is assumed that the results are a good estimate of the rupture times for the vessels, even though VessFire is not a perfect simulation tool, and results may deviate from reality. Therefore, for better results regarding the dynamics of a pressure vessel, being exposed to a fire, experiments could be conducted. This would be time consuming and expensive to do for a vast range of pressure vessels, and the deviation obtained by using a simulation software is consequently accepted.

The results obtained from the case study show similar results for all pressure vessels, as long as the vessels contain liquid. The 1st stage separator is therefore chosen as a representative case of a pressure vessel. Figure 6.1 show the rupture time of the 1st stage separator exposed to a small jet fire, a large jet fire, and a pool fire, with and without a PSV.

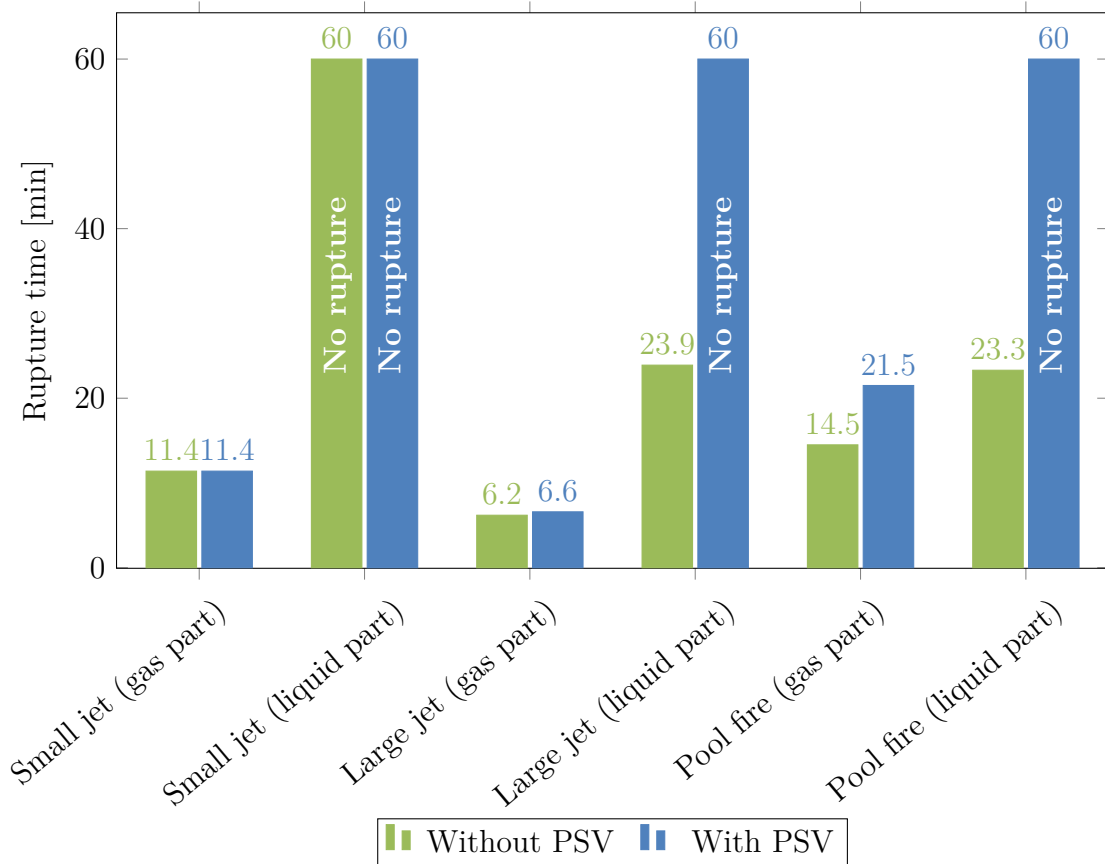


Figure 6.1: Rupture time for the 1st stage separator, with and without a PSV, when exposed to various fire scenarios. The results in the figure are found in section 4.2.

As seen in figure 6.1, the PSV is able to relieve the pressure, when the vessel is affected by a fire on the wetted area. The heat transfer coefficient for the liquid is large enough to keep the vessel wall cool and avoid rupture. The PSV offers little additional protection when the fire affects the unwetted part of the vessel. The peak heat load of the fire causes a local increase in temperature, which leads to rupture of the vessel, for small jet fire, large jet fire, and pool fire.

Alternatives to a PSV has been investigated. Blowdown of the vessel inventory was able to protect the 1st stage separator from rupture in all cases, except for the large jet fire affecting the gas part. This indicates that a BDV is able to prevent rupture of the pressure vessel in a majority of the fire scenarios.

A case with PFP on the 1st stage separator is also investigated. Layers of 50 mm, 100 mm, and 200 mm rock wool insulation was applied to the vessel. PFP was able to avoid rupture in all cases except for when a large jet fire affects the gas part of the vessel. PFP was, in the case of the large jet fire on the gas part, able to significantly extend the rupture time, and by applying a thick enough layer of

insulation, PFP was able to prevent rupture. This indicates that PFP is a possible solution in preventing rupture due to a fire, especially on the unwetted part of the vessel, but increasing the insulation thickness might not be a practical solution.

A PSV will protect the vessel from rupture when exposed to a fire on the wetted part of the vessel. A PSV will not have an effect when the vessel is exposed to a fire on the unwetted part of the vessel. This is especially a problem for completely gas filled vessels.

Increasing the wall thickness of the vessel can reduce the risk of rupture, especially for low peak heat loads. This is properly not an economically viable solution. The added weight of the vessel will require additional infrastructure and thus additional costs.

PFP can protect the vessel against all fires, but jet fires may erode the PFP, and PFP also have increased risk of corrosion and inspection problems.

BDV can protect a vessel from rupture by evacuating the inventory and lower the pressure. This is true for all fire cases, except a large jet fire affecting the unwetted part of the vessel. However, if a vessel ruptures, the pressure will be lower and the risk of a catastrophic BLEVE will be reduced.

The API guidelines for a fire PSV is originally designed for onshore refineries, for which the risk of a liquid pool spill is greater than that for an offshore production platform. The offshore production platforms generally contains more gas volumes, and thus the risk of a jet fire offshore is greater. The peak heat load of a pool fire will in most cases likely affect the liquid part of the exposed vessel, while the peak heat load of a jet fire is at equal risk of affecting either the liquid part or the gas part. Offshore pressure vessels are therefore more likely to be affected by jet fires on the gas part, and thus a PSV is more likely to not be effective.

Additionally, the results of the case study conducted, indicates that the PSV does not have a significant safety effect in this scenario, and the usefulness of a PSV is therefore limited.

According to API Standard 521 [2], it can be appropriate to use other protective measures as an alternative to a PSV, to protect against rupture from a fire exposure, if local jurisdiction permits it, and an engineering analysis indicates that the PSV only serves little or no value in reducing the likelihood of a vessel rupture.

Based on the findings in the case study, the BDV would in many cases be a way of avoiding rupture and subsequent disaster. A well designed blowdown process or even PFP could be considered as an alternative to a fire PSV.

This would also give a inherently safer design by removing the PSV, and utilizing an alternative, by having less components in the overall system.

The likelihood of all fire scenarios, including the vessel part affected, should be

taken into consideration, when deciding on either removing or replacing a PSV with an alternative. The PSV has the advantage of being a mechanical device, and does not need a support system from an electrical control system. A BDV has the advantage of being controllable either by an automatic system or manually. The disadvantage is however linked, as it is dependent on proper communication from the electrical system, and accurate sensor response. The PFP is neither controllable nor dependent on any sensors or mechanical action, as it is simply a passive safety barrier. The disadvantage is its lack of capability to withstand the momentum of a jet fire for a prolonged period of time, and as it covers all, or a part of a vessel, it limits the effectiveness of corrosion inspections.

As suggested by API 521 [2], each scenario problem should be individually assessed and engineering experience should be applied.

6.2 Sizing of pressure safety valves

If the PSV is oversized or undersized, it will have undesirable effects, for safety as well as economical considerations, and thus it is important that the PSV is properly sized. Oversizing leads to larger diameter for PSV lead and tail pipes with increased cost, and increased risk of PSV chatter with possible failure of the PSV. Undersizing gives false protection. The standard stationary sizing procedure is compared with a more detailed dynamic sizing method proposed in the project.

Stationary sizing method

In order to predict an appropriate PSV size using a stationary equation method, the heat of vaporisation and the heat load for the vessel will have to be estimated. The equation suggested by API 521 [2], to estimate the heat load, can be used in combination with the stationary sizing method, however it does not give any credit to insulation, wall material or wall thickness. The stationary sizing method does not take into consideration the change of state variables throughout the duration of the system, and as such the PSV will only be sized according to initial conditions. This further impedes the applicability of the stationary equation sizing methods, in regards to fire case scenarios.

Due to these assumptions and simplifications the sizing of a PSV, by the use of stationary sizing equation method, can be problematic.

Dynamic sizing method

The PSV size is determined by a rigorous dynamic model which predict the maximum PSV flow, based on thermodynamics and heat transfer to the vessel. This gives a better prediction of the rate of vaporisation and ensures that the PSV is

sized adequately for the entire duration of the fire scenario.

Several assumptions have been made when developing the model described in section 5. The assumptions are influencing definitions of geometry, fluid calculations, and heat transfer.

The heat transfer to the vessel is based on known equations, with assumptions, such that the equations can be applied to the practical problem of heat transfer from a flame. Additionally, the assumed energy transfer, at initial conditions, is based on standards and guidelines available in the oil and gas industry. This generalisation is useful in its applicability to a wide range of scenarios, but the accuracy in representing reality is not universal. The model assumes a view factor of unity, and thus all flame scenarios modeled will be assumed to be engulfing. The convective heat transfer coefficient is equally defined, based on guidelines and generalisations regarding flame scenarios, and could in reality vary considerably, as the surrounding air velocity highly affects the convective heat transfer.

The heat transfer through the vessel wall is modeled with assumptions of one-dimensionality, in the case of background heat load. It is effectively assumed that the vessel is infinite in the longitudinal direction, and the heat load is uniformly distributed in the circumferential and longitudinal directions. The vessel ends is not assumed to absorb or emit any heat, from the surroundings and vessel wall. The wall area affected by the peak heat load is calculated in three dimensions, with the boundary conditions in the circumferential and longitudinal direction given as Neumann boundary conditions.

The heat transfer from the wall to the gas is estimated, based on the application of vertical and horizontal plate equations. The heat transfer taking place between the wall and liquid, and the heat transfer taken place in the interface between the liquid and gas phase is equally calculated based on assumptions. The assumptions are crude, in comparison to fully developed CFD analysis, but are far more simpler, and requires less computational resources. Furthermore, the simple modeling method requires less input data, and knowledge of the flow condition of the vessel.

The gas phase, and liquid phase temperatures are assumed to be uniform, which in reality will be a good approximation for well mixed fluids. The liquid is assumed to consist of liquid hydrocarbons and water, which are perfectly mixed. This assumption could be a disadvantage when modeling a scenario concerning a three phase separator. In experiments presented by Birk [9] it is normal to observe temperature stratification and temperature gradients throughout the fluid inventory. This will also result in boundary layers, which in turn will affect the entire dynamics of the vessel system.

The stratification can cause the PSV to open sooner than if it was destratified, and thus the possible energy to be released in a rupture will be less, and the risk of a rupture becoming a BLEVE is minimized. When the PSV opens, it will cause

destratification of the temperature in liquid [9].

The model was validated with an experiment done by Moodie et al [24]. The model is able to predict the pressure rise in the vessel acceptably. The pressure change caused when the PSV opens differs from the experiment, but is similar to that calculated in VessFire. The periodic opening of the PSV, and the duration of the PSV opening, is greater than that of VessFire. This could indicate that the heat input to the fluid is excessive, compared to the experiment and VessFire, which increases the pressure more rapidly and keeps the PSV open longer. The model predicts the liquid temperature acceptably, but the gas temperature show strong stratification in the experiment, whereas the model predicts an average temperature of the gas. The maximum wall temperature of the vessel is underestimated compared to the experiment and VessFire.

The model is capable of performing simulations on horizontal vessels containing gas and liquid. VessFire is, as a tool, more complex and able to handle a wider range of cases, materials, and scenarios, including piping. The model described in this report is valid for a rather specific set of cases, but can be modified to handle various situations if needed. The model can predict the pressure, temperature, and stresses of a vessel, and is therefore fit to be used to model the depressurerisation of a vessel exposed to a fire.

Comparison of stationary and dynamic sizing methods

The stationary sizing method and dynamic sizing method have been compared for various cases, and no consequential deviation of the stationary sizing method can be defined.

Some of the cases have been underestimated, and as such the stationary sizing equations can not exclusively be used as a conservative estimation method. The cases being underestimated contained mainly light hydrocarbons in liquid and gas form. The undersized PSV is especially problematic and a dynamic sizing should therefore always be used for vessels containing light hydrocarbons.

For most of the cases regarding offshore vessels, the stationary sizing oversized the PSV. This leads to increased cost and can be optimized.

The stationary equation sizing method, in regards to fire case scenarios, should mainly be used when adequate knowledge exists, in regards to the heat load and latent heat of vaporisation, and thus a good estimate of the mass flow can be obtained.

Bibliography

- [1] API Standard 14C. *Recommended Practice for Analysis, Design, Installation, and Testing of Basic Surface Safety Systems for Offshore Production Platforms*. American Petroleum Institute, 2007.
- [2] API Standard 521. *Pressure-relieving and Depressuring Systems*. American Petroleum Institute, 2014.
- [3] The Guardian Terry Macalister. Piper Alpha disaster: How 167 oil rig workers died. <http://www.theguardian.com/business/2013/jul/04/piper-alpha-disaster-167-oil-rig>.
- [4] BBC News. <http://www.bbc.com/news/uk-scotland-22840445>.
- [5] VessFire. *A Calculation System for Blowdown of Process Segments and Process Equipment Exposed and Unexposed to Fire*. Petrell, 2005.
- [6] Scandpower. *Guidelines for the Protection of Pressurised Systems Exposed to Fire*. Scandpower Risk Management AS, 2004.
- [7] Natural Gas Asia. <http://www.naturalgasasia.com/bp-inpex-eni-get-indonesia-oil-gas-blocks-3622>.
- [8] Latest News Link. <http://latestnewslink.com/2015/02/rail-cars-on-fire-after-crude-train-derails-in-ontario-cn-says/>.
- [9] A. M. Birk. Scale effects with fire exposure of pressure-liquefied gas tanks. *Journal of Loss Prevention in the Process Industries*, 8(5), 1995.
- [10] A.M. Birk. Recent Fire Testing and BLEVE Research at Queen's University. <http://me.queensu.ca/People/Birk/Research/ThermalHazards/bleve/FieldTrials2000-2002.html>.
- [11] Nicholas P. Cheremisinoff. *Industrial Gas Flaring Practices*. Wiley & Scrivener Publishing, 2013.
- [12] API Standard 520. *Sizing, Selection, and Installation of Pressure-relieving Devices*. American Petroleum Institute, 2014.
- [13] G. Dalzell and A. Chesterman. Nothing, is safety critical. *Process Safety and Environmental Protection*, (0957-5820), 1997.
- [14] Ann Fenech, Tom Fearn, and Matija Strlic. Use of design-of-experiment principles to develop a dose-response function for colour photographs. *Polymer Degradation and Stability*, (97), 2012.

- [15] Yunus A. Çengel and Afshin J. Ghajar. *Heat and mass transfer - Fundamentals and Applications*. McGraw-Hill, 2011.
- [16] James L. Milton and William P. Goss. Stability criteria for explicit finite difference solutions of the parabolic diffusion equation with non-linear boundary conditions. *International journal for numerical methods in engineering*, (7), 1973.
- [17] EUROPEAN STANDARD. *Eurocode 3: Design of steel structures - Part 1-2: General rules - Structural fire design*. 2005.
- [18] Saburô Umino. On the specific heat of carbon steel. *Sci. Rep. Vol XV. No.3, p. 331*.
- [19] A. M. Birk, D. Porier, and C. Davison. On the response of 500 gal propane tanks to a 25% engulfing fire. *Journal of Loss Prevention in the Process Industries*, (19), 2006.
- [20] Dr. Geir Berge and Harald Olstad. Experimental study and simulation on heat exposed liquid filled process equipment. *24th International Conference on Offshore Mechanics and Arctic Engineering*, 2005.
- [21] Warren M. Rohsenow. *A method of correlating heat transfer data for surface boiling of liquids*. Massachusetts Institute of Technology, 1951.
- [22] Committee for the Prevention of Disasters. *Methods for the calculation of physical effects, Third edition*. 1997.
- [23] ASME Boiler and Pressure Vessel Code. *Rules for Construction of Pressure Vessels*. American Society of Mechanical Engineers, 2013.
- [24] K. Moodie, L.T. Cowley, R.B. Denny, L.M. Small, and I. Williams. Fire engulfment tests on a 5 tonne LPG tank. *Journal of Hazardous Materials*, (20), 1988.
- [25] VessFire. *Validation of VessFire*. Petrell, 2009.
- [26] ASME Boiler and Pressure Vessel Code. *Section II Part D Properties*. American Society of Mechanical Engineers, 2007.
- [27] F-Chart Software. *Engineering Equation Solver*, 2014.

A Appendix: Steam and liquid sizing equations

Steam relief

For the case of steam relieving equation A.1 will be used to determine the effective discharge area.

$$A = \frac{190.5 \cdot W}{P_1 \cdot K_d \cdot K_b \cdot K_c \cdot K_N \cdot K_{SH}} \quad (\text{A.1})$$

- K_N is the correction factor for the Napier equation, concerning steam loss through an orifice [12].
- K_{SH} is the superheat correction factor, applicable for temperatures above 1,200 °F (650 °C).

Liquid relief

For the special case of liquid relief equation A.2 will be used to determine the effective discharge area.

$$A = \frac{11.78 \cdot Q}{K_d \cdot K_w \cdot K_C \cdot K_V} \sqrt{\frac{G_l}{P_1 - P_2}} \quad (\text{A.2})$$

- Q is the flow rate. [L/min]
- K_V is the correction factor due to viscosity.
- G_l is the specific gravity of the liquid in relation to water at standard conditions.

B Appendix: Vessel inventory

Name	Symbol	1st stage separator Mole %	2nd stage separator Mole %	3rd stage separator Mole %	Test separator Mole %	IP suction drum Mole %	NGL KO drum Mole %	Butane vessel Mole %
Nitrogen	N ₂	0.07	0.01			0.07	0.33	0.34
Hydrogen sulfide	H ₂ S							
Carbon dioxide	CO ₂	0.31	0.12	0.07	0.31	1.39	1.43	
Water	H ₂ O	71.64	56.4	39.8	71.64	1.18		
Methane	C1	17.15	3.46	1.41	17.15	77.63	80.58	
Ethane	C2	2.15	1.41	1.28	2.15	9.45	9.47	
Propane	C3	1.47	2.06	3.86	1.47	5.84	5.37	50.0
i-Butane	iC4	0.18	0.40	0.83	0.18	0.60	0.49	
n-Butane	nC4	0.71	1.80	3.75	0.71	2.07	1.57	50.0
i-Pentane	iC5	0.21	0.74	1.39	0.21	0.42	0.26	
n-Pentane	nC5	0.34	1.28	2.33	0.34	0.59	0.33	
n-Hexane	nC6	0.45	2.08	3.23	0.45	0.37	0.14	
n-Heptane	nC7							
n-Octane	nC8							
n-Nonane	nC9							
n-Decane	nC10							
Pseudo	C7_C13	2.38	13.41	18.65	2.38	0.13		
Pseudo	C14_C18	1.01	5.82	8.08	1.01			
Pseudo	C19_C26	0.95	5.46	7.57	0.95			
Pseudo	C27_C37	0.59	3.42	4.74	0.59			
Pseudo	C38_C80	0.37	0.37	2.99	0.37			
Total		100%	100%	100%	100%	100%	100%	100%

Table B.1: Pressure vessel hydrocarbon composition.

C Appendix: Equivalent PSV size

Table C.1 shows different PSV sizes in the custom designation, imperial units, and SI units.

Custom	in ²	m ²
D	0.110	$7.09676 \cdot 10^{-5}$
E	0.196	$1.26451 \cdot 10^{-4}$
F	0.307	$1.98064 \cdot 10^{-4}$
G	0.503	$3.24515 \cdot 10^{-4}$
H	0.785	$5.06450 \cdot 10^{-4}$
J	1.287	$8.30320 \cdot 10^{-4}$
K	1.838	$1.18580 \cdot 10^{-3}$
L	2.853	$1.84064 \cdot 10^{-3}$
M	3.600	$2.32257 \cdot 10^{-3}$
N	4.340	$2.79999 \cdot 10^{-3}$
P	6.380	$4.11612 \cdot 10^{-3}$
Q	11.050	$7.12901 \cdot 10^{-3}$
R	16.000	$1.03225 \cdot 10^{-2}$
T	26.000	$1.67741 \cdot 10^{-2}$

Table C.1: PSV orifice sizes.

D Appendix: CasePlanner and Grapher

CasePlanner and Grapher are two independent Excel files, designed specifically to alleviate the cumbersome task of batch calculation in VessFire. The two files have been developed alongside the planning and designing process of the batch runs, and is simple referred to as CasePlanner and Grapher in this text.

VessFire can be used in a Graphical User Interface (GUI) environment, for single cases, and in batch mode for multiple case runs. The input files loaded by the GUI environment and the batch mode is the same, and the mode of calculation can thus be interchanged. The input files consists of a particular text string structure, and consequently some values in the files are not necessarily used, but simple present as a text string separator. To fully specify a case, it is necessary to use multiple input files, each files defining various aspects of the scenario, such as the flame heat load distribution, vessel construction, and PSV characteristics [5].

The Excel VBA programming environment has the capability to read and write text files, which is exploited in order to produce multiple input files for multiple cases, for use in the VessFire batch calculations mode. The Excel spreadsheet is used as a normal user interface, while the folder and file generation is performed in the VBA programming environment of Excel.

VessFire has implemented a report generation process in the GUI mode, but none such in the batch mode. The report contains graphs and characteristics such as rupture time. The information is stored in simple text files as output data, and can thus be read by Excel. The result files can thus be loaded into the Grapher file, and all relevant information can be calculated and shown by the built in graph capabilities of Excel. The automatic creation of Excel graphs can also be done by the VBA programming environment, and thus ease the analysis of results.

E Appendix: Thickness of shells under internal pressure

The wall thickness of a pressure vessel can be calculated by equation E.1 [23].

$$t = \frac{P \cdot R}{S \cdot E - 0.6 \cdot P} \quad (\text{E.1})$$

- t is the wall thickness. [m]
- P is the vessel gauge pressure. [MPa]
- R is the vessel radius. [m]
- S is the maximum allowable stress value. [MPa]
- E is the joint efficiency. Assumed: $E=1$.

The maximum allowable stress value is found from equation E.2.

$$S = \frac{UTS}{F_S} \quad (\text{E.2})$$

- UTS - Ultimate Tensile Strength. $UTS=441$ MPa (including 10% safety margin).
- F_S - Factor of safety. Suggested as 3.5, from ASME Boiler and Pressure Vessel Code [26].

F Appendix: CCD simulation plan

Sim. #	X ₁	X ₂	X ₃	X ₄	X ₅	X ₆	X ₇	Point
1	-1	-1	-1	-1	-1	-1	-1	Factorial
2	1	-1	-1	-1	-1	-1	-1	Factorial
3	-1	1	-1	-1	-1	-1	-1	Factorial
4	1	1	-1	-1	-1	-1	-1	Factorial
5	-1	-1	1	-1	-1	-1	-1	Factorial
6	1	-1	1	-1	-1	-1	-1	Factorial
7	-1	1	1	-1	-1	-1	-1	Factorial
8	1	1	1	-1	-1	-1	-1	Factorial
9	-1	-1	-1	1	-1	-1	-1	Factorial
10	1	-1	-1	1	-1	-1	-1	Factorial
11	-1	1	-1	1	-1	-1	-1	Factorial
12	1	1	-1	1	-1	-1	-1	Factorial
13	-1	-1	1	1	-1	-1	-1	Factorial
14	1	-1	1	1	-1	-1	-1	Factorial
15	-1	1	1	1	-1	-1	-1	Factorial
16	1	1	1	1	-1	-1	-1	Factorial
17	-1	-1	-1	-1	1	-1	-1	Factorial
18	1	-1	-1	-1	1	-1	-1	Factorial
19	-1	1	-1	-1	1	-1	-1	Factorial
20	1	1	-1	-1	1	-1	-1	Factorial
21	-1	-1	1	-1	1	-1	-1	Factorial
22	1	-1	1	-1	1	-1	-1	Factorial
23	-1	1	1	-1	1	-1	-1	Factorial
24	1	1	1	-1	1	-1	-1	Factorial
25	-1	-1	-1	1	1	-1	-1	Factorial
26	1	-1	-1	1	1	-1	-1	Factorial
27	-1	1	-1	1	1	-1	-1	Factorial
28	1	1	-1	1	1	-1	-1	Factorial
29	-1	-1	1	1	1	-1	-1	Factorial
30	1	-1	1	1	1	-1	-1	Factorial
31	-1	1	1	1	1	-1	-1	Factorial
32	1	1	1	1	1	-1	-1	Factorial
33	-1	-1	-1	-1	-1	1	-1	Factorial
34	1	-1	-1	-1	-1	1	-1	Factorial
35	-1	1	-1	-1	-1	1	-1	Factorial
36	1	1	-1	-1	-1	1	-1	Factorial
37	-1	-1	1	-1	-1	1	-1	Factorial
38	1	-1	1	-1	-1	1	-1	Factorial
39	-1	1	1	-1	-1	1	-1	Factorial
40	1	1	1	-1	-1	1	-1	Factorial

Table F.1: Quantitative variable simulation plan. Part one.

Sim. #	X ₁	X ₂	X ₃	X ₄	X ₅	X ₆	X ₇	Point
41	-1	-1	-1	1	-1	1	-1	Factorial
42	1	-1	-1	1	-1	1	-1	Factorial
43	-1	1	-1	1	-1	1	-1	Factorial
44	1	1	-1	1	-1	1	-1	Factorial
45	-1	-1	1	1	-1	1	-1	Factorial
46	1	-1	1	1	-1	1	-1	Factorial
47	-1	1	1	1	-1	1	-1	Factorial
48	1	1	1	1	-1	1	-1	Factorial
49	-1	-1	-1	-1	1	1	-1	Factorial
50	1	-1	-1	-1	1	1	-1	Factorial
51	-1	1	-1	-1	1	1	-1	Factorial
52	1	1	-1	-1	1	1	-1	Factorial
53	-1	-1	1	-1	1	1	-1	Factorial
54	1	-1	1	-1	1	1	-1	Factorial
55	-1	1	1	-1	1	1	-1	Factorial
56	1	1	1	-1	1	1	-1	Factorial
57	-1	-1	-1	1	1	1	-1	Factorial
58	1	-1	-1	1	1	1	-1	Factorial
59	-1	1	-1	1	1	1	-1	Factorial
60	1	1	-1	1	1	1	-1	Factorial
61	-1	-1	1	1	1	1	-1	Factorial
62	1	-1	1	1	1	1	-1	Factorial
63	-1	1	1	1	1	1	-1	Factorial
64	1	1	1	1	1	1	-1	Factorial
65	-1	-1	-1	-1	-1	-1	1	Factorial
66	1	-1	-1	-1	-1	-1	1	Factorial
67	-1	1	-1	-1	-1	-1	1	Factorial
68	1	1	-1	-1	-1	-1	1	Factorial
69	-1	-1	1	-1	-1	-1	1	Factorial
70	1	-1	1	-1	-1	-1	1	Factorial
71	-1	1	1	-1	-1	-1	1	Factorial
72	1	1	1	-1	-1	-1	1	Factorial
73	-1	-1	-1	1	-1	-1	1	Factorial
74	1	-1	-1	1	-1	-1	1	Factorial
75	-1	1	-1	1	-1	-1	1	Factorial
76	1	1	-1	1	-1	-1	1	Factorial
77	-1	-1	1	1	-1	-1	1	Factorial
78	1	-1	1	1	-1	-1	1	Factorial
79	-1	1	1	1	-1	-1	1	Factorial
80	1	1	1	1	-1	-1	1	Factorial
81	-1	-1	-1	-1	1	-1	1	Factorial
82	1	-1	-1	-1	1	-1	1	Factorial
83	-1	1	-1	-1	1	-1	1	Factorial
84	1	1	-1	-1	1	-1	1	Factorial
85	-1	-1	1	-1	1	-1	1	Factorial
86	1	-1	1	-1	1	-1	1	Factorial
87	-1	1	1	-1	1	-1	1	Factorial
88	1	1	1	-1	1	-1	1	Factorial
89	-1	-1	-1	1	1	-1	1	Factorial
90	1	-1	-1	1	1	-1	1	Factorial
91	-1	1	-1	1	1	-1	1	Factorial
92	1	1	-1	1	1	-1	1	Factorial
93	-1	-1	1	1	1	-1	1	Factorial

Table F.2: Quantitative variable simulation plan. Part two.

Sim. #	X ₁	X ₂	X ₃	X ₄	X ₅	X ₆	X ₇	Point
94	1	-1	1	1	1	-1	1	Factorial
95	-1	1	1	1	1	-1	1	Factorial
96	1	1	1	1	1	-1	1	Factorial
97	-1	-1	-1	-1	-1	1	1	Factorial
98	1	-1	-1	-1	-1	1	1	Factorial
99	-1	1	-1	-1	-1	1	1	Factorial
100	1	1	-1	-1	-1	1	1	Factorial
101	-1	-1	1	-1	-1	1	1	Factorial
102	1	-1	1	-1	-1	1	1	Factorial
103	-1	1	1	-1	-1	1	1	Factorial
104	1	1	1	-1	-1	1	1	Factorial
105	-1	-1	-1	1	-1	1	1	Factorial
106	1	-1	-1	1	-1	1	1	Factorial
107	-1	1	-1	1	-1	1	1	Factorial
108	1	1	-1	1	-1	1	1	Factorial
109	-1	-1	1	1	-1	1	1	Factorial
110	1	-1	1	1	-1	1	1	Factorial
111	-1	1	1	1	-1	1	1	Factorial
112	1	1	1	1	-1	1	1	Factorial
113	-1	-1	-1	-1	1	1	1	Factorial
114	1	-1	-1	-1	1	1	1	Factorial
115	-1	1	-1	-1	1	1	1	Factorial
116	1	1	-1	-1	1	1	1	Factorial
117	-1	-1	1	-1	1	1	1	Factorial
118	1	-1	1	-1	1	1	1	Factorial
119	-1	1	1	-1	1	1	1	Factorial
120	1	1	1	-1	1	1	1	Factorial
121	-1	-1	-1	1	1	1	1	Factorial
122	1	-1	-1	1	1	1	1	Factorial
123	-1	1	-1	1	1	1	1	Factorial
124	1	1	-1	1	1	1	1	Factorial
125	-1	-1	1	1	1	1	1	Factorial
126	1	-1	1	1	1	1	1	Factorial
127	-1	1	1	1	1	1	1	Factorial
128	1	1	1	1	1	1	1	Factorial
129	0	0	0	0	0	0	0	Center
130	-1	0	0	0	0	0	0	Axial
131	1	0	0	0	0	0	0	Axial
132	0	-1	0	0	0	0	0	Axial
133	0	1	0	0	0	0	0	Axial
134	0	0	-1	0	0	0	0	Axial
135	0	0	1	0	0	0	0	Axial
136	0	0	0	-1	0	0	0	Axial
137	0	0	0	1	0	0	0	Axial
138	0	0	0	0	-1	0	0	Axial
139	0	0	0	0	1	0	0	Axial
140	0	0	0	0	0	-1	0	Axial
141	0	0	0	0	0	1	0	Axial
142	0	0	0	0	0	0	-1	Axial
143	0	0	0	0	0	0	1	Axial

Table F.3: Quantitative variable simulation plan. Part three.

G Derivation of stability criteria

This chapter will provide the derivation of the numerical stability criterion of the transient heat transfer equations in 1-D and 3-D. In the following, some common definitions are presented which are used in the derivations.

$$\tau_r = \frac{\alpha \cdot \Delta t}{\Delta r^2} \quad (\text{G.1})$$

$$\tau_\varphi = \frac{\alpha \cdot \Delta t}{(r_m \Delta \varphi)^2} \quad (\text{G.2})$$

$$\tau_z = \frac{\alpha \cdot \Delta t}{\Delta z^2} \quad (\text{G.3})$$

$$\alpha = \frac{k}{\rho c_p} \quad (\text{G.4})$$

1-D inner node stability criterion, in cylindrical coordinates

The discretized equation of 1-D heat transfer is given from equation 5.9 page 57 as:

$$T_m^i = T_m^{i-1} + \frac{t^i - t^{i-1}}{\rho \cdot c_p} \left(\frac{-k \cdot r_{m-\frac{1}{2}} \left(\frac{T_m^{i-1} - T_{m-1}^{i-1}}{r_m - r_{m-1}} \right) + k \cdot r_{m+\frac{1}{2}} \left(\frac{T_m^{i-1} - T_{m+1}^{i-1}}{r_m - r_{m+1}} \right)}{r_m \cdot (r_{m+\frac{1}{2}} - r_{m-\frac{1}{2}})} \right) \quad (\text{G.5})$$

- m indicates the position of the node.
- i indicates the iteration.

The equation is rewritten in terms of r_m and Δr , $t^i - t^{i-1}$ is set as Δt and the definition of α is applied:

$$T_m^i = T_m^{i-1} + \alpha \Delta t \left(\frac{-(r_m - \frac{1}{2} \Delta r) \left(\frac{T_m^{i-1} - T_{m-1}^{i-1}}{\Delta r} \right) + (r_m + \frac{1}{2} \Delta r) \left(\frac{T_m^{i-1} - T_{m+1}^{i-1}}{-\Delta r} \right)}{r_m \cdot \Delta r} \right) \quad (\text{G.6})$$

The stability criterion is set and only terms with T_m^{i-1} is kept:

$$0 \leq T_m^{i-1} + \alpha \Delta t \left(\frac{-(r_m - \frac{1}{2}\Delta r) \left(\frac{T_m^{i-1}}{\Delta r}\right) - (r_m + \frac{1}{2}\Delta r) \left(\frac{T_m^{i-1}}{\Delta r}\right)}{r_m \cdot \Delta r} \right) \quad (\text{G.7})$$

The coefficients of T_m^{i-1} is kept:

$$0 \leq 1 + \alpha \Delta t \left(\frac{-(r_m - \frac{1}{2}\Delta r) \left(\frac{1}{\Delta r}\right) - (r_m + \frac{1}{2}\Delta r) \left(\frac{1}{\Delta r}\right)}{r_m \cdot \Delta r} \right) \quad (\text{G.8})$$

The numerator in the fraction is rearranged, based on the common factors.

$$0 \leq 1 + \alpha \Delta t \left(- \left(\frac{1}{\Delta r^2}\right) \left(\frac{1}{r_m}\right) \left((r_m - \frac{1}{2}\Delta r) + (r_m + \frac{1}{2}\Delta r) \right) \right) \quad (\text{G.9})$$

The terms of $\frac{1}{2}\Delta r$ with opposite signs cancel out, and $2r_m$ then remains.

$$0 \leq 1 + \alpha \Delta t \left(- \left(\frac{1}{\Delta r^2}\right) \left(\frac{1}{r_m}\right) (2 \cdot r_m) \right) \quad (\text{G.10})$$

Rearranging:

$$0 \leq 1 - 2 \cdot \frac{\alpha \cdot \Delta t}{\Delta r^2} \quad (\text{G.11})$$

The definition of τ_r is applied:

$$0 \leq 1 - 2 \cdot \tau_r \quad (\text{G.12})$$

1-D boundary condition stability criterion, in cylindrical coordinates

The discretized equation of 1-D heat transfer, at the boundary condition, is given from equation 5.17 page 59 as:

$$T_m^i = T_m^{i-1} + \frac{2 \cdot (t^i - t^{i-1})}{\rho \cdot c_P} \left(\frac{r_{m+\frac{1}{2}} k \left(\frac{T_m^{i-1} - T_{m+1}^{i-1}}{r_m - r_{m+1}}\right) - r_m h (T_m^{i-1} - T_{fluid}^{i-1})}{\left(r_{m+\frac{1}{4}}\right) (r_{m+\frac{1}{2}} - r_{m-\frac{1}{2}})} \right) \quad (\text{G.13})$$

The equation is rewritten in terms of r_m and Δr , the stability criterion is set and the coefficients of T_m^{i-1} is kept, and the definition of α is applied:

$$0 \leq 1 + 2\alpha\Delta t \left(\frac{(r_m + \frac{1}{2}\Delta r) \left(\frac{1}{-\Delta r}\right) - r_m \frac{h}{k}}{(r_m + \frac{1}{4}\Delta r) (\Delta r)} \right) \quad (\text{G.14})$$

The definition of τ_r is applied, and the signs of the terms in the fraction is rearranged.

$$0 \leq 1 - 2\tau_r \left(\frac{(r_m + \frac{1}{2}\Delta r) + r_m \frac{h}{k} \Delta r}{(r_m + \frac{1}{4}\Delta r)} \right) \quad (\text{G.15})$$

The two terms of the numerator is split into two fractions:

$$0 \leq 1 - 2\tau_r \left(\frac{(r_m + \frac{1}{2}\Delta r)}{(r_m + \frac{1}{4}\Delta r)} + \frac{r_m \frac{h}{k} \Delta r}{(r_m + \frac{1}{4}\Delta r)} \right) \quad (\text{G.16})$$

The large parentheses are eliminated, and the terms are rearranged:

$$0 \leq 1 - 2\tau_r \left(\frac{r_m + \frac{1}{2}\Delta r}{r_m + \frac{1}{4}\Delta r} \right) - 2\tau_r \frac{h}{k} \Delta r \left(\frac{r_m}{r_m + \frac{1}{4}\Delta r} \right) \quad (\text{G.17})$$

In the case of $r_m \rightarrow \infty$, the fractions will tend towards unity, and thus the stability criterion will resemble that of a wall.

3-D inner node stability criterion, in cylindrical coordinates

The differential equation is defined from equation 5.22 page 61 as:

$$\rho \cdot c_P \frac{\partial T}{\partial t} = \frac{1}{r} \frac{\partial}{\partial r} \left(r \cdot k \frac{\partial T}{\partial r} \right) + \frac{1}{r^2} \frac{\partial}{\partial \varphi} \left(k \frac{\partial T}{\partial \varphi} \right) + \frac{\partial}{\partial z} \left(k \frac{\partial T}{\partial z} \right) \quad (\text{G.18})$$

The equation is discretized, rewritten in terms of r_m and Δr , and the definition of

α is applied:

$$\begin{aligned}
T_m^i &= T_m^{i-1} - \alpha \Delta t \left(\frac{(r_m - \frac{1}{2}\Delta r) \left(\frac{T_m^{i-1} - T_{m-1}^{i-1}}{\Delta r} \right) + (r_m + \frac{1}{2}\Delta r) \left(\frac{T_m^{i-1} - T_{m+1}^{i-1}}{\Delta r} \right)}{r_m \cdot (\Delta r)} \right) \\
& - \alpha \Delta t \left(\left(\frac{1}{r_m^2} \right) \frac{\left(\frac{T_m^{i-1} - T_{m-1}^{i-1}}{\Delta \varphi} \right) + \left(\frac{T_m^{i-1} - T_{m+1}^{i-1}}{\Delta \varphi} \right)}{\Delta \varphi} \right) \\
& - \alpha \Delta t \left(\frac{\left(\frac{T_m^{i-1} - T_{m-1}^{i-1}}{\Delta z} \right) + \left(\frac{T_m^{i-1} - T_{m+1}^{i-1}}{\Delta z} \right)}{\Delta z} \right)
\end{aligned} \tag{G.19a}$$

The stability criterion is set and the coefficients of T_m^{i-1} is kept:

$$0 \leq 1 - \alpha \Delta t \left(\frac{(r_m - \frac{1}{2}\Delta r) \left(\frac{1}{\Delta r} \right) + (r_m + \frac{1}{2}\Delta r) \left(\frac{1}{\Delta r} \right)}{r_m \cdot (\Delta r)} \right) \tag{G.20a}$$

$$- \alpha \Delta t \left(\left(\frac{1}{r_m^2} \right) \frac{\left(\frac{1}{\Delta \varphi} \right) + \left(\frac{1}{\Delta \varphi} \right)}{\Delta \varphi} \right) \tag{G.20b}$$

$$- \alpha \Delta t \left(\frac{\left(\frac{1}{\Delta z} \right) + \left(\frac{1}{\Delta z} \right)}{\Delta z} \right) \tag{G.20c}$$

The terms are rearranged:

$$0 \leq 1 - \frac{2\alpha \Delta t}{\Delta r^2} - \frac{2\alpha \Delta t}{(r_m \Delta \varphi)^2} - \frac{2\alpha \Delta t}{\Delta z^2} \tag{G.21}$$

The definitions of τ_r , τ_φ , and τ_z are applied:

$$0 \leq 1 - 2\tau_r - 2\tau_\varphi - 2\tau_z \tag{G.22}$$

3-D boundary condition stability criterion, in cylindrical coordinates

The equation is discretized, and the definition of α is applied, and sign of the numerator is rearranged:

$$\begin{aligned}
T_m^i = T_m^{i-1} - 2\alpha\Delta t & \left(\frac{(r_m + \frac{1}{2}\Delta r) \left(\frac{T_m^{i-1} - T_{m+1}^{i-1}}{\Delta r} \right) + r_m \frac{h}{k} (T_m^{i-1} - T_{fluid}^{i-1})}{(r_m + \frac{1}{4}\Delta r) (\Delta r)} \right) \\
& - 2\alpha\Delta t \left(\left(\frac{1}{r_m^2} \right) \frac{\left(\frac{T_m^{i-1} - T_{m-1}^{i-1}}{\Delta \varphi} \right) + \left(\frac{T_m^{i-1} - T_{m+1}^{i-1}}{\Delta \varphi} \right)}{\Delta \varphi} \right) \\
& - 2\alpha\Delta t \left(\frac{\left(\frac{T_m^{i-1} - T_{m-1}^{i-1}}{\Delta z} \right) + \left(\frac{T_m^{i-1} - T_{m+1}^{i-1}}{\Delta z} \right)}{\Delta z} \right)
\end{aligned} \tag{G.23a}$$

The stability criterion is set and the coefficients of T_m^{i-1} is kept:

$$\begin{aligned}
0 \leq 1 - 2\alpha\Delta t & \left(\frac{(r_m + \frac{1}{2}\Delta r) \left(\frac{1}{\Delta r} \right) + r_m \frac{h}{k}}{(r_m + \frac{1}{4}\Delta r) (\Delta r)} \right) \\
& - 2\alpha\Delta t \left(\left(\frac{1}{r_m^2} \right) \frac{\left(\frac{1}{\Delta \varphi} \right) + \left(\frac{1}{\Delta \varphi} \right)}{\Delta \varphi} \right) \\
& - 2\alpha\Delta t \left(\frac{\left(\frac{1}{\Delta z} \right) + \left(\frac{1}{\Delta z} \right)}{\Delta z} \right)
\end{aligned} \tag{G.24a}$$

The terms are rearranged:

$$\begin{aligned}
0 \leq 1 - \frac{2\alpha\Delta t}{\Delta r^2} & \left(\frac{(r_m + \frac{1}{2}\Delta r)}{(r_m + \frac{1}{4}\Delta r)} + \frac{r_m \frac{h}{k} \Delta r}{(r_m + \frac{1}{4}\Delta r)} \right) \\
& - 2\alpha\Delta t \left(\left(\frac{1}{r_m^2} \right) \frac{2}{(\Delta \varphi)^2} \right) \\
& - 2\alpha\Delta t \left(\frac{2}{\Delta z^2} \right)
\end{aligned} \tag{G.25a}$$

The large parentheses are eliminated, the definition of τ_r , τ_φ , and τ_z is applied , and the factors and terms are rearranged:

$$0 \leq 1 - 2\tau_r \left(\frac{r_m + \frac{1}{2}\Delta r}{r_m + \frac{1}{4}\Delta r} \right) - 2\tau_r \frac{h}{k} \Delta r \left(\frac{r_m}{r_m + \frac{1}{4}\Delta r} \right) - 4\tau_\varphi - 4\tau_z \quad (\text{G.26})$$

H Appendix: Fluid conductivity

Conductivity of water

The conductivity of water is dependent of the temperature and the dependency of pressure is neglected. Values for the conductivity of water is found from EES [27] in a temperature range of 274.15 K to 505 K, and the values are shown in figure H.1.

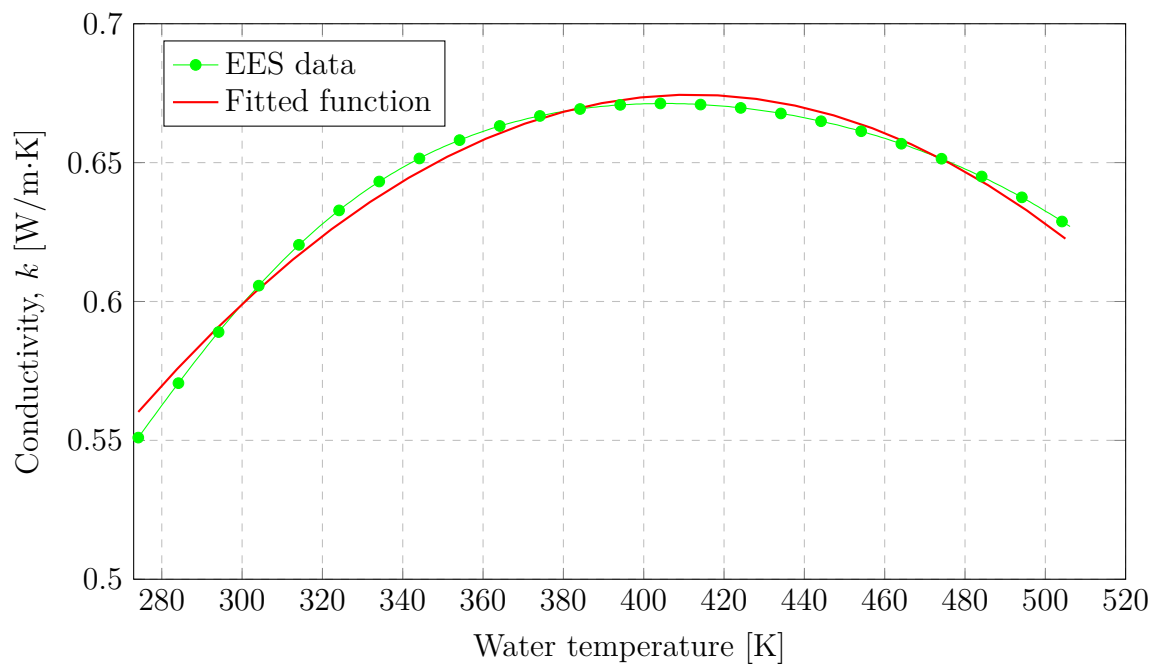


Figure H.1: Conductivity of water as a function of temperature. EES data is sampled at 30 bara.

A function is fitted to the data and used for the conductivity of water in the model. The function is shown in equation H.1.

For $274.15\text{K} \leq T < 505\text{K}$

$$k_{water} = -6.0041 \cdot 10^{-6} \cdot T^2 + 0.0049483415 \cdot T - 0.3450957097 \quad (\text{H.1a})$$

Conductivity of hydrocarbon liquid

The oil liquid in the inventory consists of different hydrocarbons, which all have individual conductivities. The conductivity, for a range of hydrocarbons, as a function of temperature and at a pressure of 30 bara, can be seen in figure H.2. It is out of the scope of this report to calculate the mixture conductivity of the liquid phase, and therefore an assumption has been made. The conductivity of the mixture is modelled as a fixed value of $k = 0.1 \text{ W/m}\cdot\text{K}$.

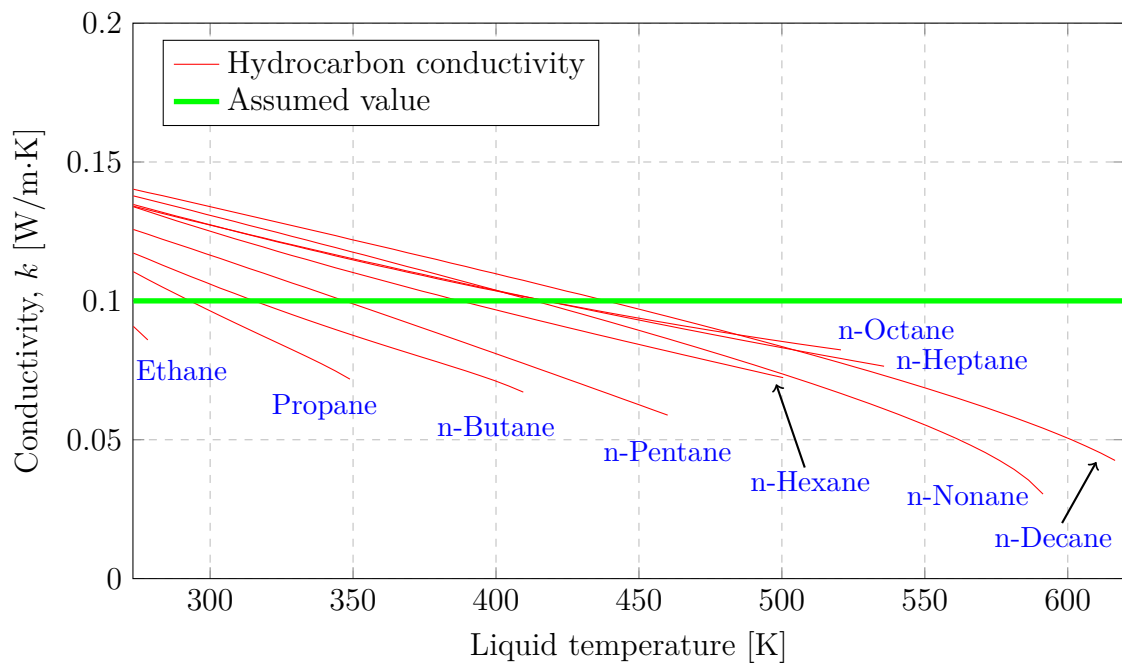


Figure H.2: Conductivity for hydrocarbon liquid as a function of temperature and an assumed value for the conductivity. EES data is sampled at 30 bara.

Conductivity of hydrocarbon gas

Similarly to the liquid phase, the gas phase consists of different hydrocarbon components. The conductivity of the components can be seen in figure H.3. An assumption for the conductivity of the gas mixture is also made. The conductivity of the gas mixture is assumed to be $0.03 \text{ W/m}\cdot\text{K}$. This is equivalent to the conductivity of air at $80 \text{ }^\circ\text{C}$ [15].

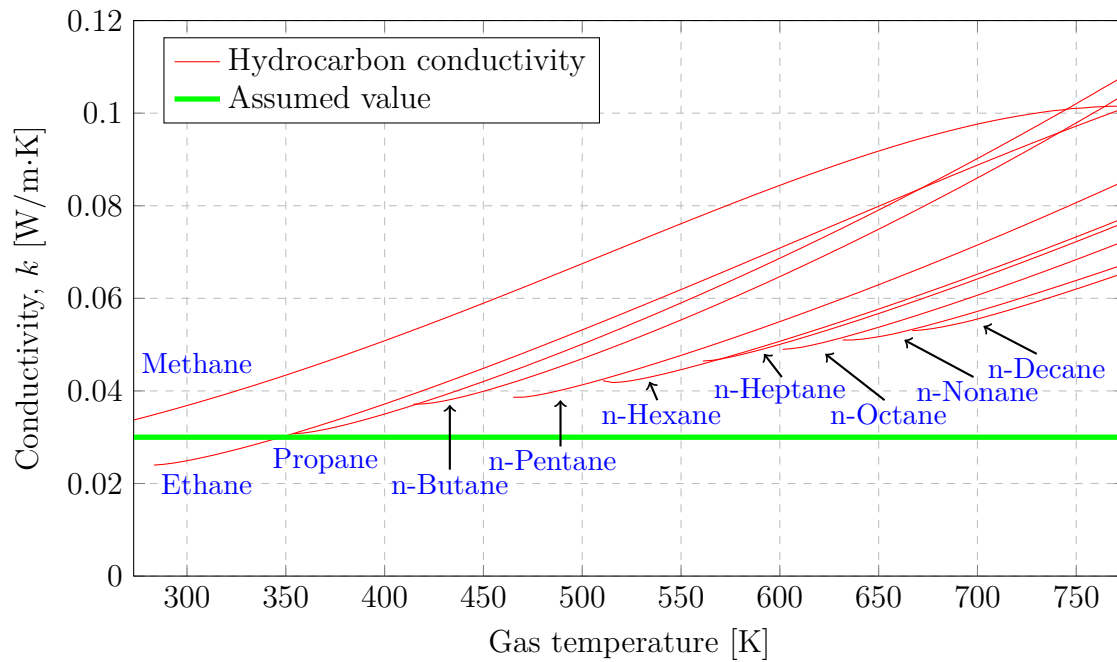


Figure H.3: Conductivity for hydrocarbon gas as a function of temperature and an assumed value for the conductivity. EES data is sampled at 30 bara.